MICRO/NANOPATTERNING APPROACHES FOR MOLECULAR MANIPULATION

A Thesis
Presented to
The Academic Faculty

by

Zhan Liu

In Partial Fulfillment
of the Requirements for the Degree
Doctor of Philosophy in the
School of Material Science and Engineering

Georgia Institute of Technology
December 2010

MICRO/NANOPATTERNING APPROACHES FOR MOLECULAR MANIPULATION

Approved by:

Professor Mark G. Allen, Advisor
School of Electrical and Computer Engineering
Georgia Institute of Technology

Professor David G. Bucknall
School of Material Science and Engineering
Georgia Institute of Technology

Professor Anselm C. Griffin
School of Material Science and Engineering
Georgia Institute of Technology

Professor Donggang Yao
School of Material Science and Engineering
Georgia Institute of Technology

Professor Yonathan S. Thio
School of Material Science and Engineering
Georgia Institute of Technology

Date Approved: 10 November 2010

To my beloved family

ACKNOWLEDGEMENTS

First and foremost, I would like to express my gratitude to my adviser Prof. Mark G. Allen for his faith, patience and encouragement of me, his mental and financial support of me, as well as his vision and extensive technical guidance on my research projects throughout these years. Thanks Prof. Allen for giving me the opportunity to work together with him, to broaden my knowledge and experience in MEMS/NEMS and micro/nanofabrication, to explore and work on many exciting, interdisciplinary and very challenging projects with inspired creative ideas, and to let me understand how to work hard and smart. I am deeply impressed by his professional research attitudes, solid and broad knowledge, sharp mind and big vision, creativity, leadership, management and communication skills. He would be a role model for me to learn.

Another person I am grateful to is my co-adviser Prof. David G. Bucknall. He is always willing to share his life experiences, his knowledge and hands-on skills as well as his beliefs and attitudes towards research and career with his students like me, which I have kept as a precious gift. I can still clearly remember the time when David taught me how to characterize challenging polymer samples by using AFM. David's respect and patience to his students, in-depth knowledge and extensive experience in polymers and materials, research enthusiasm, curiosity as well as creativity have deeply impressed me. Thanks David for putting time and effort in motivating and advising me throughout these years.

I would also like to thank my proposal and defense committee members, Prof. Anselm C. Griffin, Prof. Donggang Yao and Prof. Yonathan S. Thio, for their time and evaluation of my work. Your suggestions and support are important and invaluable for me to accomplish this work and achieve the PhD degree.

I am grateful for the former and current MSMA (Microsensors and Microactuators) group members, in particular Dr. Y. K Yoon, Dr. Seong-Hyok Kim, Dr. Seong-O Choi, Dr. Yanzhu Zhao, Dr. Xiaosong (Sharon) Wu, Dr. Seung-Keun Choi, Dr. Florian Herrault, Dr. Maxine McClain, Ms. Nisarga Naik and Mr. Preston Galle. They gladly gave me their help. In addition, Ms. Purnima Sharma and Mr. Richard Shafer deserve my special gratitude and respect. Without them the group and the lab would not be able to be running smoothly and efficiently. They have been important to every MSMA group member. It has been a real privilege to work in such a wonderful group.

I also want to thank DB's group members and alumni. They are very helpful and friendly. In addition many thanks go to Mr. Ryan Kincer (PTFE & MSE) for the technical help on chemical reactions, Mr. Wei Zhang (PTFE & MSE) for the polymer viscosity characterization, Dr. Toni South (Chemistry) for the UV-vis spectroscopy characterization.

I would like to specially thank the administrative staff in PTFE & MSE - Ms. Angie Abbott and Ms. Hope Payne; the former and current cleanroom staff in MiRC - Mr. Kevin Martin, Mr. Gary Spinner, Mr. Joel Pikarsky, Mr. Devin Brown, Mr. Tran-Vinh Nguyen and Dr. Hang Chen. I believe they have assisted and helped countless students, and I am just one of them. I still want to express my thankfulness to all of them.

I want to give many of my sincere thanks to a few of my friends I have met at Georgia Tech for their generous and selfless help in my research and study - Prof. Muhannad Bakir, Dr. Wanting Ren, Dr. Ruilan Guo, Dr. Bo Pan, Dr. Zhensheng Jia, Dr. Gang Huang, Dr. Jin Liu, Dr. Yuan Li, Dr. Jun Jia, Mr. Ye Luo, Mr. Xin Gao, Mr. Qishu Qin, Mr. Qing Li, Mr. Hongfeng Ren and Ms. Yubin Shen. The memory of our time together at Georgia Tech is very pleasant and cannot be erased, and I will miss all of you.

Finally I would like to use the last paragraph to acknowledge my family members: my mother Jine Ma, my father (passed away) Chunhuai Liu, my older brother Peng Liu and my sister-in-law Jizheng Wang for their great love and selfless sacrifices, constant encouragement and endless support of me. I grew up under their love and care, and I am very proud of having them. I do hope that I can do something for them soon. Lastly an important thank you goes to Deshen Lin (my fiance) and his parents. Thanks Deshen for always supporting my studies both in China and in the US, being open-minded and coming to the US for our future. You will always be my life partner.

TABLE OF CONTENTS

LIST OF TABLES

LIST OF FIGURES

SUMMARY

Nanotechnology is having a steadily increasing impact on worldwide research and business activities. One application area for nanotechnology is the control of material structure, assembly, or reaction on the molecular scale. This work explores advanced micro/nano patterning approaches for molecular manipulation. The objectives are to (1) build a proper bridge from a few microns to the 100-10 nm range and below as well as to (2) combine "top-down" precise design with the "bottom-up" size scale to create designed surfaces, areas and volumes that can interact with molecules in a designed way. Three investigations were designed and studied accordingly.

The first investigation of "top-down" Inclined Nanoimprinting Lithography (INIL) enables the production of three-dimensional (3-D) nanopatterns of varying heights in a single step. INIL is an extension of dewetting in which a shear force, generated by inclining a template mass in contact with a dewetting polymer film, induces directionality in the dewetting. The degree of resulting asymmetry can be controlled by the magnitude of the inclination angle. The feature size is reduced from micron scale of the template to a resultant nanoscale pattern. The underlying INIL mechanism is investigated. It is primarily due to the shear force induced when the inclination angle is not zero leading to anisotropic dewetting of the polymer and consequent asymmetric 3D nanopatterns of varying heights. Various 3-D nanostructures are successfully demonstrated including nanolines, nanocircles and nanosquares. INIL removes the need to prepare expensive 3D nanotemplates or multiple template-to-substrate alignments. INIL enables 3D nano-scale devices including angle-resolved photonic and plasmonic crystals.

The second investigation demonstrates the success of "bottom-up" molecular imprinting of the water soluble X-ray contrast agent iodixanol in a synthetic polymer matrix poly(4-vinylpyridine-*co*-ethylene glycol dimethacrylate). The resulting tailor-made molecularly imprinted polymers (MIPs) show significantly improved absorption capacity and efficiency for iodixanol relative to non-imprinted polymers both in aqueous and blood plasma solutions. The best binding capacity achieved from the optimized MIPs was 284 mg/g in aqueous solution, 8.8 times higher than that of the non-imprinted polymers. The best binding capacity obtained in sheep plasma was 232 mg/g, 4.5 times higher than the non-imprinted polymers. The molecular imprinting strategy enables feature size reduction from macromolecules to the molecular scale. The demonstrated MIPs are encouraging for biomedical implementations including clinical dialysis and nanosensors.

The third investigation, nanolithography-based molecular manipulation (NMM), explores a hybrid approach by combining "top-down" electron-beam lithography (EBL) with "bottom-up" surface initiated polymerization (SIP). It reduces the nanopattern's feature size to sub-10 nm and simultaneously tunes its surface chemistry through functional polymer brushes. The demonstrated prototype molecular manipulation templates have 3D surface nanostructures with sub-10 nm feature size and anisotropic surface functionalities. They mimic biocatalyst enzymes to "bottom-up" assemble nanoparticle targets at specific locations producing 3D nanostructures in a designated way. Various 3D synthetic nanostructures have been demonstrated including polystyrene "nanomushrooms", "nanospikes", "nanofibers" and polystyrene−iron oxide "nanoflowers". Potential applications of these synthetic 3D nanostructures can be improved therapeutic agents. This hybrid strategy realizes the integration of "top-down" design with "bottom-up" molecular scale to create designed nanopatterned surfaces that can interact with molecules in a designated way.

CHAPTER I

INTRODUCTION

1.1 Nanotechnology and Molecular Nanotechnology

Nanotechnology has been experiencing broad and rapid development since the early 1980s. It is generally defined as design, production, characterization and application of materials, structures, devices and systems at atomic, molecular and macromolecular scales (normally 1 to 100 nm), where their properties would be significantly different from those at a macro scale. It has brought major impact to worldwide research and business activities. Nanotechnology is a highly multidisciplinary field ranging from applied physics, materials science, interface and colloid science to chemical engineering, mechanical engineering, and electrical engineering. Their common objective is to control matters and fabricate devices at atomic and molecular scale.

The concept of nanotechnology was first described by physicist Richard Feynman in his classic talk "There's Plenty of Room at the Bottom" on December 29^{th}, 1959. In his presentation, he introduced the concept of manipulating individual atoms and molecules by using a sequential size reduction approach where a set of tools would be used to fabricate and operate a proportionally smaller set, while repeating such process until achieving the desired scale. Consequently, a series of advanced tools and techniques are required to drive the development of nanotechnology. Recent technology advances have demonstrated the feasibility to examine, probe and manipulate macromolecules, molecules and even atoms with great precision. Examples include electron beam lithography (EBL), nanoimprinting lithography (NIL), focused ion beam (FIB) and atomic force microscopy (AFM). Although most of them are still under development, it is anticipated that nanotechnology will have a revolutionary

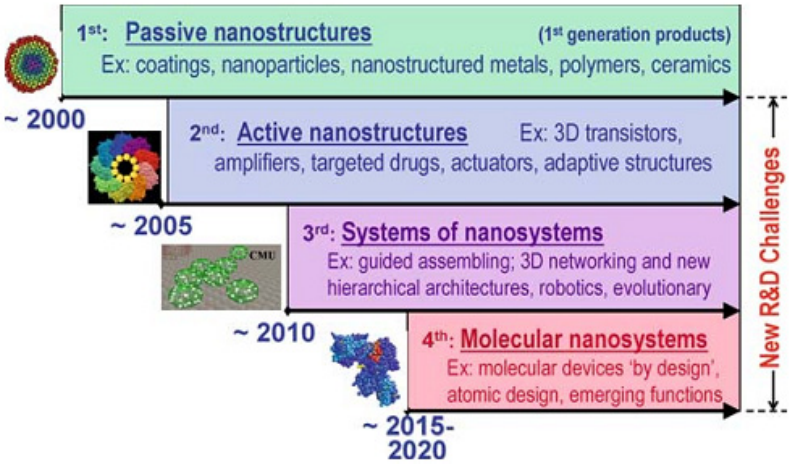

Figure 1.1: Four generations of products: timeline for beginning industrial prototyping and nanotechnology commercialization [103].

impact during the 21^{st} century.

The predicted trend of nanotechnology development and implementation between 2000-2040 is shown in Figure 1.1. Currently, the main research areas relate to passive and active nanostructures as the 1^{st} and 2^{nd} generations of nanotechnology, while the future of nanotechnology is to create nanosystems and molecular nanosystems as its 3^{rd} and 4^{th} generations respectively.

As an advanced form of nanotechnology, molecular nanotechnology (MNT) focuses on engineering functional nanomechanical machines and systems at the molecular scale. Such molecular machines and systems are used for desirable mechanosynthesis in specific locations and orientations. It is distinct from nanoscale or nanostructured materials which greatly rely on the principles given by nature. MNT is targeting a proper combination of engineering design, process control and fabrication accuracy at molecular scale in a designated manner. It would employ designed processes to exactly obtain the expected results similar to what nature does.

Potential applications of MNT are very diverse. The first example is smart materials, which are referred to any sort of material designed and engineered at nanometer scale to perform a specific task, e.g. to selectively recognize and respond differently

to various molecules. Another example is a nanosensor that could incorporate such a smart material within a larger machine/system to react to its environment. The third example are so called metamaterials that are defined as engineered artificial materials to provide properties which may not be readily available in nature, such as negative refractive index. These materials usually gain their unusual properties from structure, periodicity and scale rather than composition. Molecular assemblers are proposed devices that are able to guide chemical reactions by precisely positioning molecular reactants. Nano-robots would be more complex systems containing special molecular building blocks for replication and healthcare. In summary, molecular nanotechnology is a promising field. Although it is still in the conceptual stage, it shows large potential to attract increasing attentions.

Generally, there are two dominant fabrication methodologies widely used in nanotechnology: "bottom-up" and "top-down" strategies. In the "bottom-up" approach, materials and devices are built up from molecular components by molecular recognition and self-assembly (e.g. polymer manufacturing [23, 37, 91, 141]). In the "top-down" approach, nano-objects are machined from bulky entities without atomic-level control, such as photolithography [59], EBL [101], NIL [28] and soft lithography [72].

Both "top-down" and "bottom-up" strategies have their pros and cons. The "top-down" approach is used for mass production of micro devices, but it is very challenging to ideally realize molecular level resolution and functionality. The "bottom-up" approach strongly relies on the spontaneous geometric assemblage available from nature. It is difficult to use it to organize a sufficient amount of nanostructures into well-defined patterns at specific locations for fabricating useful devices. Although it is an appropriate method to have molecular resolution, it is opposed to the MNT's principle of design and fabrication in a designated way.

A third strategy is recently emerging and seems promising to address these issues. It integrates "top-down" and "bottom-up" approaches together and could compensate

for the limitations of each. Examples include scanning probe lithography (SPL)-based molecular manipulation [40, 35] as well as nanotube and nanowire integrated functional structures and devices [25, 39, 88, 124].

The motivation of this research is to explore novel and feasible micro/nano patterning approaches by developing both "top-down" and "bottom-up" methods, to create a proper bridge across the physical gaps between microns, nanometers and further down to molecular scale (<10 nm), and to combine "top-down" precise design with "bottom-up" molecular scale to create designated surface and volume which can properly interact with molecules in a designated way. The achievement of this goal can be a big step towards molecular nanotechnology (MNT) realizing MNT at an earlier time. A literature survey of the current progress of nanotechnology and molecular nanotechnology associated with minimizing feature size and molecular manipulation has been performed. It covers "top-down", "bottom-up" and "top-down"/"bottom-up" hybrid strategies. Section 1.2 will give detailed reports and discussions.

1.2 Literature Survey

1.2.1 "Top-down" Approaches for Nanofabrication

1.2.1.1 Potolithography

Photolithography is the most common type of patterning with great convenience for batch production. It is extensively used in microelectronics and microelectromechanical systems (MEMS). A single iteration of photolithography consists of several steps in sequence including wafer preparation, photoresist coating, UV exposure and development, etching, and photoresist removal. The principle of UV light diffraction is used to create a reduced feature size. The minimum feature size is given approximately by equation 1.1:

$$F = k \cdot \frac{\lambda}{NA} \tag{1.1}$$

where F is the minimum feature size; k is a coefficient that encapsulates process-related factors, and typically equals 0.5; λ is the light wavelength; and NA is the numerical aperture of the lens.

According to equation 1.1, the feature size can be minimized by either decreasing the wavelength or increasing the numerical aperture, i.e. making lenses larger and bringing them closer to the wafer. With regard to light wavelength, deep ultraviolet (DUV) lithography with wavelengths of 248 nm and 193 nm are state-of-the-art for optical lithography. With regard to numerical aperture, the use of a micro-stepper with high numerical aperture (NA) lens, phase-shifting masks (PSM), and fluoropolymer resists demonstrated a feature size reduction down to less than 50 nm [52]. Up to now the feasibility of photolithography to fabricate various patterns with a reduced feature size, e.g. less than 50 nm, has been demonstrated. In addition, non-conventional UV photolithographic techniques by manipulating either the mask and the light path or the photoresist have also been widely investigated. Various 3D complex nanostructures are demonstrated for potential applications in MEMS, optics and fluidics. For example, Rogers *et al*. demonstrated complex 3D nanostructures using high-resolution PDMS elastomer conformable phase masks (Figure 1.2) [59]. The PDMS phase mask has relief features that are comparable in dimension to the UV wavelength (370-430 nm). The resulting 3D nanostructures have feature size as small as 50 nm.

Generally speaking UV photolithography for nanofabrication is feasible but limited due to the need for complex equipment, expensive masks, photoresist materials, and optical fundamentals.

1.2.1.2 Electron Beam Lithography

The primary advantages of electron beam lithography (EBL) are that it is maskless and can beat the diffraction limit of light, thereby producing patterns with very high resolution. In a typical EBL process, a pattern is carved out line-by-line by scanning

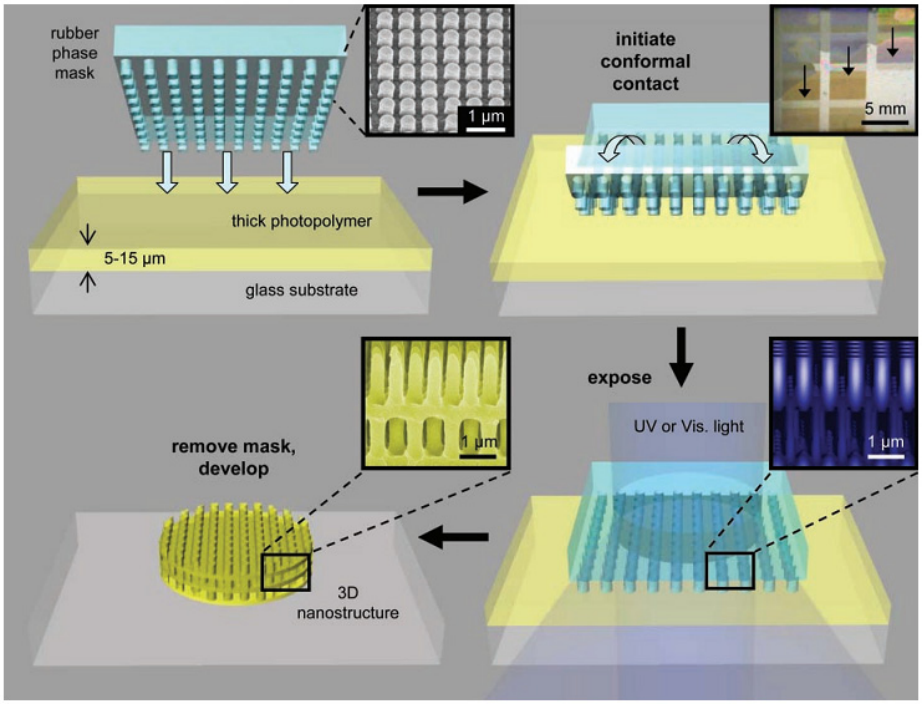

Figure 1.2: Schematic illustration of fabrication steps using a high-resolution conformable, elastomeric phase mask to produce 3D nanostructures [59].

a high-energy (>10 kV) beam of electrons across a surface using a CAD file instead of a physical mask. Current dedicated EBL systems have pushed line resolution below 10 nm.

The resolution of EBL is essentially determined by high-energy secondary electrons and the scattering of electrons from the primary beam within the resist and from the substrate, but the actual resolution is affected by other factors, such as pattern design, photoresist properties, development of the resist after exposure, and pattern transfer processes. Very recently, by using the high-resolution inorganic resist hydrogen silsesquioxane (HSQ), sub-6 nm EBL was developed in [115]. Gatech has demonstrated 6.5 nm wide nanoline using HSQ resist and 3.5 nm gap using poly(methyl methacrylate) (PMMA) resist respectively by JBX-9300FS EBL system [2]. Vieu *et al.* indicated that the intrinsic resolution of writing in PMMA can be as small as 3 to 5 nm at high electron energy, but the practical resolution is limited

by the post processes after exposure [120]. Moreover the high resolution mentioned above is only for isolated features rather than nested features. Nested features exacerbate the proximity effect, whereby electrons from the exposure of an adjacent feature spill over into the exposure of the currently written feature effectively enlarging its image and reducing its contrast. Dense arrays of periodic structures in PMMA are demonstrated at a pitch of 30 nm, leading to a density close to 700 Gbit/in^2. For most resists, it is difficult to go below 25 nm lines and spaces.

A number of unique and interesting nanostructures have been successfully demonstrated by EBL to experimentally investigate fundamental theories, device physics and the feasibility of molecular manipulation. Qi *et al.* [101] fabricated 3D photonic nanocrystals that are particularly suited for optical device integration using an EBL-based layer-by-layer approach (Figure 1.3). Point-defect micro-cavities are introduced during fabrication. The obtained optical measurements at near-infrared are in good agreement with numerical simulations. Kinkhabwala *et al.* [71] utilized EBL to fabricate bowtie nanoantennas in sub-25nm feature size (Figure 1.4). The produced nanoantennas present highly enhanced optical fields. The observed enhancement of a single molecule's fluorescence is up to a factor of 1,340, ten times higher than other reports, in agreement with the electromagnetic calculations.

1.2.1.3 Soft Lithography

Soft lithography is a suite of techniques that use organic materials to enable replication and pattern transfer on multiple length scales from nanometers to centimeters. The term "soft" refers to the stamp, e.g. poly(dimethylsiloxane) (PDMS), and/or the organic ink, e.g. polymers or self-assembled monolayers.

PDMS silicone rubber is widely used for the mold material because of a number of useful properties: (a) PDMS is inert to many chemicals and unreactive towards most materials being patterned or molded; (b) it has a low surface free energy (= 21.6

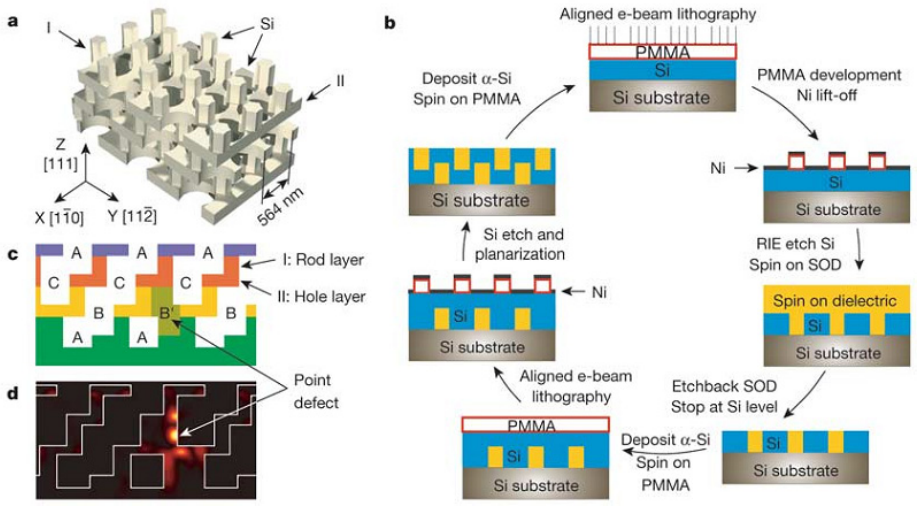

Figure 1.3: Schematic of the 3D PhC and its fabrication in silicon (Si). (a) Computer rendering of an ideal 3D PhC. (b) An illustration of the layer-by-layer EBL-based approach. (c) Cross-sectional view in the [110] plane. (d) Calculated $\varepsilon \mid E^2 \mid$ (where ε is the dielectric constant, and E is the electric field) of the point-defect state at a resonant wavelength of $1.3\mu m$ [101].

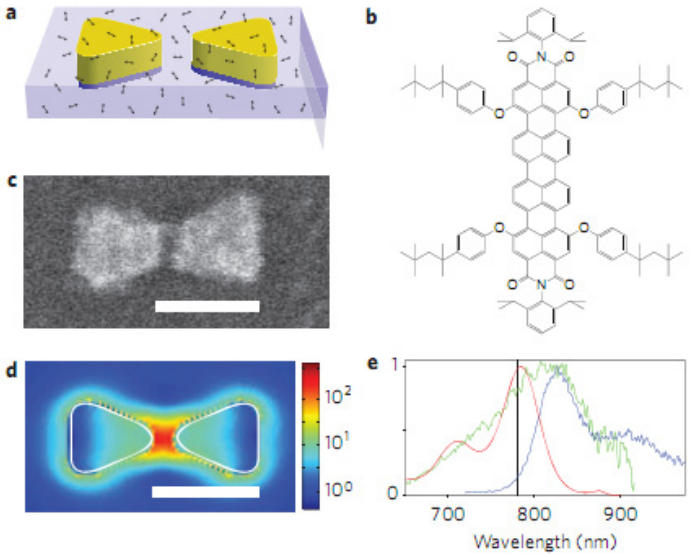

Figure 1.4: (a) Schematic of bowtie nanoantenna (gold). (b) Molecular structure of TPQDI. (c) SEM image of a gold bowtie nanoantenna. Scale bar, 100 nm. (d) FDTD calculation of local intensity enhancement. (e) Normalized absorption and emission spectra adapted from [71].

dyn/cm^2) that facilitates the separation from templates and printed structures; (c) PMDS is optically transparent down to 300 nm and thermally stable (below 150 °C) which permits UV or thermally-induced cross-linking of materials being molded; (d) it is physically tough with a tensile modulus of 4.77 MPa; and (e) it is flexible with a elastic modulus of 1.8 MPa and up to 160% elongation value [127]. A series of soft lithographic methods have been developed to fabricate micro/nano size patterns using PDMS stamps. Some classic examples include replica molding (RM) [69, 128], microtransfer molding (μTM) [142] and micromolding in capillaries (MIMIC) [99, 131]. These methods can successfully and conformally transfer the structure from the stamp to the ink layer at micro/nano scale.

A recently developed molded de-wetting (MD) process [72, 139] is distinct from the above well-known soft lithographic techniques. It is developed in polymer thin films (less than 50 nm) and capable of producing 2D nanoscopic polymer patterns simply using a microscopic patterned PDMS mold. The feature size of the resulting polymer patterns can be much smaller than that of the PDMS stamp. Moreover, the nanopatterns are highly regular and reproducible. The fabrication procedure is shown in Figure 1.5 including contacting, annealing-induced de-wetting, and stamp separation. Three requirements are suggested for the applicability of MD: (1) the polymer melt wets the PDMS mold pretreated by O_2 much better than the Si substrate; (2) the film is thin compared to the feature depth of the PDMS stamp; (3) a sufficient annealing temperature or incubation time is required.

The MD process has successfully demonstrated high yield in 2D nanopatterns. However, to obtain 3D nanopatterns of varying heights, it seems necessary to repeat it accompanied by careful alignment. Layer-by-layer MD-based fabrication is feasible but not desirable. To address this concern more investigation has to be carried out to further explore the de-wetting behavior of polymer thin film as well as 3D nanofabrication feasibility.

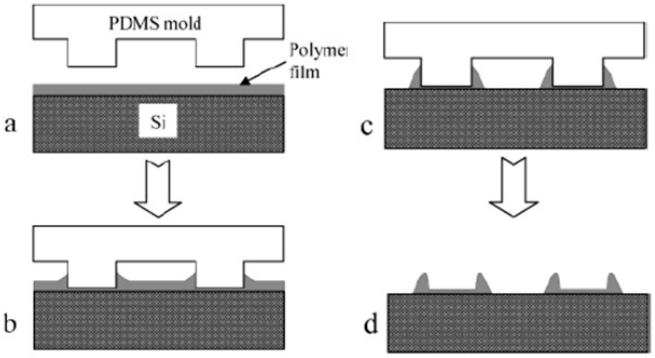

Figure 1.5: Schematic illustration of MD process adapted from [139]. (a) contact; (b) annealing at a temperature above the T_g of the polymer; c) further annealing to complete the polymer dewetting; d) cooling the assembly below T_g and the stamp separation.

Nanotransfer printing (nTP) is also recently developed to build a range of complex 2D/3D structures with feature sizes between tens of microns and tens of nanometers using PDMS stamps [85, 137]. nTP approach uses micro/nanopatterned PDMS stamps coated with a thin solid metallic "ink" layer. The surface adhesion or chemical bonding interactions between the substrate and the ink layer enables the efficient transfer of the metal thin film from the stamp to the substrate. Figure 1.6 shows the schematic process of transferring 2D and 3D gold metal films onto the substrate. Whether 2D or 3D structures can be transferred is dependent on the profile of the PDMS stamp and the coated "ink" layer. A stamp with slightly sloping sidewalls would lead to a continuous metal layer coating. Consequently 3D metal thin films can be transferred. Repeating the transfer would result in more complex 3D nanostructures. nTP can be used to fabricate various organic electronics and plasmonic crystals.

This interesting nTP technique is simple and cost-effective, yet tricky in terms of 3D fabrication at the nano and molecular scale. It requires a 3D nanoscopic high resolution PDMS stamp, greatly relying on the manipulation of surface chemistry. To date, only gold has been successfully demonstrated primarily due to the thiol-based

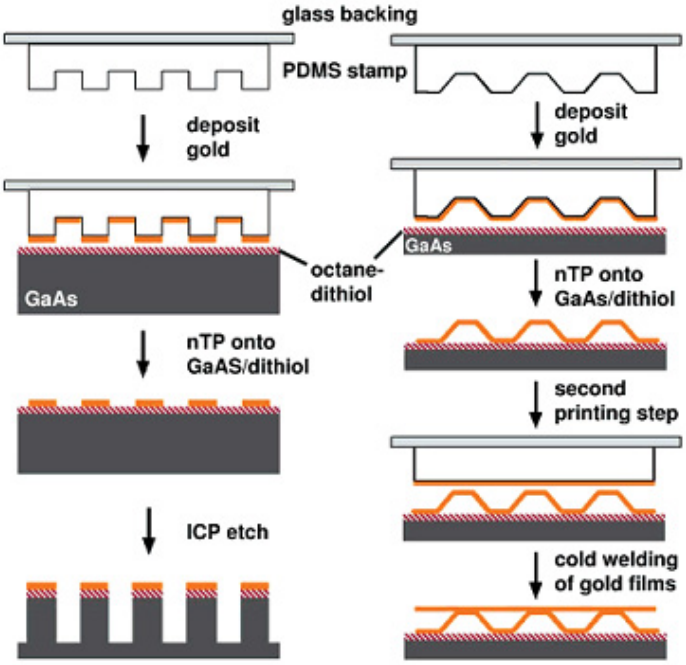

Figure 1.6: Schematic illustration of nanotransfer printing. Depending on the profile of the stamp, two-dimensional (left) or three-dimensional (right) Au films can be transferred onto the substrate adapted from [137].

surface interaction.

1.2.1.4 Nanoimprinting Lithography

Nanoimprint lithography (NIL) is a novel method of fabricating nanometer scale patterns [45]. The process is simple, with high-yield and high-resolution. There are many different types of NILs. Two most important ones are thermoplastic NIL (T-NIL) [28] and photo NIL (P-NIL) [50, 111]. T-NIL is the earliest nanoimprint lithography developed by Professor Chou's group [28, 30, 31, 140]. A typical T-NIL process is shown in Figure 1.7 consisting of three steps: (1) imprinting by using a mold to create a thickness contrast in a resist, (2) mold removal, and (3) pattern transfer by using anisotropic etching. A typical P-NIL process is shown in Figure 1.8. In P-NIL, a photo (UV) curable liquid organic resist is applied to the sample substrate. The mold is normally made of a transparent material such as quartz or fused silica. After

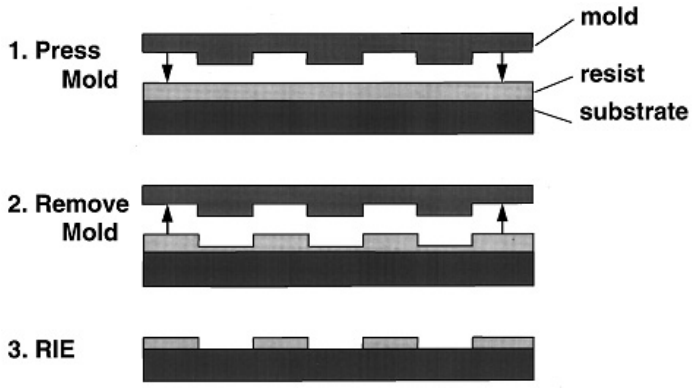

Figure 1.7: Schematic of nanoimprint lithography process adapted from [45].

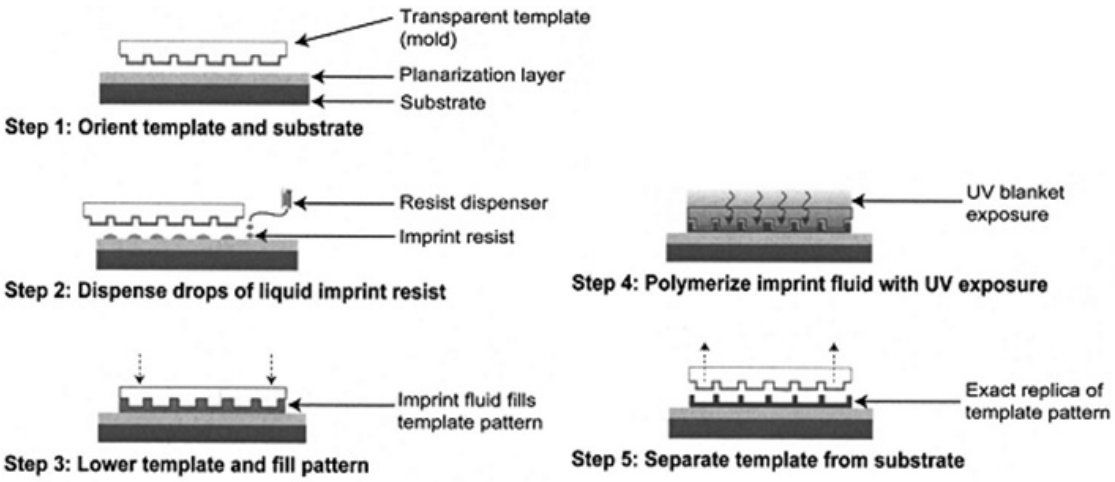

Figure 1.8: Process schematic of step and flash nanoimprint lithography adapted from [111].

the mold and the substrate are pressed together, the resist is cured under UV light followed by mold separation. NIL has been used to pattern a number of nanodevices in microelectronics, optics and fluidics [45, 79, 88, 140]. It can replicate structures with aspect ratios up to 10:1 and lateral dimensions as small as 10 nm [31]. The highest resolution so far is down to sub-6 nm by T-NIL [8, 9] and to 2 nm by P-NIL [50].

3D nanopatterns can be fabricated by NIL either using 3-D templates [78] or a layer-by-layer fabrication strategy to repeatedly transfer nanopatterns from template

to the substrate [11]. Neither approach is relatively simple, convenient and technically desirable. Critical issues for NIL include pattern defects, the technical challenge, and the increased cost of fabricating nano templates especially with 3D structures, although these can be mitigated with the use of effective template cleaning and EBL or FIB strategies respectively.

1.2.2 "Bottom-up" Approaches for Nanofabrication

"Bottom-up" approaches seek to have smaller (usually molecular) components arranged into more complex assemblies. They generally use the concepts of molecular self-assembly and/or molecular recognition. Early examples from "bottom-up" approaches include Langmuir-Blodgett films, molecular crystallization, epitaxial growth, synthesis of polymers and many processes common to living systems. Recently an increasing number of chemical growth methods have been developed to form nanostructural new materials, such as molecular imprinted technology (MIT) and surface grafting polymerization (SIP).

1.2.2.1 Molecular Imprinting Technology

Molecular imprinting technology (MIT) is an attractive biomimetic approach to nature at the nano/atomic scale. The imprinting process can be likened to a process of making artificial "locks" for "molecular keys". A brief outline of the process is shown in Figure 1.9 [1]: (a) the selected key molecule is first mixed with a variety of lock building blocks; (b) then lock building blocks and the key are allowed to attach to each other; (c) such formed complexes are subsequently "glued" together in order to fix the building block positions around the key; (d) the molecular key (template) is removed to leave the lock with a imprinted site that ideally can only recognize the original key and will not recognize any other key. Consequently the synthetic polymer material of MIT is named as molecularly imprinted polymers (MIPs).

In principle, the molecular template may be of any type ranging from small

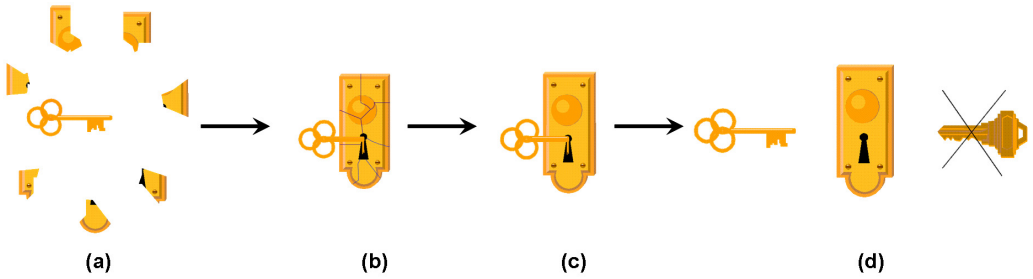

Figure 1.9: A brief outline of imprinting procedure in MIT adapted from [1].

molecules, such as drug substances and amino acids, to larger molecules, such as nucleic acids and proteins. In general, the difficulty of making the imprinted polymer materials increases with the size, functionality and structural complexity of the selected key molecule.

MIT is classified into covalent imprinting, non-covalent imprinting, and semi-covalent imprinting [5, 23]. Different imprinting strategies have their own pros and cons. Amongst them, the non-covalent imprinting method has been studied more than the others due to the reduced cost, the technical convenience and simplicity and the adaptability to various molecular templates. There are several modes of non-covalent interactions between the molecular keys and functional monomers or the resulting MIPs matrix including hydrogen bonds, hydrophobic effects, and $\pi - \pi$ stacking and relatively strong ionic bonds. The wide variety of possible interactions implies that molecular recognition of a target molecule may be dominated by one mode of molecular interaction or controlled by a combination of different recognition mechanisms. In general, the combination of two or more interaction modes can be expected.

Many parameters are involved in this chemical MIT and would affect the resulting MIPs' binding performance and capability. The important information associated with the resulting binding sites in MIPs includes the size, the shape, the polarity of the polymer matrix, the steric arrangement of functionalities, and the electronic

properties (charge, polarity and van der Waals forces). Besides, the porogen also plays an important role, since it can be applied to increase the porosity of resulting polymers and the consequent binding capacity. Therefore a successful MIT is determined by a combination of (1) feasible imprinting strategy, (2) careful selection of monomer, crosslinker and solvent/porogen as well as (3) proper synthesis recipe.

Several applications have been envisaged by the molecularly imprinted polymers (MIPs) [16, 43, 91, 126, 135], including (1) separation and isolation, (2) antibody and receptor mimics in immunoassay-type analyses, (3) enzyme mimics in catalytic applications, and (4) biosensor-like devices.

1.2.2.2 Surface Inititated Polymerization

Surface initiated polymerization (SIP) [12, 37, 141] is generally used to grow polymer brushes on a substrate surface. It enables one to tailor the surface of patterned inorganic substrates/materials by functional polymers. In general, there are two ways applicable to functionalize material surface through polymers: (1) chemically and (2) physically (by physisorption) as shown in Figure 1.10.

For polymer physisorption (Figure 1.10(A)), block copolymers adsorb onto a suitable substrate with one block interacting strongly with the surface and the other block interacting weakly with the substrate. It is a non-covalent adsorption making the adsorbed layer unstable and thus not favored in certain applications. In contrast, chemical grafting techniques are preferred in most cases. It consists of "grafting to" (Figure 1.10(B)) and "grafting from" (Figure 1.10(C)). In the "grafting to" approach, preformed end-functionalized polymer molecules react with an appropriate substrate to form polymer brushes. "Grafting from" is also called surface initiated polymerization (SIP), that is, the surface of inorganic materials/substrates is first chemically modified with initiators followed by polymerization. The "grafting from" approach is more promising to produce high grafting density, because the steric barrier imposed

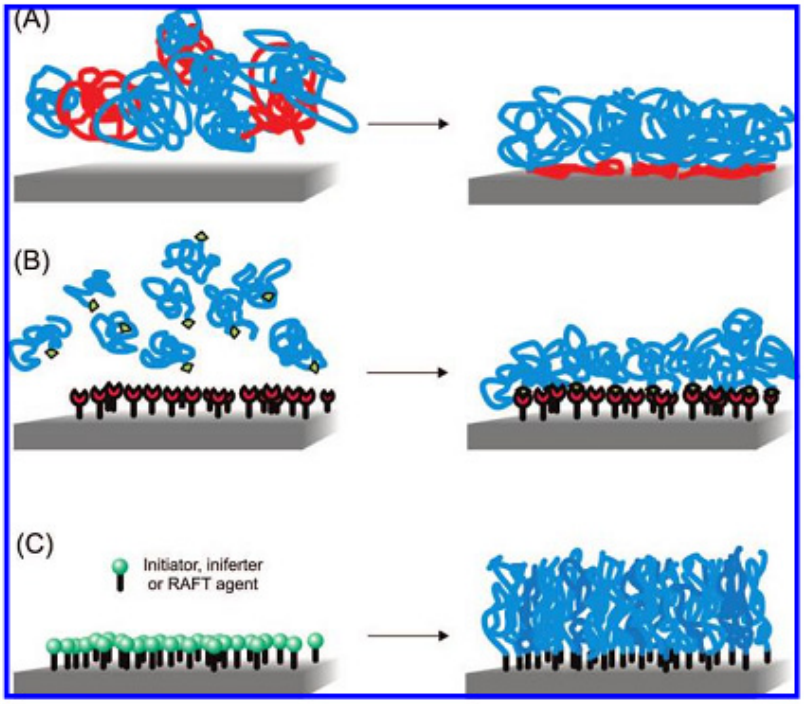

Figure 1.10: Synthetic strategies for the preparation of polymer brushes: (A) physisorption of diblock copolymers via preferential adsorption of the red blocks to the surface; (B) chemisorption via reaction of appropriately end-functionalized polymers with complementary functional groups at the substrate surface ("grafting to"); (C) polymer brushes grown via surface-initiated polymerization ("grafting from") [12].

by the in situ grafted chains does not limit the access of smaller monomer molecules to the active initiation sites, while in the case of "grafting to" the steric barrier would greatly affect the access of preformed macromolecules [37]. For the purpose of uniformity we will only use the term of SIP rather than "grafting from" for the following chapters of this dissertation.

In addition, it is possible for SIP to control the produced polymer chain length or the polymer layer thickness by using controllable polymerization methods. So far polymerization mechanisms that have been used to synthesize polymer brushes include cationic, anionic, free radical, TEMPO-mediated radical, atom transfer radical polymerization (ATRP) and ring-opening polymerization. Free radical polymerization is primarily preferred due to the less stringent reaction conditions and cost.

According to many reported systems using SIP via a conventional free radical polymerization mechanism, the immobilization of radical initiators would involve a series of steps. Typically, an anchor molecule would be immobilized on the solid substrate surface and then the initiators are linked to the anchor molecules in one or more additional steps. For example Ueda *et al.* [117] treated silica beads with 3-aminopropyltriethoxysilane (γ-APS) to obtain amino functional groups on the surface. Azo initiators were then immobilized onto the surface through the formation of amide bonds between the γ-APS modified surface and the acid-chloride-functionalized azo initiators. Subsequently, surface initiated radical polymerization was carried out to produce tethered polymer chains.

Applications of SIP would be in (1) responsive surfaces, for instance to target molecules, ions, temperature and pH value; (2) nonbiofouling surfaces, i.e. surfaces that resist the nonspecific adsorption of proteins, cells or other biological species which are important for a wide variety of applications in fields ranging from medical implants to contact lenses, drug delivery as well as biosensors; (3) adhesive surfaces to specific targets e.g. cells, proteins and DNA; (4) chromatography; (5) membranes and coatings [12].

1.2.3 Hybrid "Top-down"/ "Bottom-up" Approaches for Nanofabrication

Both "top-down" and "bottom-up" approaches have their inherent drawbacks as have been briefly discussed above. It seems that fusing "top-down" and "bottom-up" together would be a promising strategy to overcome those inherent limitations. Very recently a number of studies have been started to explore various hybrid fabrication approaches.

Some examples include (1) fabrication of polymeric micro/nanostructures using a combination of SIP with various lithographic techniques [57, 62, 108, 121], (2) self-assembled block copolymers as masks for conventional lithography [38, 96], (3)

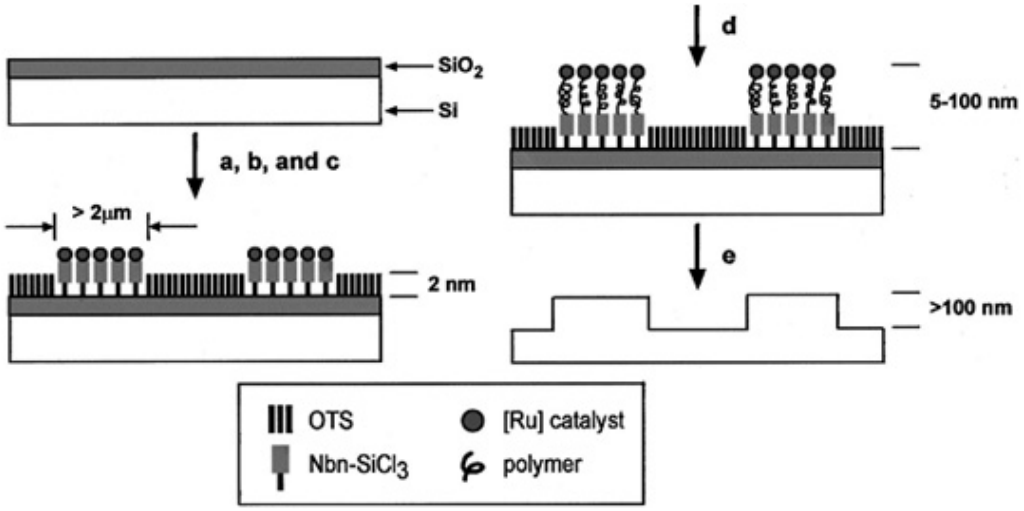

Figure 1.11: Schematic representation of patterned polymer formation by μCP, activation, and ring-opening metathesis polymerization on the surface of SiO_2/Si [57].

scanning probe lithography (SPL) based molecular manipulation [35, 40], (4) fabrication of nanowires, nanoparticles, nanotube integrated functional structures and devices [25, 39, 82, 88, 124].

In terms of the first hybrid approach, one of the earliest research work associated with this strategy was reported by Whitesides *et al.* [57]. The process includes μCP, chemical activation (initiator grafting), ring-opening metathesis polymerization on the surface of SiO_2/Si, followed by ion etching for pattern transfer as shown in Figure 1.11. The smallest lateral feature from the grown polymer layer was 2 μm determined by the PDMS stamp in the μCP process which would not be the intrinsic limit of the method. However there is no further report regarding to the smallest feature size this method can realize.

Timothy *et al.* reported a hybrid approach that combines μCM with SIP to control the size and chemistry of micro/nanoscopic features [121]. In that process, a highly

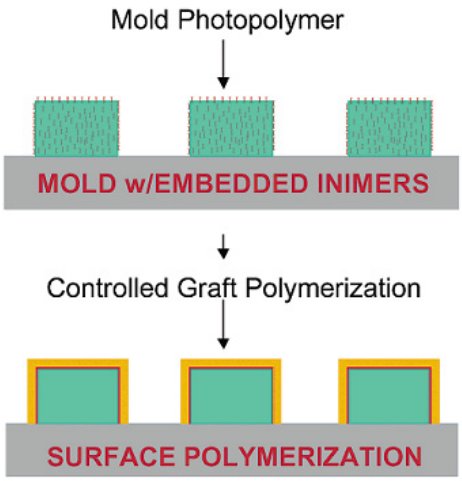

Figure 1.12: Graphical representation of surface tuning for nanoscopic pattern replication [121].

cross-linked photopolymer, based on a methacrylate/acrylate mixture, is first patterned into submicron sized features on a silicon wafer using a contact molding technique. Living free radical polymerization is then employed to grow polymer brushes from these patterned features as shown in Figure 1.12. A critical component of that process is the photopolymer contains an imbedded inimer (***ini***tiators/mono***mers***, having both an initiator and monomer fragment) which can be both molded in step one and chemically activated for polymerization in step two. Demonstrated lateral features ranged in size from 5 μm to sub-60 nm. However this approach involves several complicated synthesis steps for preparing commercially unavailable inimers, and thus is not a simple or convenient method.

Kaholek *et al.* [65] fabricated stimulus-responsive poly(N-isopropyl-acrylamide) nanopatterns from monolayers of omega-mereaptoundecyl bromoisobutyrate on gold-coated surfaces. The fabrication process combines "nanoshaving", a scanning probe lithography (SPL) method, with surface-initiated polymerization (SIP) in aqueous methanol. Thick polymer brush layers (up to 500 nm in the swollen state) are demonstrated after polymerization. The minimum feature size is determined by the scanning

time and circles under defined parameters. Their work demonstrated the possibility of triggered control of interfacial properties on the nanometer scale holding a significant promise for actuation in bio-nanotechnology applications. However, SPL is performed in a raster manner with a low scanning speed in order to precisely manipulate the surface chemistry at the nano scale, it is not very suitable for high-volume manufacturing with low cost.

Obviously, increasing attention and efforts have been paid to various novel hybrid approaches in nanofabrication because of the vast flexibility and potential for the anticipated nano/molecular-sized functional structures, devices and complex nanosystems approaching Molecular Nanotechnology (MNT). A bright future is expected ahead.

1.3 Objectives and Organization of Dissertation

The research motivation of this work is to reduce the pattern's feature size from micrometers through nanometers down to the molecular scale with precise control by exploring various fabrication and manipulation techniques. Another research motivation is to combine "top-down" precise design with the "bottom-up" size scale to create a designated surface and volume that can interact with molecules in a designated way. Molecular manipulation becomes paramount in the pursuit of these targets. Three objectives are set to develop advanced nanotechniques minimizing the pattern feature size. They are "top-down" Inclined Nanoimprinting Lithography (INIL), "bottom-up" Molecularly Imprinted Polymers (MIPs) and hybrid Nanolithography-based Molecular Manipulation (NMM) fabrication strategies. The "top-down" Inclined Nanoimprinting Lithography (INIL) and the hybrid Nanolithography-based Molecular Manipulation (NMM) projects are focusing on minimizing the feature size from micrometers to a few hundred nanometers till sub-10nm by manipulating polymers' physical and chemical properties. The study of Molecularly Imprinted Polymers

(MIPs) further reduces the scale to molecular size by manipulating the X-ray contrast agent of iodixanol and its associations with the synthetic polymer matrix.

1.3.1 Inclined Nanoimprinting Lithography (INIL)

INIL is a "top-down" 3-D nanofabrication approach. It can produce three-dimensional (3-D) nanopatterns of varying heights in a single imprinting step. This approach enables us to manipulate macromolecules' anisotropic de-wetting behavior by controlling the inclination angle. The size reduction is from the micrometer to the nanometer scale. A few applications can be envisaged by the produced 3D nanostructures such as angle-resolved photonic crystals and plasmonic crystals. The study associated with this technique will be presented and discussed in Chapter 2.

1.3.2 Molecularly Imprinted Polymers (MIPs) for X-ray Contrast Agent

Molecular Imprinting Technology (MIT) is a "bottom-up" chemical approach. In this work MIT is used to produce Molecularly Imprinted Polymers (MIPs) as proper absorbent materials to efficiently absorb X-ray contrast agent molecules (iodixanol) in aqueous and plasma solutions. The binding mechanism is analogous to the recognition between antibody and antigen. This approach provides the capability of further reducing the feature size down to the atomic scale by chemically controlling affinities between the target molecules and MIPs matrix. The synthetic tailor-made MIPs are suitable for a number of biomedical applications including dialysis, nanosensors and nanomedicines. Chapter 3 will focus on this investigation.

1.3.3 Nanolithography-based Molecular Manipulation (NMM)

Nanolithography-based Molecular Manipulation (NMM) is proposed as a hybrid nanofabrication strategy to create designed nanostructures, devices and systems with molecular-level resolution and functionality. In our work, a combination of "bottom-up" surface initiated polymerization (SIP) with "top-down" nanolithography of electron-beam

lithography (EBL) is used to create a series of prototype molecular manipulation templates with different surface 3D sub-10nm nanostructures and anisotropic surface functionalities. The produced templates are able to recognize and assemble molecular targets into various 3D nanostructures in a designated manner with potential applications as improved therapeutic agents. This hybrid NMM strategy allows us to combine "top-down" design with "bottom-up" molecular scale to create designed surface and volume that can interact with molecules in a designated way. The work associated with this investigation will be discussed in Chapter 4.

The last chapter of this dissertation provides the summary, the contributions of this work, and some suggestions to future work.

CHAPTER II

INCLINED NANOIMPRINTING LITHOGRAPHY (INIL)

2.1 Introduction

The ability to fabricate 3D nanopatterns/nanostructures is a significant technical driver not only to realize systems with similar scale, topography and function to those found in nature [4], but also in photonics [17, 32, 44, 59, 101], plasmonics [10, 14, 22, 34, 47, 71, 93, 100, 112, 116], metamaterials [86, 93, 100], micro- and nanofluidics [27, 67, 132], nanobiochemistry [4, 13, 64] and nanoelectromechanical systems (NEMS) [27, 64]. To these ends, nanoimprinting lithography (NIL) [3, 29, 41, 45] and soft lithography [58, 134, 137, 139] have been recently exploited since they offer the ability to form the desired 3D structures with the promise of low cost and high throughput as are discussed in Chapter 1. However, to properly achieve true 3D nanostructures of varying heights on a planar substrate, they would require either templates with 3D nanostructures over a large area for direct 3D nanoimprinting, or a precise registration and alignment between the templates and substrates to repetitively transfer 2D structures from templates onto the single substrates as an indirect route for 3D nanofabrication. This would inevitably increase fabrication difficulties and process complexities.

In this chapter, we demonstrate a nanofabrication approach, Inclined Nanoimprinting Lithography (INIL), for producing 3D nanostructures of varying heights in a single imprinting step by utilizing an inclined poly(dimethylsiloxane) (PDMS) stamp mold micropatterned with 1D/2D structures. INIL derives from the anisotropic dewetting process of polymer thin films [24, 139], augmented by the observation that the degree of anisotropy is controlled by the angle of inclination during the process.

The underlying mechanism of INIL is discussed both theoretically and experimentally. INIL can not only maintain the low cost and high throughput advantages of NIL and soft lithography, but also remove the need for either nanoscale 3D templates or precise template-to-substrate alignments. Moreover, the feasibility of transferring such 3D nanostructures from the imprinted polymer layer into other materials, such as silicon, silicone rubber (e.g. PDMS) and metals (e.g. gold), is studied for various device fabrication, e.g. angle-resolved photonic crystals. The polymer resist material used in INIL should possess both suitable imprinting properties and amenable properties for the post-INIL processes, such as reactive ion dry etching compatibility for 3D nanopattern transfer into Si substrates.

In this work we utilized a nanolithography polymer resist ZEP [89], poly(methyl-α-chloroacrylate-*co*-α-methylstyrene), to demonstrate INIL. The shear-force-driven 3D nanopatterning mechanism is primarily investigated. Moreover the produced 3D ZEP nanostructures are successfully transferred into silicon substrates, PDMS silicone rubber and gold (Au) film by a proper integration of INIL with reactive ion dry etching (CHF_3/H_2) [130], PDMS molding [41] and a nanotransfer printing process (nTP) [137]. Several applications can be envisaged by the produced 3D nanostructures in the fields of photonics and plasmonics. Details of the fabrication, characterization, and mechanism study of INIL as well as process integration will be given in the following sections of this chapter.

2.2 INIL Process Development

2.2.1 Template Fabrication

Fabrication of a PDMS stamp used for the INIL process consists of (1) fabrication of a topographically-patterned Si master template with the desired structures by conventional photolithography or electron-beam lithography (EBL) and (2) casting and curing PDMS prepolymer (Sylgard 184, Dow Corning) at 45 °C for 24 hours on the

prepared Si master template, resulting in the desired PDMS stamp. In the PDMS molding procedure, the anti-adhesion agent (3,3,3-trifluoropropyl dimethylchlorosilane) is used to treat the Si master surface in advance to eliminate the adhesion between the Si master template and cured PDMS rubber, thereby aiding separation. Various patterns are investigated, such as trenches (1 μm in width, 1 μm in depth and separated by a lateral pitch of 2 μm), cylindrical pillars (1 μm in diameter, 1 μm in depth and a 2 μm lateral pitch) and square columns (1 μm in side width, 1 μm in depth and separated by a lateral pitch of 2 μm).

2.2.2 INIL Process

Figure 2.1 schematically illustrates the INIL fabrication process. The PDMS stamp is pretreated by O_2 plasma (1 min) for surface energy enhancement and then brought into contact with a Si substrate bearing a thin ZEP film (30nm-50nm), and intimate contact is maintained by applying a glass plate to the top (Figure 2.1(a)). The entire assembly is then inclined at a small angle θ, typically $0\,^\circ$ to $5\,^\circ$, followed by annealing for approximately 12 hours in vacuum at a temperature (e.g. T = 170 °C) above the glass transition temperature of the polymer ZEP (T_g = 105 °C). During annealing, the polymer tends to de-wet from the Si substrate, and preferentially wets the PDMS sidewalls. When $\theta = 0\,^\circ$ (Figure 2.1-I), symmetrical polymer flow results in a symmetric polymer profile of the same height in the region between two PDMS sidewalls with nanometer feature size (Figure 2.1-I(b)). This nanopattern is then fixed by cooling the assembly to room temperature and revealed after stamp separation. The resulting uniform nanoline pattern has 1 μm pitch with much smaller features than the original patterns of PDMS stamp (Figure 2.1-I(c)), e.g. for a film of initial thickness of 30 nm the resulting line height is ∼100 nm and the full width half-maximum (FWHM) is ∼300 nm as shown in Figure 2.2(a). As θ is changed from $0\,^\circ$, the polymer flows anisotropically (Figure 2.1-II(b)). As a result, 3D nanoline

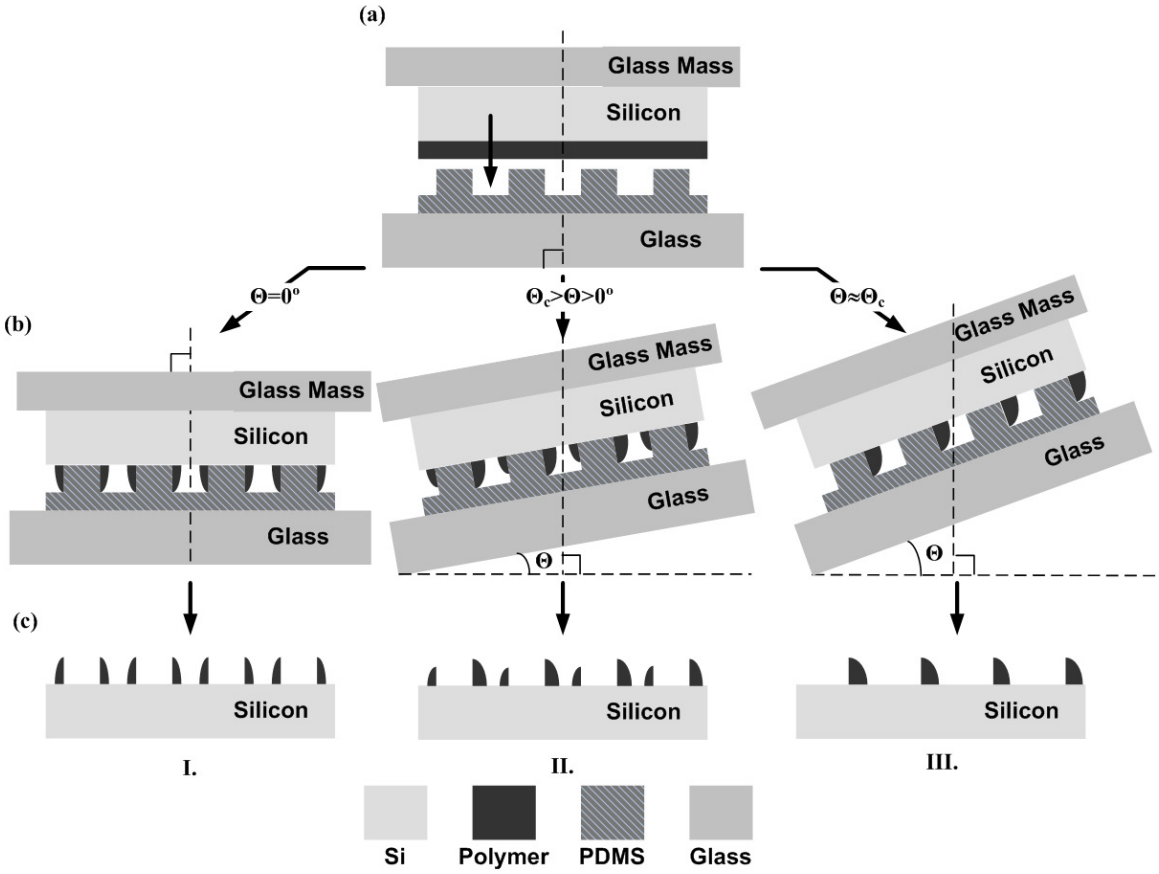

Figure 2.1: Schematic illustration of INIL fabrication process. (I) $\theta = 0\,^{\circ}$, (II) $0\,^{\circ} < \theta < \theta_c$, (III) $\theta \approx \theta_c$ ($\approx 5\,^{\circ}$). (a) An intimate contact between the polymer thin film and the PDMS stamp. (b) Inclining the assembly by θ degree and annealing it at a temperature higher than polymer glass transition temperature for a few hours. (c) cooling down the assembly and separating the substrate from the PDMS stamp.

patterns with different heights and widths are obtained (Figure 2.1-II(c)). When θ is increased to a threshold inclination angle θ_c, the profile evolves to be extrememly asymmetric (Figure 2.1-III(b)). Only one nanoline can be obtained per 2 μm pitch spacing (Figure 2.1-III(c)).

2.2.3 Experimental Results and Discussion

Figure 2.2 shows the AFM images of resulting 3D nanolines produced by INIL at different θ in a 30 nm thick ZEP polymer layer. As observed, different heights are obtained when the inclined angle is varied from $0\,^{\circ}$ to $5\,^{\circ}$. The height of the symmetric

line (Figure 2.2(a)) is ∼100 nm, and the full width half maximum (FWHM) of the lines is ∼300 nm. It is instructive to calculate the volumes of the film patterns before and after INIL. Since the lines are extruded in one dimension, e.g. the y-axis, an area calculation (in the x-z plane) can be performed instead of volume. Based on the symmetric profile, the cross-sectional area occupied by polymer nanolines over 2 μm pitch of the original mold is calculated as 100 nm × 300 nm × 2 (line width × line height × line number per 2 μm). This is consistent with the cross-sectional area of non-patterned polymer thin film per 2 μm distance, 30 nm × 2000 nm (film thickness × 2 μm pitch). For asymmetric lines the height and width are changed due to the geometry, but the volume of polymer is conserved.

In order to understand the effect of the inclined angle θ a series of polymer films with similar thickness, equal to ∼30 nm, are studied using the same trench mold. The experimental conditions are the same in all cases except for the inclined angle θ. The line height difference $\triangle$h as a function of the inclined angle θ is plotted in Figure 2.3. These data show that under same conditions the height difference of the nanolines is primarily dependent on the magnitude of the inclined angle θ. When θ is above 4 °, the height difference $\triangle$h saturates at the point and the extreme asymmetric structure appears as seen previously in Figure 2.2(e).

Moreover, the effect of the initial thin film thickness on the resulting nanoline height difference is also studied. Two series of polymer films are examined with thicknesses equal to ∼30 nm and ∼50 nm respectively. The line height difference obtained from these two series, $\triangle h_{30}$ and $\triangle h_{50}$, are plotted as a function of the inclined angle ((-■-) and (-▲-) plots in Figure 2.4). It is clearly revealed that the 50 nm film leads to a larger nanoline height difference than the 30 nm film at the same inclined angle, $\triangle h_{50} > \triangle h_{30}$. In other words, the 50 nm film requires a smaller magnitude of the inclined angle than 30 nm film does to obtain the same $\triangle$h. Moreover, the resulting height difference of $\triangle h_{50}$-$\triangle h_{30}$ is increased by increasing the inclined angle

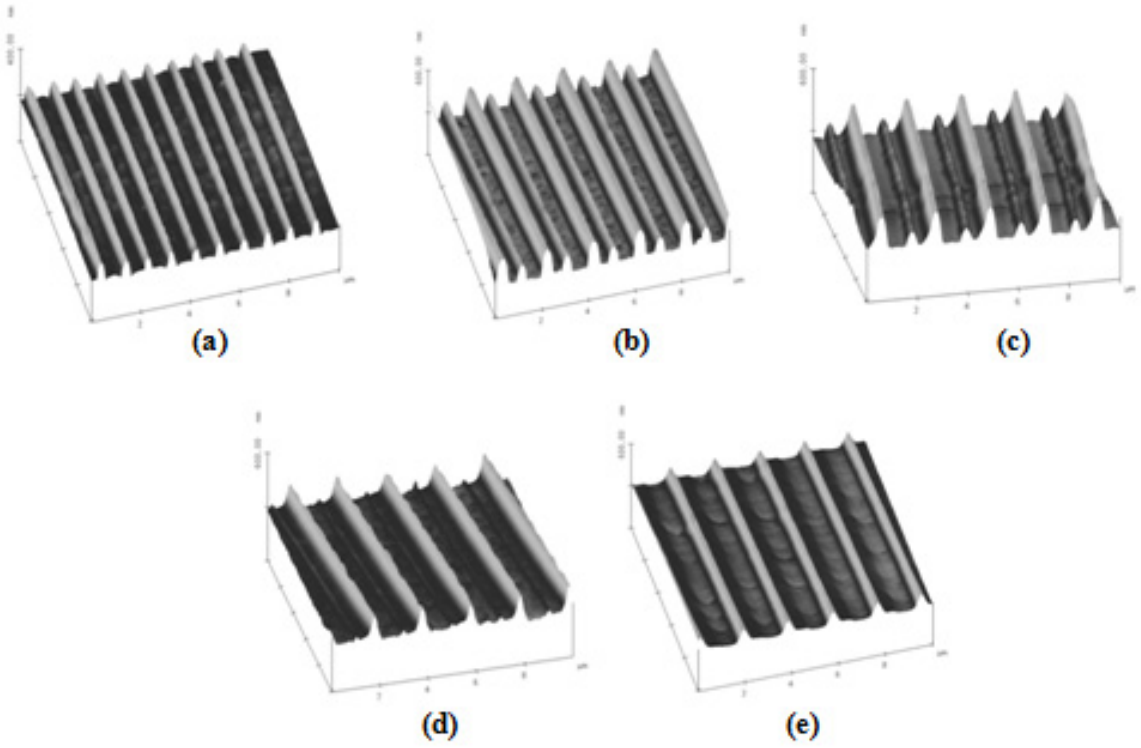

Figure 2.2: AFM images of the resulting 3D nanolines with multiple heights in various θ (polymer film thickness is 30 nm) (a) $\theta = 0^\circ$ (z scale bar = 400 nm), (b) $\theta = 1.4^\circ$ (z scale bar = 600 nm), (c) $\theta = 2.8^\circ$ (z scale bar = 600 nm), (c) $\theta = 4.3^\circ$ (z scale bar = 600 nm), (e) $\theta = 5.7^\circ$ (z scale bar = 600 nm). The x-y area in all AFM images is 10 μm $\times$ 10 μm.

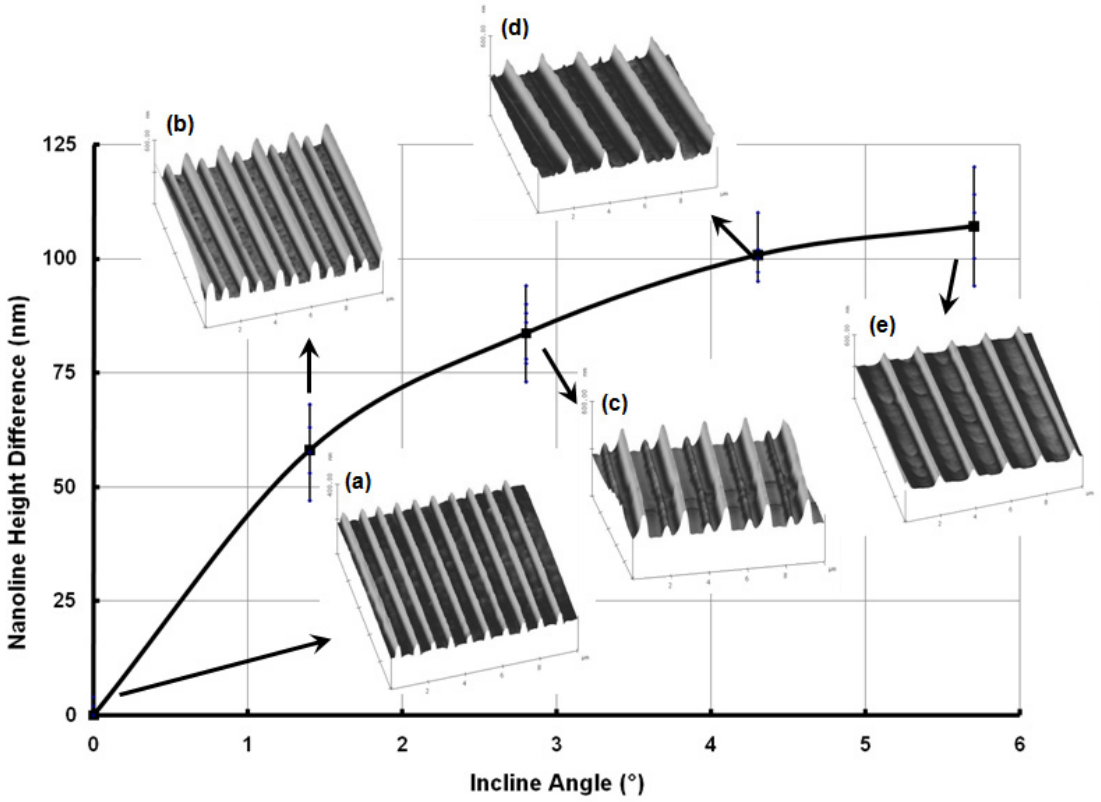

Figure 2.3: Plot of nanoline height difference as a function of the inclined angle θ. Inserted images are representative AFM section analyses corresponding to each testing θ respectively.

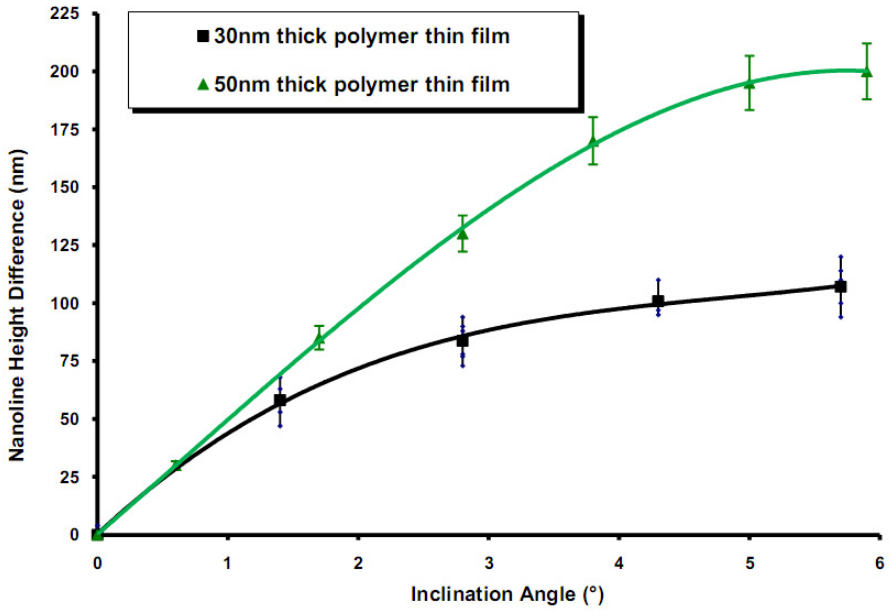

Figure 2.4: Plot of nanoline height difference as a function of the inclined angle θ produced in (-▲-) 50 nm and (-■-) 30 nm ZEP thin film by INIL.

θ . When $\theta \approx 5\,^{\circ}$, the height differences of both series of films reach the maximal values, $\triangle h_{50max}$ and $\triangle h_{30max}$, and the extreme asymmetric structures appear respectively. $\triangle h_{50max}$ is approximately two times larger than $\triangle h_{30max}$ due to the initial film thickness difference. These observations indicate that the resulting nanostructure is also influenced by the film thickness. More discussion with respect to the INIL mechanism will be given in section 3.3.

Other shapes have also been successfully demonstrated by INIL, such as the symmetric and asymmetric nanocircles by using the cylindrical pillar PDMS stamp as well as the symmetric and asymmetric nanosquare-loops (Figure 2.5).

2.3 INIL Mechanism Study

In general, the de-wetting phenomenon of polymer thin films can be explained by analyzing the free energy of the system [77, 102]. The simplest systems are uniform thin films on horizontally flat surfaces. De-wetting leads to a film morphology change, e.g. into droplets or other patterns. When a PDMS mold with topographic features

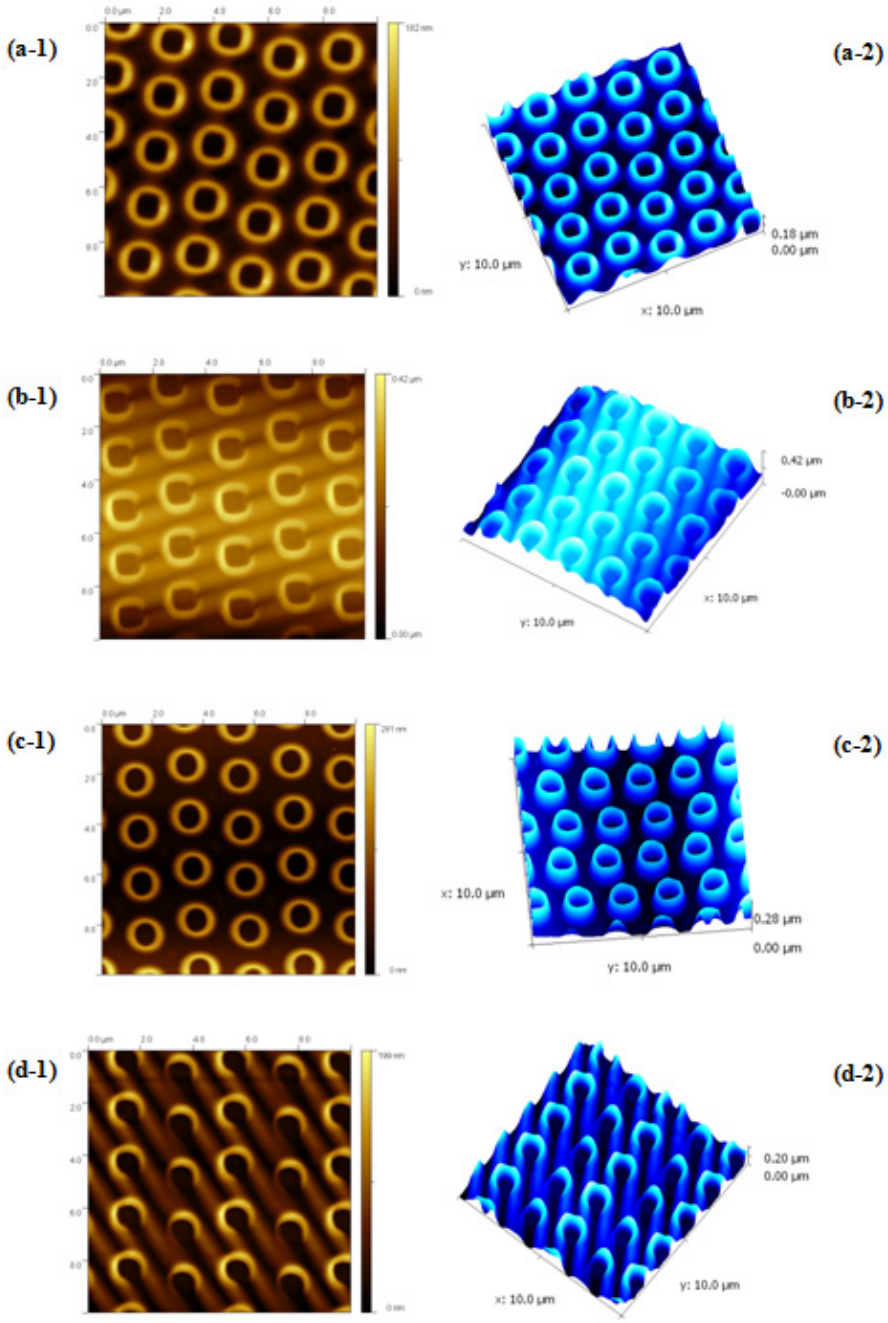

Figure 2.5: AFM images of nanosquare loops and nanocircles produced by INIL in 2D (left) and 3D (right) views. (a-1) and (a-2) symmetric nanosquare-loops ($\theta = 0\,^{\circ}$), (b-1) and (b-2) asymmetric nanosquare-loops ($\theta = 5.7\,^{\circ}$), (c-1) and (c-2) symmetric nanocircles ($\theta = 0\,^{\circ}$), (d-1) and (d-2) asymmetric nanocircles ($\theta = 5.7\,^{\circ}$).

is introduced to the system, the film is consequently in contact with two different surfaces, the mold and the substrate, and tends to reach the system equilibrium, minimum free energy, deforming in a three-dimensional frame. An example is the uniform 3D nanopatterns of the same height as shown in Figure 1.5 in Chapter 1.

It is clear that the formed 3D nanopatterns result from a balance of the different forces and energies experienced by the polymer as it interacts with two different surfaces: the Si substrate and the PDMS side wall. Although energy arguments are important in determining the ultimate dewetting state of the polymer, the kinetics associated with the transition to this ultimate state must also be considered, especially for these viscous polymers. Therefore we primarily investigated the process mechanism by analyzing the forces from the kinetics point of view. The forces of interest consist of the wetting and dewetting forces associated with the PDMS mold and silicon substrate surface respectively, as well as the force $F_{mass} = mg$, exerted by the INIL apparatus on the polymer film due to the total mass of glass and silicon acting on the polymer (m). The gravitational body force of the polymer itself is several orders of magnitude smaller than F_{mass} as well as surface wetting/dewetting forces ($F_{surface\ tension} = \gamma\ L$, where γ is polymer surface tension coefficient and L is the contact length) and is therefore negligible.

When $\theta = 0\,^{\circ}$, the symmetric wetting and dewetting forces result in 3D nanopatterns with the same height, as demonstrated in our work as well as [139]. In [139] (see Figure 1.5), the PDMS mold is placed onto the polymer thin film spin-coated on a substrate. This can be likened to an "inverted" INIL process ($\theta = 0\,^{\circ}$). [139] demonstrates that wetting and dewetting forces lead polymer to flow in the opposite direction relative to gravity. This observation confirms that the gravitational force of the polymer thin film itself is negligible compared to the wetting force. We also studied and compared this "inverted" INIL process ($\theta = 0\,^{\circ}$) to the standard INIL process. The annealing time and temperature are identical to those for the INIL

structure shown in Figure 2.1-I. We observed that the INIL structure (Figure 2.3(a)) shows clear separation between the dewetting lines, which does not occur in the "inverted" INIL case (Figure 2.6). However, if the "inverted" INIL example is annealed for a longer time at a higher temperature, a structure that closely resembles Figure 2.3(a) can be observed. Clearly, inverting the system does not affect the ultimate structural form, but does affect the kinetic behavior of the polymer. The difference is attributed to the larger normal force (F_{mass}) in INIL induced by the top glass and silicon acting on the polymer (Figure 2.7(a)). This force is greatly reduced in "inverted" INIL case, therefore a longer time scale at a higher temperature and lower polymer viscosity is required to reach a given state.

When $\theta > 0^\circ$ (Figure 2.7(b)) F_{mass} generates (1) a lateral shear on the polymer, equal to $F_{mass}sin\theta$, and (2) a normal force pressing on the polymer thin film, equal to $F_{mass}cos\theta$. The magnitudes of these two forces are dependent on the inclination angle. However, the wetting or dewetting force is not affected by the inclination angle [24]. When θ is very small or close to 0°, $F_{mass}sin\theta$ is negligible, and the wetting/dewetting and $F_{mass}cos\theta$ are the primary forces influencing the movement of the polymer; as θ increases from zero, the shear force $F_{mass}sin\theta$ becomes significant, leading to asymmetric dewetting of the polymer. The wetting and $F_{mass}cos\theta$ are in the same direction driving the polymer flow to move downward along the PDMS sidewall. Consequently, more polymer material builds up on one of the PDMS mold walls compared to the other.

When imposing this angle-dependent shear force onto the polymer in this INIL configuration, it is possible to derive the time (t) taken for the polymer with a viscosity of $\eta(T)$ to move a distance (d) at an average velocity ($\bar{v} = d/t$). For a Newtonian polymer fluid as we assumed for the polymer material used in INIL, the average shear stress τ is proportional to strain rate ($\dot{\gamma}$) where the polymer viscosity ($\eta(T)$) is the constant factor of proportionality as shown in equation 2.1. The average shear stress

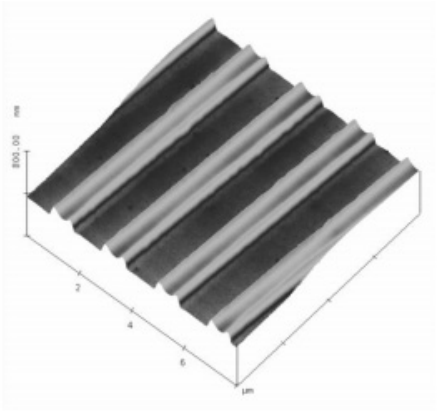

(a)

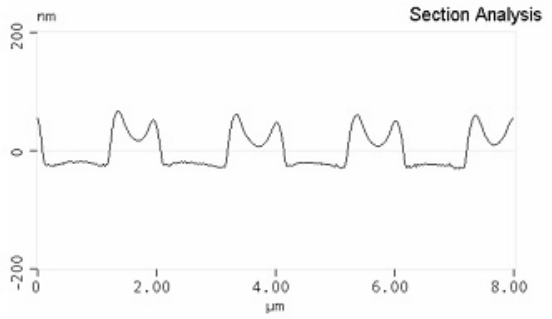

(b)

Figure 2.6: AFM image of nano-line without a complete development from the "inverted" INIL process (8 μm x 8 μm). (a) AFM 3-D image; (b) section analysis result of (a).

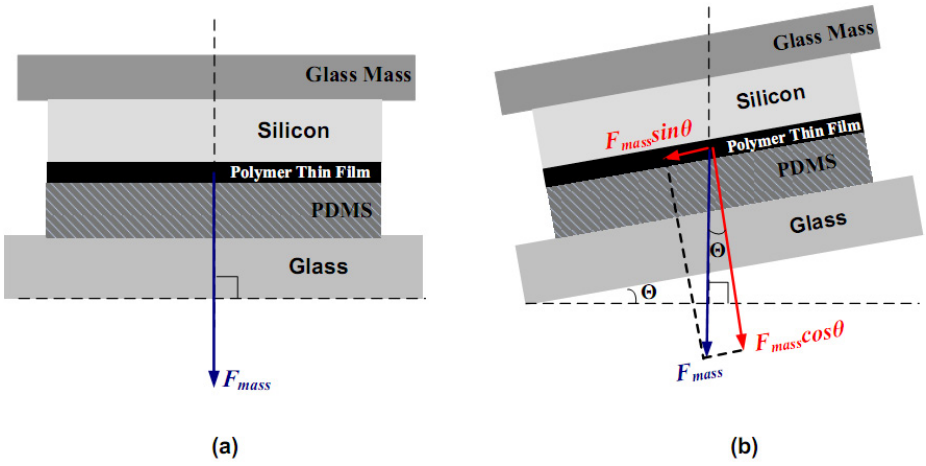

Figure 2.7: Schematic illustration of the inclined assembly in INIL process (a) $\theta = 0\,^{\circ}$, and (b) $\theta > 0\,^{\circ}$.

(τ) applied to the fluidic polymer thin film can be equated to the force load ($mgsin\theta$) per cross-section area (A) as shown in equation 2.2.

$$\tau = \eta(T)\dot{\gamma} \doteq \eta(T)\frac{\bar{v}}{y} = \eta(T)\frac{d}{yt} \tag{2.1}$$

where y is the polymer film thickness, $\eta(T)$ is the polymer viscosity and can be obtained from the empirical Williams-Landel-Ferry (WLF) model as shown in equation 2.3.

$$\tau = \frac{mgsin\theta}{A} \tag{2.2}$$

where g is the gravitational constant equal to 9.8 m·s^{-2}.

$$\eta = \eta_0\ exp[\frac{-C_1(T - T_1)}{C_2 + T - T_r}] \tag{2.3}$$

where T is the experimental temperature, T_r is the reference temperature chosen as 148 °C, η_0 is the zero-shear viscosity, $C_1 = 8.86$ and $C_2 = 101.6$ K [7]. The value η_0 of ZEP polymer at T$_r$ (= 148 °C) was obtained using a rotational rheometer with parallel-plate geometry [133] and is equal to 3.2×10^5 Pa·s, as shown in Figure 2.8.

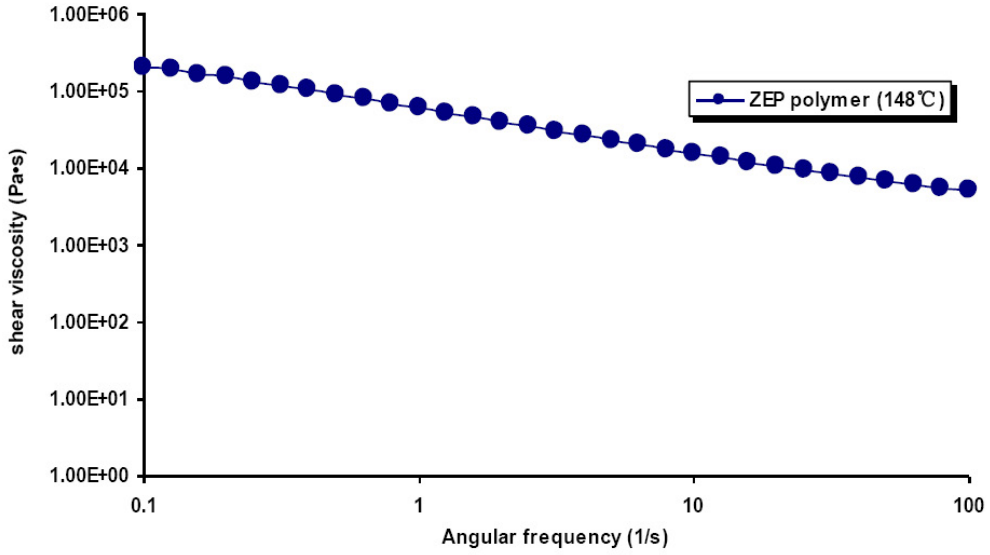

Figure 2.8: Shear viscosity of ZEP polymer versus angular frequency at 148 °C.

$$t \doteq \frac{dA}{ymgsin\theta}\ \eta(T) = \lambda \cdot \eta(T) \tag{2.4}$$

where the coefficient $\lambda = \frac{dA}{ymgsin\theta}$.

Equation 2.4 can be derived from equations 2.1∼2.3. It indicates the time (t) taken for the polymer fluid to move through a certain distance (d) at an average velocity ($\bar{v}$). When d is equal to the distance between two nearest sidewalls of PDMS, e.g. 1μm of the trench stamp, t can be calculated as a function of process temperature with the given information of A, y, m and θ. t then represents the INIL process time. In particular, the factor of λ is calculated to be equal to 0.56 Pa^{-1} when $d = 1 \times 10^{-6}$ m, $A = 1 \times 10^{-4}$ m^2, $y = 5 \times 10^{-8}$ m, $m = 7$ g and $\theta = 3\,°$.

Figure 2.9 shows the value of $t(T)$ (•) determined experimentally (T = 150 °C, 170 °C, 210 °C, 230 °C) by examining a series of similar samples processed by using a PDMS trench stamp with a feature size $d = 1 \times 10^{-6}$ m where λ is equal to 0.56 Pa^{-1}. The actual INIL process time at each temperature of interest is obtained by characterizing the nanoline pattern at different time intervals of INIL, e.g. 0.5 hours,

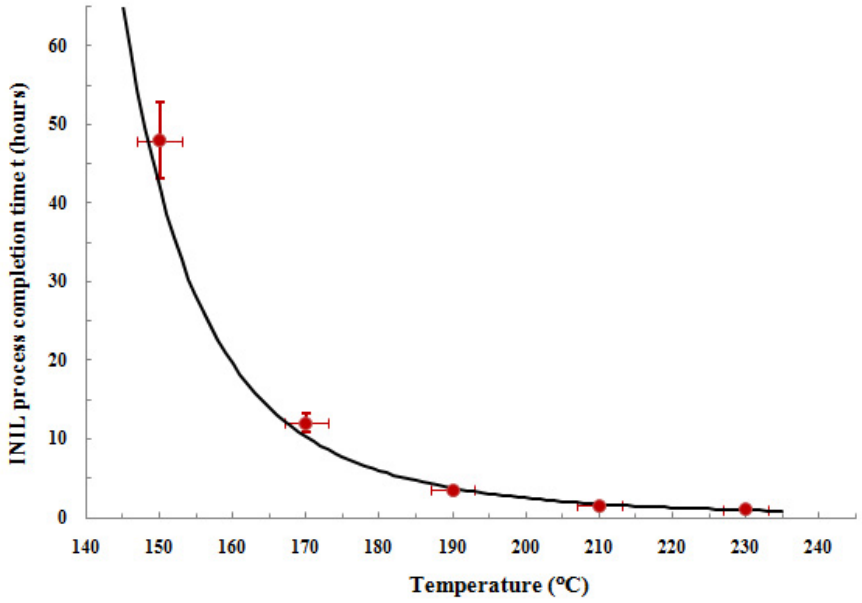

Figure 2.9: Plot of INIL process time as a function of process temperature $t(T)$. (•) experimental and (-) theoretical data. Vertical error bars represent the maximum and minimum measurement values of 5 samples at each temperature point.

2 hours, 8 hours, 12 hours, until the time when completely developed nanoline pattern is observed, as illustrated in Figure 2.10. Each data point obtained in Figure 2.9 is averaged from five samples examined. Vertical error bars represent the maximum and minimum time values achieved. The predicted behavior of $t(T)$ according to equation 2.4 in the same temperature range as the experimental measurements and setting (λ = 0.56 Pa^{-1}) is also plotted in Figure 2.9 (-). It is clear that the experimental data fit the theoretical $t(T)$ model well, especially when the temperature is above 170 °C. The difference observed in the low temperature region ($T < 170$ °C) is most probably associated with the relatively high viscosity where non-Newtonian polymer fluid properties may be observed, leading to discrepancies between the experimental and estimated data.

In summary, the underlying INIL mechanism has been primarily investigated from

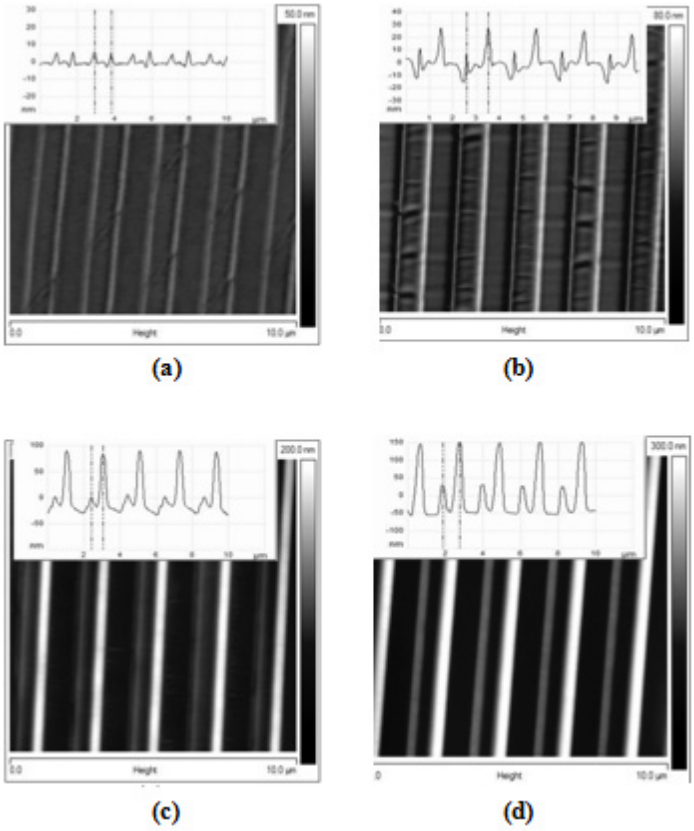

Figure 2.10: AFM images of the nanolines obtained at different time intervals ($A = 1 \times 10^{-4}$ m^2, $y = 5 \times 10^{-8}$ m, $m = 7$ g, $\theta = 3\,^{\circ}$, $T = 170\,^{\circ}$C). The inserted images are representative AFM section analyses respectively. (a) 0.5 hour, the obtained nanoline height difference $\triangle h = 0$ nm, (b) 2 hours, the obtained nanoline height difference $\triangle h = 30 \pm 5$ nm, (c) 8 hours, the obtained nanoline height difference $\triangle h = 85 \pm 5$ nm, (d) 12 hours, the obtained nanoline height difference $\triangle h = 120 \pm 10$ nm. The x-y area in all AFM images is 10 μm$\times$10 μm.

the kinetics point of view. Study indicates that the angle-dependent 3D nanostructures produced in INIL are due to the mass-generated force incident on the polymer film when the inclined angle is greater than zero. Numerical simulation study and thermal dynamics analysis will be conducted in future to comprehensively study the process theory. The following section 2.4 will be focusing on the process integration of INIL with other techniques to transfer such 3D nanostructures from polymer ink layer into Si, PDMS and metal gold (Au) thin film materials for the potential applications in angle resolved nanophotonic crystals and plasmonic crystals.

2.4 INIL-based 3D Nanofabrication

2.4.1 Background and Motivation

Photonic crystals (PhCs) and nanophotonic crystals have been a fascinating research field in the past decade owing to their ability to influence light through their periodic dielectric structure. Compared to 1D/2D PhC-based devices [14, 17, 32], it has been a considerable challenge to cost-effectively fabricate high quality 3D PhCs and integrate them for various optical devices in a convenient manner. Nanolithography has been a promising approach to produce high quality 3D PhCs in silicon with appropriate device integration capability by means of mature microelectronics manufacturing equipment including EBL, FIB and deep-UV lithography. However, issues associated with this strategy are the high equipment cost and process complexities.

Plasmonics is a recently emerging field. It attracts much research interest in various metallic nanostructures, where confined electrons are forced to oscillate by an incident light or electromagnetic wave. Such electron oscillation can exhibit strong local-field enhancement at a particular wavelength known as localized surface plasmon resonances (LSPRs). This electron-photon coupled resonance is essential to increase nearly all light-matter interactions including surface-enhanced Raman scattering (SERS) [10, 14, 47, 112, 116] and surface-enhanced fluorescence [34, 71]. Many

applications are envisaged by plasmonic crystals including bio-diagnostics [112], imaging [34, 71], sensing [10, 47, 71, 116] and metamaterials [100]. The plasmon resonance frequency is largely determined by the metal nanostructure itself [100]. Therefore there has been a surge of interest in exploring proper nanofabrication approaches that can control the shape, size and/or spacing of metal structures at the nano/micro scale.

In this section 3D silicon, PDMS silicone rubber and Au nanostructures are demonstrated by integrating INIL with reactive ion etching (RIE), PDMS molding and metal nanotransfer molding (nTP) respectively. Details of the process integration and characterization will be presented in the following parts of this section.

2.4.2 INIL-based Nanofabrication Process

Figure 2.11 schematically illustrates the fabrication process for 3D nanostructures with symmetric (Figure 2.11(I)) and asymmetric (Figure 2.11(II)) geometries. It starts with 3D polymer nanostructures produced by INIL (Figure 2.11(a)). Plasma dry etching (CHF_3/H_2) (Figure 2.11(b)) is applied to transfer the polymer nanopattern to the underlying Si substrate followed by removal of ZEP polymer residue either using dry etching (CHF_3/O_2 plasma) or wet etching (piranha solution at 120 °C for 10 min). The resulting Si nanostructure is used as a mold master for subsequent PDMS molding to transfer the opposite Si nanostructure to a PDMS stamp (Figure 2.11 (c)-(d)). The produced nanopatterned PDMS stamp is then mounted on a glass backing and surface uniformly coated with a continuous thin metal film by sputtering (typically 40nm Au/5nm Ti, where Ti is an adhesion layer in the subsequent nanotransfer printing (nTP) process) (Figure 2.10 (e)). In the nTP process the 3D thin film, which can be thought of as a nanostructured Au sheet, is transferred to the adhesive polymer substrate due to its high surface energy (e.g. Kapton tape backed by a glass substrate or photocurable polyurethane (PU) spin coated on a glass substrate).

In this process the freshly metal-coated PDMS stamp mold is immediately brought into contact with the flat polymer substrate, and a gentle pressure applied (Figure 2.11 (f)). After this contact is established, the metal layer on the stamp is thoroughly adhered and transferred to the high surface energy polymer substrate. After mold separation, freestanding nanostructures that replicate the silicon mold master 3D nanostructures are obtained (Figure 2.11(g)). The resulting 3D Si nanostructures can be potentially used as 3D PhCs, while the resulting 3D Au nanostructures can be used as angle-resolved plasmonic crystals for surface enhanced resonance sensing (SERS).

2.4.3 Experimental Results and Discussion

2.4.3.1 3D Si Nanostructures

Figures 2.12 and 2.13 display a set of SEM and AFM images of resulting 3D Si nanostructures as a result of plasma dry etching illustrated in Figure 2.11(b). Figure 2.12(a) shows the resulting symmetric nanolines, approximately 250nm wide and 200 nm in height. Figures 2.12(b) and 2.13 (a-1, a-2) are the resulting asymmetric nanolines. Figures 2.12(c) and 2.13 (b-1, b-2) present the resulting symmetric nanocircles. The symmetric nanocircle inner diameter is 1 μm, the circle width is approximate 250 nm by a lateral pitch of 2 μm. Figures 2.12(d) and 2.13 (c-1, c-2) present the resulting asymmetric nanocircles. Figures 2.12(e) and 2.13(d-1, d-2) are the resulting symmetric nanosquare loops. The symmetric nanosquare loop inner square width is 1 μm, and the loop width is approximately 250 nm with a lateral pitch of 2 μm. It is observed that the corners of the resulting symmetric nanosquare loops are apparently rounded, not an ideal 90°. This effect is attributed to the deformation of PDMS stamp. Figures 2.12(f) and 2.13(e-1, e-2) are the resulting asymmetric nanosquare loops. For the asymmetric nanostructures obtained (Figures 2.12(b,d,f) and 2.13(a-1,a-2, c-1, c-2, e-1, e-2)), the resulting width and height are varied according to the

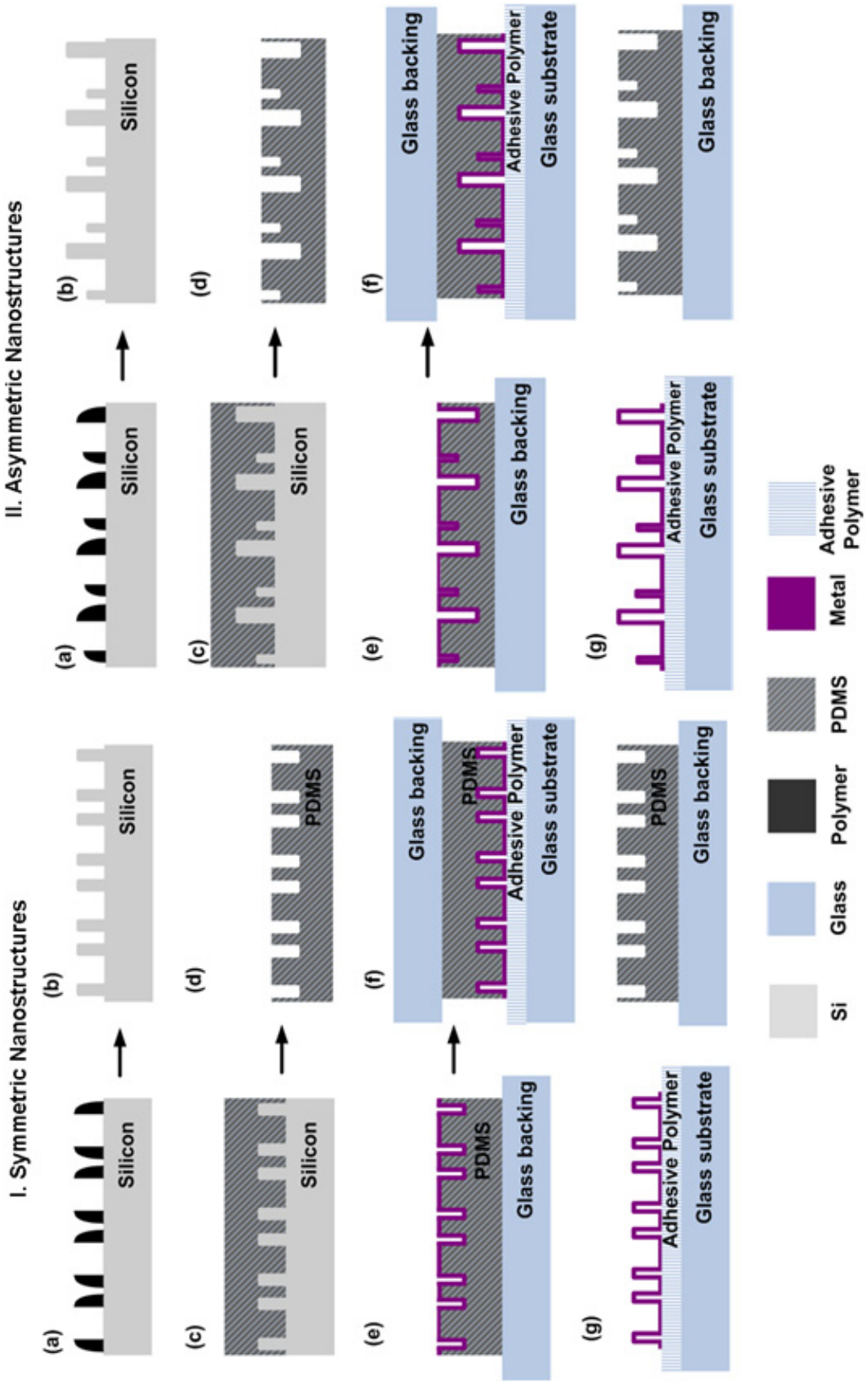

Figure 2.11: Schematic illustration of the fabrication process of 3D Si and metal nanostructures.

INIL fabrication process. Moreover, a careful comparison of the resulting Si nanostructures (Figures 2.12 and 2.13) with the polymer nanopatterns produced by INIL (Figures 2.2 and 2.4) indicates the success of pattern transfer from the ZEP polymer ink layer to the Si substrate. These resulting 3D periodic silicon nanostructures with multiple heights can be applied as angle-resolved photonic crystals for exploiting and tuning their optical properties owning to their structural characteristics.

2.4.3.2 3D Silicone Rubber Nanostructures

The prepared Si nanostructures are further used as molding masters for PDMS molding to transfer the nanopatterns into PDMS silicone rubber (Figure 2.11(d)). Figure 2.14 shows a series of AFM images of the resultant PDMS stamps. As can be observed, the 3D nanostructures of Si mold masters are successfully transferred into PDMS.

In this PDMS molding step, it is found critical to pre-treat Si mold master surface by an anti-adhesion agent (3,3,3-trifluoropropyl dimethylchlorosilane). This thin layer can greatly reduce the adhesion between the nanostructured Si master and cured PDMS, leading to a successful separation (Figure 2.11(d)) without damaging the Si master or leaving any PDMS residue on the Si master surface. In comparison, a sample without applying the anti-adhesive agent is examined. As a result, a large amount of PDMS rubber is strongly adhered and left on Si master surface. It is hard to properly separate the cured PDMS from the Si master by a gentle force. However, applying a harsh de-molding force can easily damage the Si mold nanostructures. Moreover, some of the broken Si nanostructures are glued and embedded into the PDMS rubber as shown in Figure 2.15. A similar observation was lately reported by Fujita *et al*. [55]. Instead, they extensively studied such phenomena and applied it for fabricating PDMS/SiO_2 nanocomposites with embedded uniform and regular SiO_2 nanostructures.

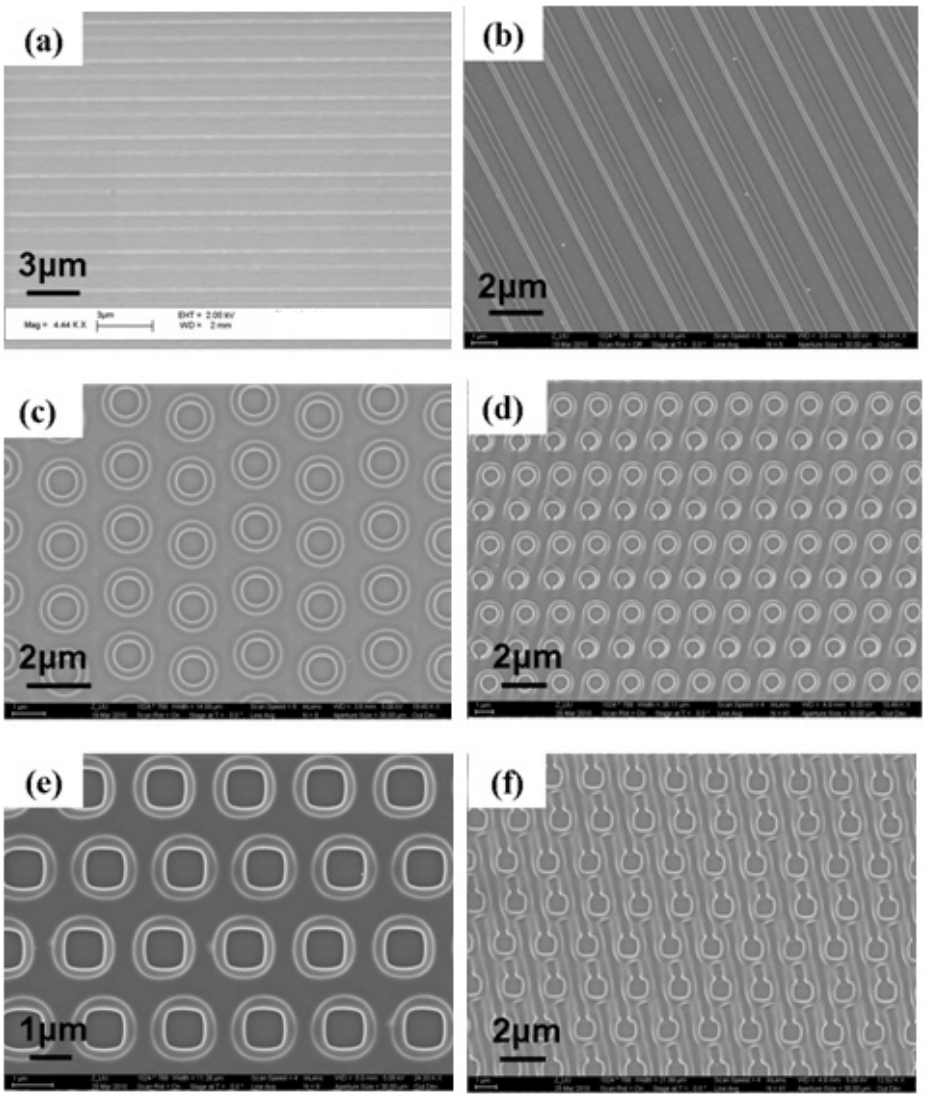

Figure 2.12: SEM images of 3D Si nanostructures. (a) symmetric nanolines, (b) asymmetric nanolines, (c) symmetric nanocircles, (d) asymmetric nanocircles, (e) symmetric nanosquare loops, (f) asymmetric nanosquare loops.

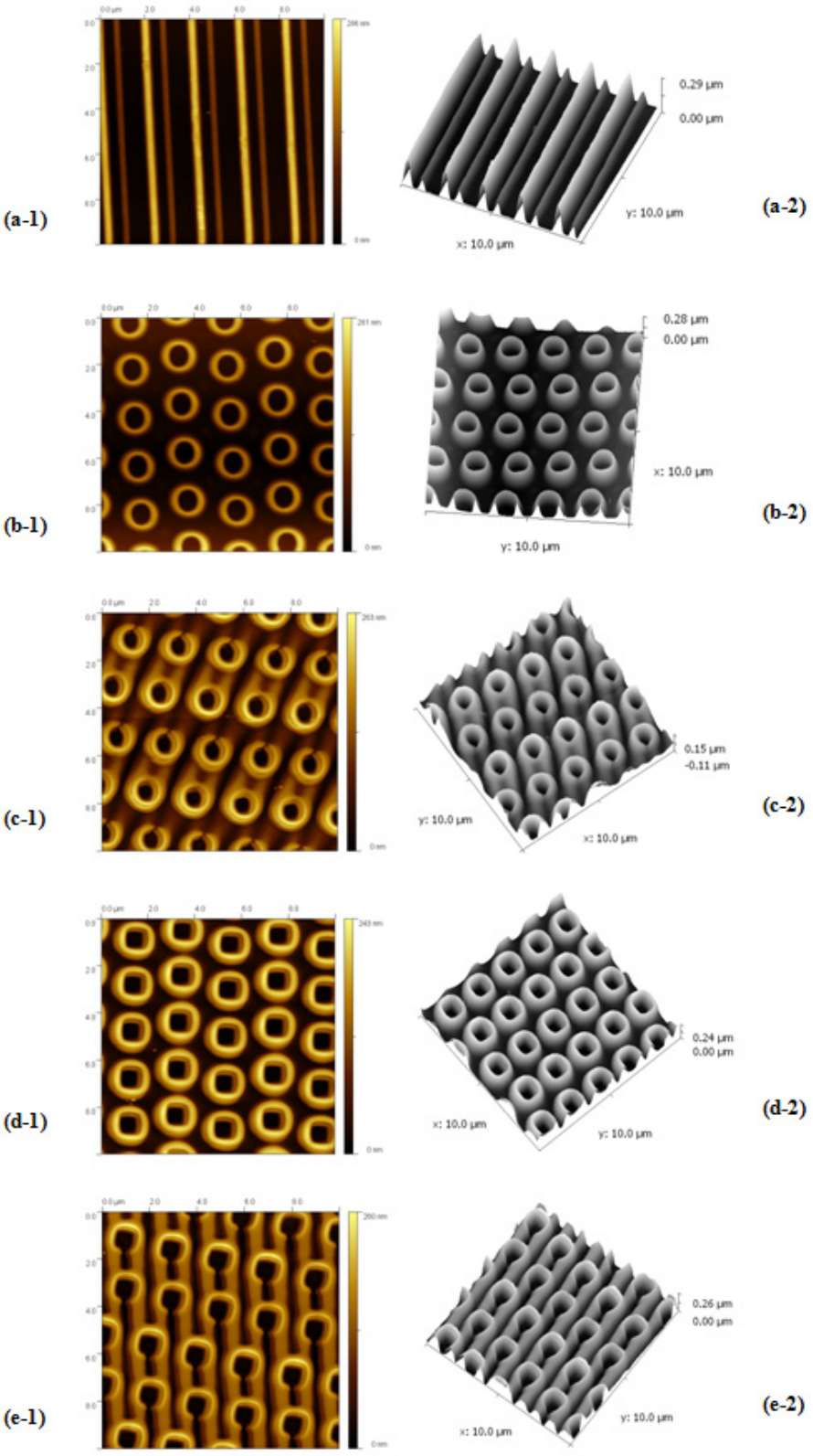

Figure 2.13: AFM images of 3D Si nanostructures in 2D (left) and 3D (right) views. (a-1)-(a-2) asymmetric nanolines, (b-1)-(b-2) symmetric nanocircles, (c-1)-(c-2) symmetric nanosquare loops, (d-1)-(d-2) asymmetric nanocircles, (e-1)-(e-2) asymmetric nanosquare loops.

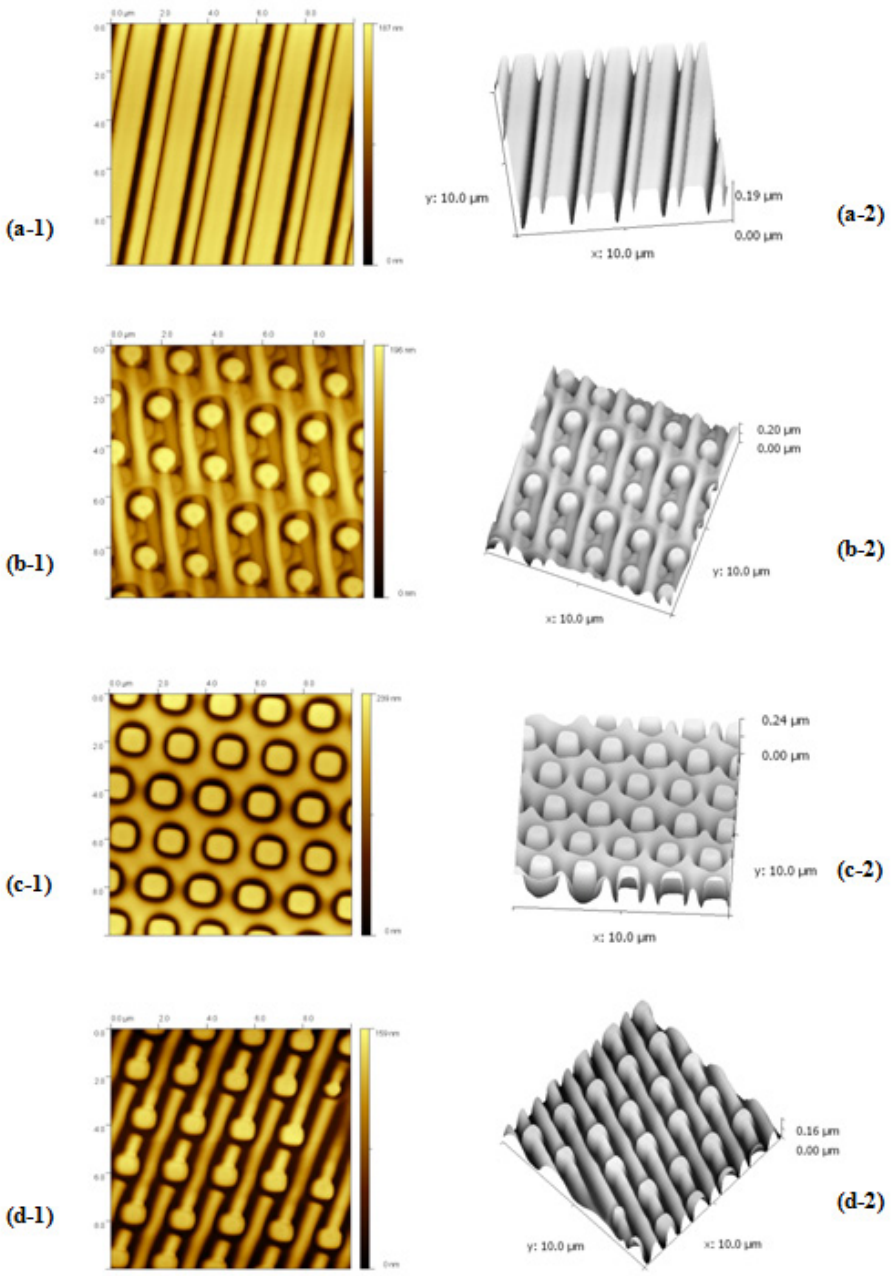

Figure 2.14: AFM images of 3D PDMS nanostructures in 2D (left) and 3D (right) views. (a-1)-(a-2) asymmetric nanolines, (b-1)-(b-2) asymmetric nanocircles, (c-1)-(c-2) symmetric nanosquare loops, (d-1)-(d-2) asymmetric nanosquare loops.

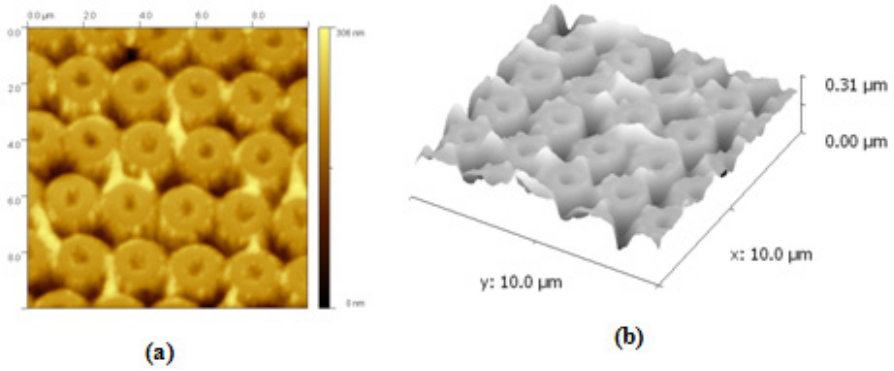

Figure 2.15: AFM images of the PDMS rubber embedded with silicon nanostructures in (a) top and (b) 3D views.

2.4.3.3 3D Gold Nanostructures

Figure 2.16 shows a set of SEM images of resulting 3D Au nanostructures on the adhesive polymer substrates at low and high magnifications. Figure 2.17 shows a series of AFM images of the resulting 3D Au nanostructures in 2D and 3D views. First of all, it can be clearly seen from the SEM images that the Au thin film is completely and successfully transferred from the PDMS mold to the adhesive polymer substrate surface with freestanding nanostructures. The transferred Au layer thickness is approximately 40 nm as determined by the metallization step in fabrication. The stronger cohesion of Au [137] leads those non-contact Au parts to be effectively transferred to the adhesive substrate as illustrated in Figure 2.11(g). Furthermore, a careful comparison of the resulting Au nanostructures with those in the Si mold masters indicates that the nanostructures of varying heights are properly preserved in the freestanding Au thin film. Typically, the resulting symmetric Au nanosquare loop pattern is approximate 250 nm in width, 150 nm in height. Its inner square width is 1 μm, and the lateral pitch between two nearest two loops is 2 μm (Figures 2.16(e, f) and Figures 2.17 (c-1, c-2)). For asymmetric nanostructures of varying heights, the width, height and periodicity of resulting Au nanostructures are varied according to the 3D PDMS stamps. Some random nanocracks can be observed on

the Au nanostructures. These cracks are believed to be due to the cracks formed on PDMS silicone rubber surface as well as stamp deformation during transfer printing. It is challenging to completely eliminate them. In our work, crack elimination can be achieved by a combination of using glass backing to support the PDMS stamp, using a thin PDMS stamp (∼0.5 mm thick), as well as applying a gentle printing force. The demonstrated 3D Au nanostructures with multiple heights can be potentially applied as plasmonic crystals with incident angle-dependent optical properties due to their asymmetric nanostructures for sensing and imaging applications.

2.5 Chapter Summary

In summary of this chapter, inclined nanoimprinting lithography (INIL) is successfully demonstrated. The capability of fabricating 3D nanostructures of varying heights over large surface areas on the planar substrate in a single step is enabled. The underlying INIL mechanism is investigated, and a theoretical $t(T)$ model is studied both theoretically and experimentally. The investigation indicates that the shear force generated at non-zero inclination angle leads to the asymmetry of polymer flow ultimately resulting in 3D nanopatterns with multiple heights. INIL removes the need for conventional 3D nanolithography of either 3D templates or multiple repeating steps. In addition, the process integration of INIL with plasma dry etching, PDMS molding and nanotransfer printing (nTP) is demonstrated to transfer various INIL produced 3D structures into other materials including silicon, PDMS and metal gold. The developed INIL combined with proper pattern design shows great promise to fabricate various nano-scale devices including angle-resolved photonic and plasmonic crystals, solar cells and biomimic anisotropic self-cleaning surfaces.

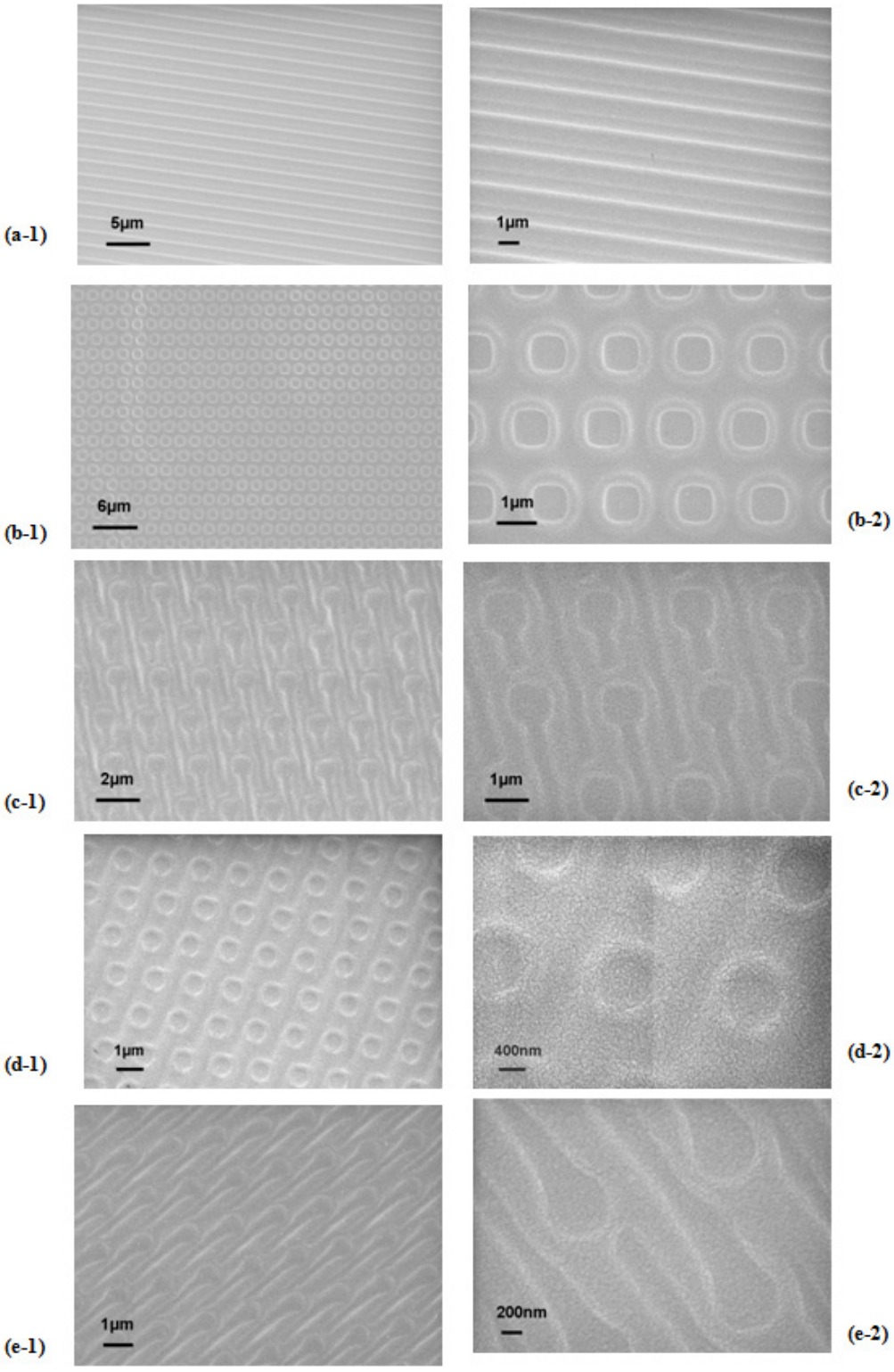

Figure 2.16: SEM images of 3D gold nanostructures on adhesive glass substrate. (a-1)-(a-2) asymmetric nanolines, (b-1)-(b-2) symmetric nanosquare-loops, (c-1)-(c-2) asymmetric nanosquare-loops, (d-1)-(d-2) asymmetric nanocircles with a small degree of asymmetry, (e-1)-(e-2) asymmetric nanocircles with a large degree of asymmetry.

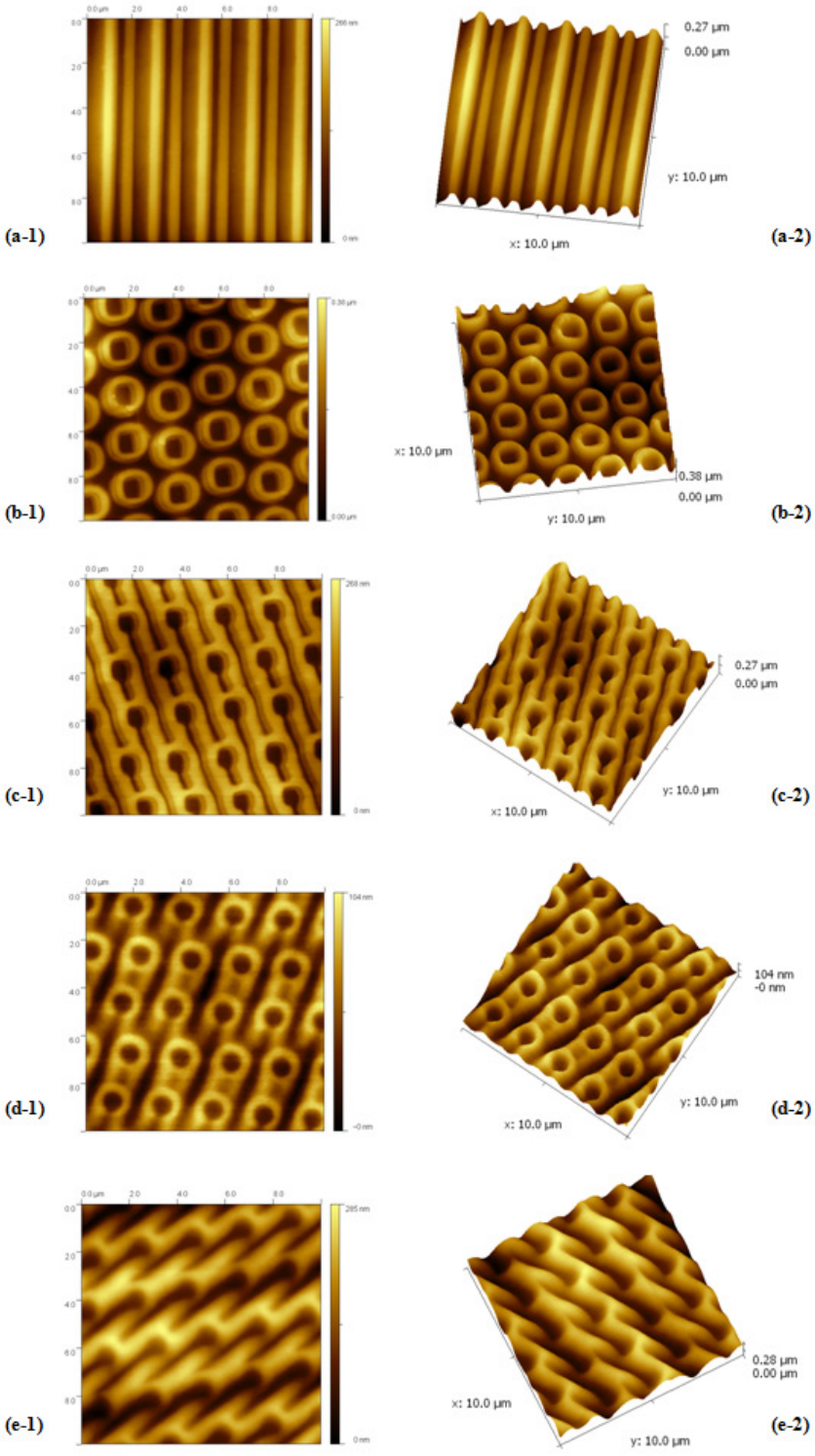

Figure 2.17: AFM images of 3D Au nanopatterns on adhesive glass substrate in top (left) and 3D views (right). (a-1)-(a-2) asymmetric nanolines, (b-1)-(b-2) symmetric nanosquare loops, (c-1)-(c-2) asymmetric nanosquare loops, (d-1)-(d-2) asymmetric nanocircles with a small degree of asymmetry, (e-1)-(e-2) asymmetric nanocircles with a large degree of asymmetry.

CHAPTER III

MOLECULARLY IMPRINTED POLYMERS (MIPS) FOR X-RAY CONTRAST AGENT

3.1 Introduction

3.1.1 Background and Motivation

Nowadays most countries face high and increasing rates of cardiovascular disease. Each year, it kills more Americans than cancer [73]. In the clinic, a radiologic (X-ray) examination is used as a reliable method to help diagnose cardiovascular disease by imaging certain disorders. Typically, a contrast agent (dye) is injected into the bloodstream, and the flow of this dye is used to diagnose vessel blockages. Because the dye should be opaque to X-rays, a biocompatible material with high atomic number is required.

The biomedical molecule iodixanol (sold commercially under the trade name of Visipaque (Figure 3.1) has been widely used as a water-soluble, iodinated x-ray contrast agent in such examination [6]. Normally it is given in the hospital, administered by injection and ultimately excreted by the kidneys. Although clinical trials demonstrate that iodixanol has lower rates of adverse renal events than other available iodinated contrast agents, it has still been linked to high rates of acute renal failure - resulting in a disease called contrast induced nephropathy (CIN) [122]. Moreover this risk becomes much higher in patients with cardiovascular diseases. In a study of Swedish cardiac patients, 1,108/47,543 patients (2.3%) who used iodixanol were re-hospitalized with renal failure [83]. In addition, iodixanol is evaluated no less toxic than any other iodinated contrast agent in patients with constant kidney disease [105]. Apparently CIN leads to increased incidence of mortality. Thus increasing attention

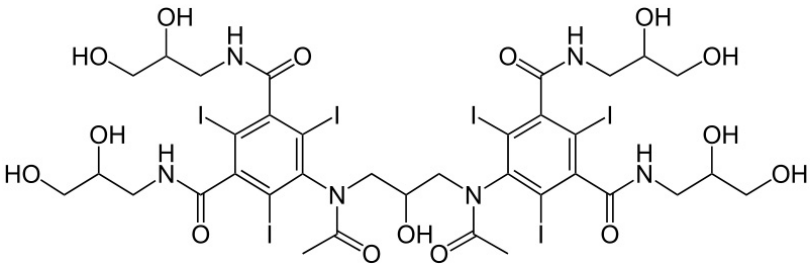

Figure 3.1: Molecular structure of iodixanol.

and efforts have been paid to such at-risk patients. Nevertheless clinical practices have not found desirable solutions to prevent CIN associated with iodixanol. Current methods are simply to limit the administrative dosage, to hospitalize patients for post-procedure observation, or to not recommend any contrast agent for patients with serious diseases.

Existing techniques studied to remove iodixanol from blood possess inherent problems and can not ideally alleviate the incidence of CIN. For example, dialysis is feasible in principle to protect kidneys by partially extracting iodixanol [15, 53]. However, current dialysis methods are based on a physical/mechanical filtration using commercially available hollow fiber membranes, such as polysulfone and cellulose triacetate. These filtration materials have neither specificity nor high binding capacity to iodixanol. This results in not only a low extraction efficiency, but also the potential for additional complications associated with removing some natural blood constituents which should preferably be retained in the blood. Therefore a highly efficient filtration material that can selectively capture significant quantities of iodixanol substances from the blood is required.

3.1.2 Molecular Imprinting

Molecular imprinting has become increasingly recognized as a powerful "bottom-up" technique to chemically manipulate molecules and cost-effectively produce synthetic

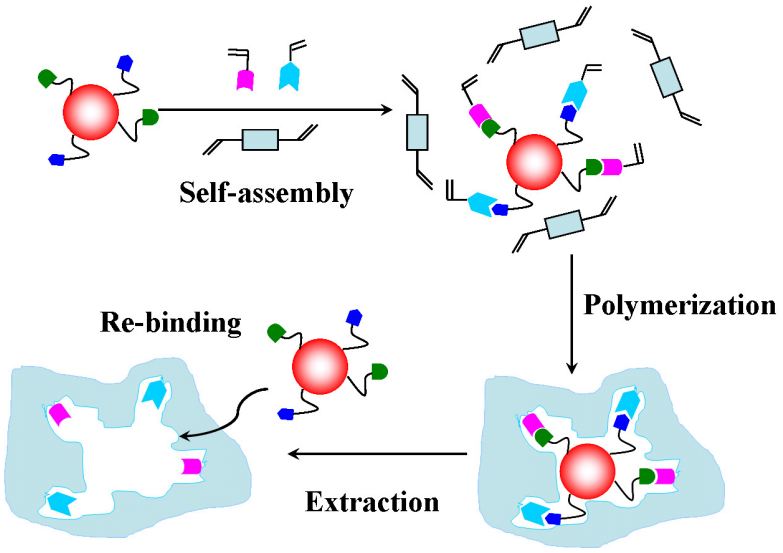

Figure 3.2: The principle of non-covalent molecular imprinting and recognition.

polymers that contain tailor-made recognition sies for binding specific molecule targets. The polymeric products are named as molecularly imprinted polymers (MIPs). The imprinting and recognition principle is based on the concepts of molecular "keys", polymeric "locks", the non-covalent affinities/associations and consequently bindings between them mimicking the recognition between antibodies and antigens as shown in Figure 3.2. A number of biomedical applications have been envisaged by MIPs including separation chromatography, solid phase extraction, molecular sensors and immunoassay-type analyses [16, 20, 43, 91, 106, 118, 126, 135].

Molecular imprinting is generally classified into covalent and non-covalent imprinting approaches. The first demonstration of covalent imprinting was reported by Wulff [126] and similarly non-covalent imprinting by Mosbach [46]. Compared to covalent imprinting, the non-covalent approach is technically less challenging due to the reduced process complexity and better adaptability to a greater range of potential template molecules, including not only small molecules but also macromolecules and giant molecules, such as antigens [26], proteins [56] and virus [18, 19]. The non-covalent imprinting process is basically performed by copolymerizing functional monomers and

cross-linkers in the presence of a molecular template. After elution of the templates, complementary binding sites are exposed and ready for exclusively recognizing and efficiently binding target molecules within the polymer network. Compared to covalent imprinting, non-covalent imprinting removes the chemical reaction steps that are necessary for covalent imprinting, such as (1) covalently bonding functional monomers to molecular templates before polymerization and (2) chemically dissociating such formed covalent bonds during solution extraction in order to properly remove the molecular templates from the imprinted sites. The inherent drawback of non-covalent imprinting compared to covalent imprinting is the possibility of producing heterogeneous binding sites resulting from relatively weak non-covalent interactions. Despite this drawback, the non-covalent approach has been widely utilized because of its apparent reduced process complexity and greater adaptability/feasibility, especially for macromolecular templates (considering the templates' large shape and multiple functionalities). Based on it non-covalent imprinting is particularly studied to imprint the macromolecular template of iodixanol of interest in this work.

For the last several years, a great number of publications have reported non-covalent imprinting of relatively small molecules such as sugars [94, 125], steroids [49], pesticides [46], pigments [143] and certain drugs [118]. By contrast, molecular imprinting of water-soluble macromolecules, to date, has been increasingly studied but only achieved limited success [18, 19, 26, 75, 80, 109, 110], since the template molecules have complex conformations, low solubility in organic monomers/crosslinkers solutions, slow diffusion rates and interference due to other components in the imprint systems [16, 43, 135]. A recently notable development in non-covalent bulk imprinting in aqueous solutions is the work of Kofinas *et al.* where they studied various templates and achieved increased imprinting factors, including viruses (imprinting factor of 2.3, compared to the non-imprinted reference polymers) [18, 19], antigens (imprinting factor of $\sim$5) [26] and proteins (imprinting factor of 4.5, compared to

the non-imprinted reference polymers) [56] in addition to glucoses (imprinting factor of 2.9, compared to the non-imprinted reference polymers) [125]. In practice, many parameters involved in the imprinting system and preparation process can affect the information associated with the binding sites, such as functional monomers/polymers, crosslinkers, and solvents/porogens [16, 98]. Thus both the imprinting feasibility and proper preparation condition require explorations regarding the iodixanol template.

In this study, we hypothesize that molecular imprinting of suitable polymers can be used to enhance their absorption capacity for iodixanol to the point where clinically useful amounts of this contrast agent can be absorbed. We further hypothesize that the specificity of the imprinting procedure will allow this enhanced absorption to be maintained even in the presence of the variety of molecules extant in blood plasma. The proposed biomedical applications based on such imprinted polymer particles can be either *in vivo* or *in vitro* healthcare treatments, where the MIPs materials are used as the key components to remove iodixanols from the blood matrix providing reliable, predictable and efficient solutions in the clinic. Two conceptual applications are illustrated in Figure 3.3. The *in vitro* application can be dialysis treatments using MIPs-packed filtration columns to exclusively absorb and efficiently excrete previously administered contrast agents from the blood stream in a manner similar to an artificial kidney. The *in vivo* application can be implantable wireless microsensors or nanomedicines which involve MIPs materials encapsulated into or coated onto MEMS based microfabricated "vascular stents" or "stent grafts", in a manner similar to an interventional medical device. It could then be inserted into the blood stream, and guided into specific sites inside the body to monitor contrast concentration as well as to facilitate contrast filtration.

In this work synthetic iodixanol-imprinted polymers are prepared by a non-covalent imprinting approach in aqueous ethanol. 4-vinylpyridine (4-VP) is used as the functional monomer due to its various potential associations with iodixanol, such as the

interactions between basic pyridines and acidic hydroxyl groups and π-π stacking between pyridine and benzene rings. 4-VP is also compared with another functional monomer candidate of methacrylic acid (MA) in terms of the resulting imprinted polymers' binding capability. Ethylene glycol dimethacrylate (EGDMA) is applied as the cross-linker. Their binding performance is investigated in aqueous and plasma media. Several factors including the quantity of iodixanol templates, the crosslink density and the solvents/porogens are studied to optimize the binding capacity and imprinting effect of synthetic MIPs. In addition, the binding capacities of MIPs as a function of the initial assay solution concentration as well as the examination time are also addressed. Details of the preparation and characterization of iodixanol-imprinted polymers for biomedical applications will be presented in the following sections of this chapter.

3.2 Experimental

3.2.1 Materials

Iodixanol was obtained from Sigma-Aldrich Chemical Company as an aqueous solution with a concentration of 600 mg/ml. 4-vinylpyridine (4-VP) monomer, ethylene glycol dimethacrylate (EGDMA), 2,2'-azo-bis(isobutyronitrile) (AIBN) and all solvents were from Sigma-Aldrich Chemical Company as A.C.S. grade. Sterile filtered sheep plasma was purchased from Hemostat Laboratories (Dixon, CA, USA). AIBN is used after twice re-crystallization. 4-VP was used after vacuum distillation to remove the inhibitor and impurities. Other chemicals and solvents were used without further purification.

3.2.2 Synthesis of MIPs

A typical iodixanol-imprinted polymer, poly(4-VP-*co*-EGDMA), is synthesized using the following procedure as shown in Figure 3.4. Iodixanol (template), 4-VP (monomer), EGDMA (crosslinker) and AIBN (initiator) are weighed and added in 10

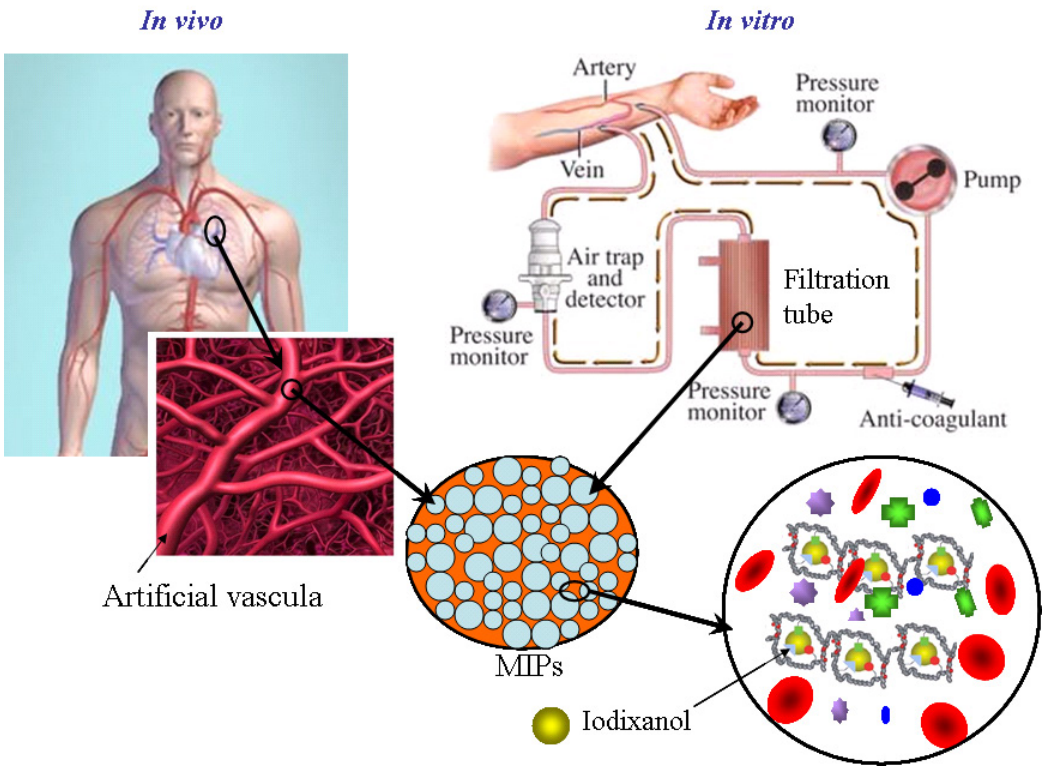

Figure 3.3: Conceptual illustration of two biomedical applications of the proposed iodixanol-imprinted MIPs, adapted from $3DScience.com$ and *nucleusinc.com*. (left) *in vivo* application of MIPs for microsensors and nanomedicines, (right) *in vitro* application of MIPs for blood dialysis.

ml ethanol/DI water (5:1) solvent mixture with the specific ratios listed in Table 3.1. The solution is stirred for 1 hour to ensure equilibration of non-covalent associations between templates and monomers followed by nitrogen gas bubbling to remove oxygen. The solution is then placed in an oven at 60 °C for 6 hours till the completion of free radical thermal polymerization. Non-imprinted polymers (NIPs) are prepared following the same procedure described above but without the addition of iodixanol templates.

Table 3.1 summarizes the details of the various experimental conditions used for each MIPs and NIPs synthesis. Each sample is labeled with a prefix of either M or N to represent MIP and NIP materials, respectively. The first series of polymers (M1∼M6) are prepared with an equimolar ratio [monomers]:[crosslinkers] of 1:1 and variable ratio, x, of the template. The theoretical value of x is approximately 0.07:1 represented by sample M2. This value is primarily determined based on the template's structural analysis. The template of interest (iodixanol) has 15 functional groups including hydroxy, amine and benzene components, thereby 15 functional monomers would be required in theory to form proper non-covalent associations with the template. This hypothesis suggests the ideal x ratio to be 0.07:1 between template and functional monomer. Experimentally, this x ratio is adjusted in a certain range from 0.006:1 to 0.167:1. The optimal value would be determined based on the materials' testing result - binding capacity (BC) and imprinting effect (IE). In fact, the optimal x ratio is experimentally determined to be 0.026:1 represented by sample M4, which will be discussed later. In addition, since the [monomers]:[crosslinkers] ratio for this series is kept constant, only one type of NIP control polymer is prepared and named as N1. The second series of polymers (M41 M45 and M4) are prepared using a constant ratio [templates]:[monomers] of 0.026:1 (optimal) and a variable crosslinker ratio, y. Various MIPs produced with different crosslink densities (y) from much greater than 1 to much smaller than 1 are studied. The analogous control polymers (N2∼N6) are

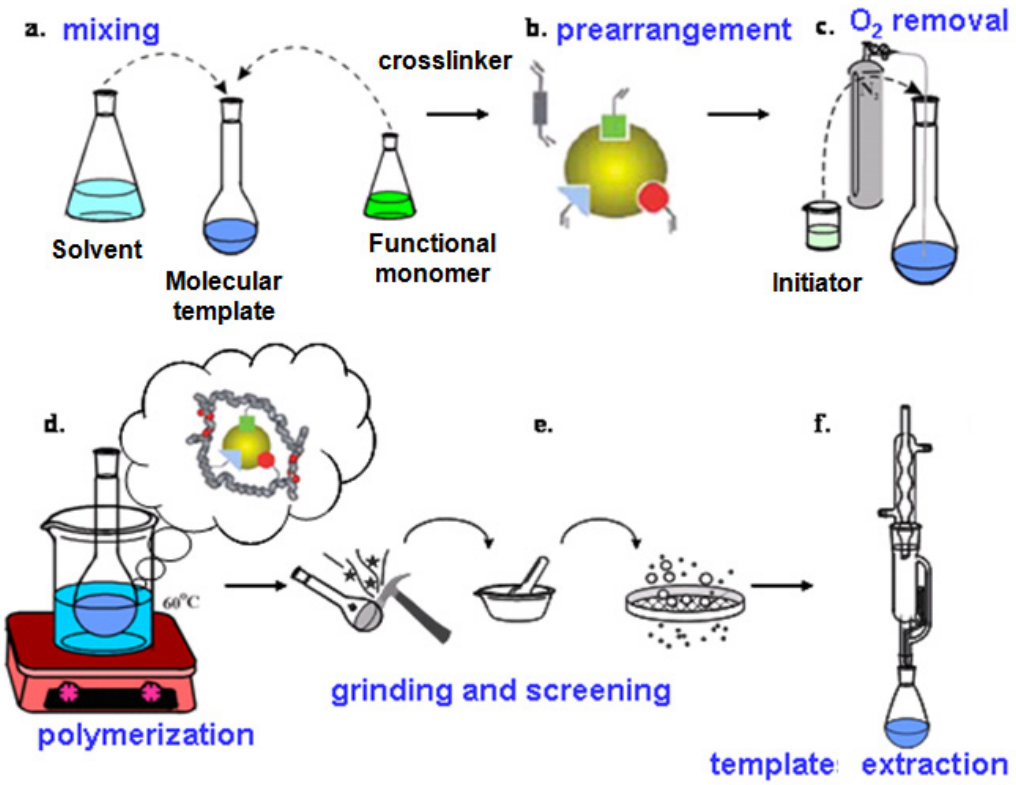

Figure 3.4: Schematic illustration of MIPs fabrication procedure. (a) mixing of template molecules (iodixanol), functional monomers (4-VP) and porogent/solvent (aqueous ethanol); (b) prearrangement by non-covalent associations between functional monomers and template molecules for 1 hour; (c) adding initiator (AIBN) and bubbling the system by N_2 for 10 min to remove O_2; (d) thermal polymerization at 60 °C for 6 hours; (e) grinding and sieving highly crosslinked polymers to powders with a desirable size of less than 25 μm; (f) tetrahydrofuran (THF) extraction to remove the potential linear oligomers/polymers embedded in the polymer matrix followed by water incubation and extraction to remove the molecular templates from binding sites.

Table 3.1: Details of sample codes and molar feed ratios of iodixanol-imprinted polymers and their control samples NIPs.

Polymer Code Number	Molar Ratio of Components			Solvents	Category
	Iodixanol Templates	4-VP Monomers	EGDMA Crosslinkers		
M1	0.167	1	1	aqueous ethanol	The 1st series x:1:1
M2	0.077	1	1		
M3	0.038	1	1		
M4	0.026	1	1		
M5	0.018	1	1		
M6	0.006	1	1		
N1	0	1	1		
M41	0.026	1	0.333	aqueous ethanol	The 2nd series 0.026:1:y
N2	0	1	0.333		
M42	0.026	1	0.667		
N3	0	1	0.667		
M4	0.026	1	1		
N1	0	1	1		
M43	0.026	1	1.333		
N4	0	1	1.333		
M44	0.026	1	1.667		
N5	0	1	1.667		
M45	0.026	1	2		
N6	0	1	2		
M46	0.026	1	1	DMSO	The 3rd series
N7	0	1	1		

synthesized and numbered correspondingly. The optimized crosslink density y is of 1:1 based on the testing results which will be discussed later. Moreover dimethyl sulfoxide (DMSO) solvent is also examined, replacing the ethanol-water solvent in the method described above, and the MIP and NIP produced using DMSO are labeled as M46 and N7.

The resulting solid polymers are powdered and sieved through a 25 μm mesh, and the powder size is verified by scanning electron microscopy (SEM). The polymer powders are washed in tetrahydrofuran (THF) for 24 hours using Soxhlet extraction to remove the potential residual monomers, crosslinkers, and linear oligomers/polymers from the polymer matrix. After filtering, the powders are dried in a vacuum at room temperature for 24 hours. The powders are then rinsed in DI water for 12 hours at room temperature to extract the iodixanol templates and then filtered to obtain the

solid powders. This washing and filtration cycle is typically repeated 9-10 times to remove most of the iodixanol templates. The powders are finally dried to a constant weight in vacuum at 60 °C. The removal of template molecules is verified by monitoring the amount of iodixanol in the rinse water using UV-Vis spectrophotometric measurements at 245 nm [54]. This analysis indicated that about 95% of the template molecules are removed with respect to the total amount added in the polymer preparation.

3.2.3 Characterization

3.2.3.1 Structural and Chemical Composition Characterization

Fourier transform infrared (FT-IR) spectroscopy (Bruker Vector 22) was used to characterize MIPs and quantitatively determine the actual copolymer composition ratios of monomers (4-VP) to crosslinkers (EGDMA) according to the integrated area ratios of two characteristic peaks at 1600 cm^{-1} (4-VP) and 1727 cm^{-1} (EGDMA). The polymer powder size and its surface morphology were characterized by SEM (FEI Nova Nanolab 200 FIB/SEM). The surface porosity was determined by nitrogen adsorption/desorption BET analysis (SA 3100 Surface Area & Pore Size Analyzer, Beckman Coulter, Inc.).

3.2.3.2 Binding Characterization in Aqueous and Blood Plasma Solutions

A UV-vis spectrophotometer (Shimadzu UV-160A) was used to determine the iodixanol concentration in both aqueous and sheep plasma solutions by measuring the UV absorbance at 245 nm. The calibrated molar absorptivity of iodixanol in aqueous solutions is 64.7 ± 0.3 $ml{\cdot}mg^{-1}cm^{-1}$ calculated from the slope of a plot of absorbance versus solution concentration in accordance with the Beer-Lambert law. This plot is obtained by measuring the absorbance of a series of iodixanol solutions with known concentrations. The molar absorptivity of iodixanol in diluted plasma solution is determined in a similar way and equal to 79.4 ± 0.5 $ml{\cdot}mg^{-1}cm^{-1}$.

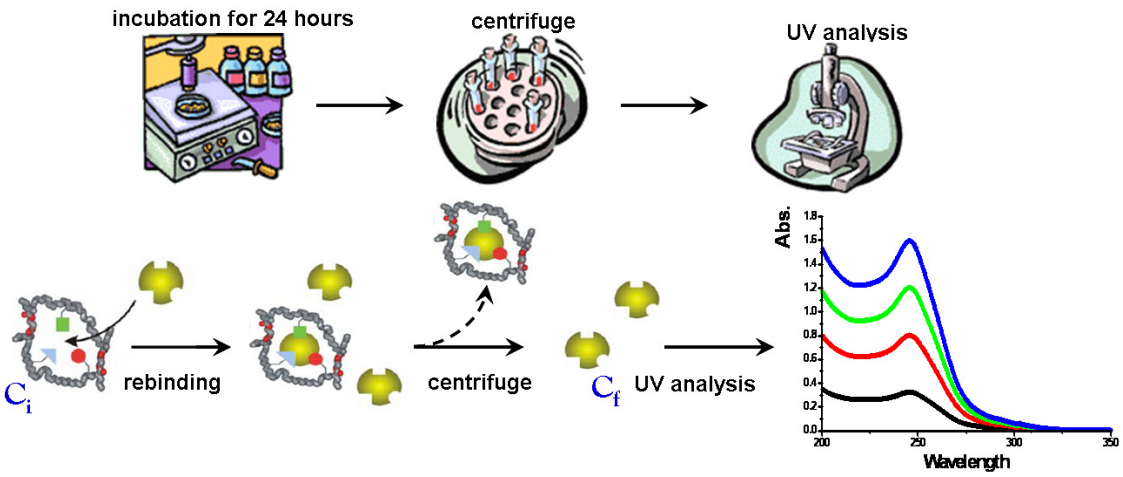

Figure 3.5: Binding test procedure of MIPs and their control polymers NIPs in aqueous and sheep plasma iodixanol solutions.

Binding tests are performed on both imprinted (MIPs) and non-imprinted polymers (NIPs). In a typical procedure (Figure 3.5), 50 mg of dry polymers are added to a vial of 10 ml iodixanol aqueous solution with an initial concentration (C_i) of 15 mg/ml. The use of a concentration of 15 mg/ml mimics a typical iodixanol concentration in blood after administration of iodixanol for angiography. This calculation is based on the average adult having a blood volume of 5 liters, being administered an injection dose of 450 ml iodixanol. The test solution and powdered polymer is slowly stirred by magnetic stirrer for 24 hours. The solution is then centrifuged to remove the polymer powders, and diluted by DI water in 650 times to ensure the UV absorbance in the spectra region is not saturated, followed by UV-Vis spectroscopy characterization to determine the final iodixanol concentration (C_f). A typical UV-Vis spectrum of diluted iodixanol aqueous solution (650 times) is shown in Figure 3.6 (a).

The binding performance of MIPs and NIPs in the aqueous and blood plasma media is quantitatively evaluated by binding capacity (BC) and imprinting effect (IE) calculated using equations 3.1 and 3.2.

$$BC = \frac{\triangle m_t}{m_p} = \frac{(C_i - C_f)V}{m_p} \tag{3.1}$$

$$IE = \frac{BC_{MIPs}}{BC_{NIPs}} \tag{3.2}$$

where C_i and C_f are initial and final concentrations of iodixanol in the solution respectively, V is the solution volume, $\triangle m_t$ is the amount of iodixanol targets bound to polymers, m_p is the mass of polymers. BC_{MIPs} and BC_{NIPs} are binding capacities of MIPs and NIPs. Using these definitions, the binding capacity, BC, represents the total mass of iodixanol absorbed per mass of polymer, while the imprint effect, IE, quantifies the improvement of absorption efficacy of imprinted polymers relative to non-imprinted polymers (references). The mean of these values is determined from three independent tests.

The absorption profile of MIPs in iodixanol aqueous solutions with different initial concentrations from 0.15 mg/ml to 25 mg/ml is also studied, since the actual injected amount of iodixanol for radio-imaging is varied by physicians according to patient body conditions and their actual tolerances, which consequently require different initial iodixanol concentration, C_i.

Subsequently, sterile filtered sheep plasma media is examined using a similar test procedure as described above, where a series of 10 ml sheep plasma solutions with an initial iodixanol concentration of 15 mg/ml are tested and characterized by UV-Vis spectroscopy (at 245 nm). Although the plasma components would have some UV-Vis absorption at 280 nm [26] (see Figure 3.6(b)), this absorbance becomes negligible after dilution by DI water of 750 times. By contrast, the UV absorbance at 245 nm associated with iodixanol is still clearly observed (see Figure 3.6(c)). Therefore, after calibration of known concentrations of iodixanol sheep plasma solution, the UV absorbance intensity at 245 nm is used to determine the concentration of remaining iodixanol in sheep plasma.

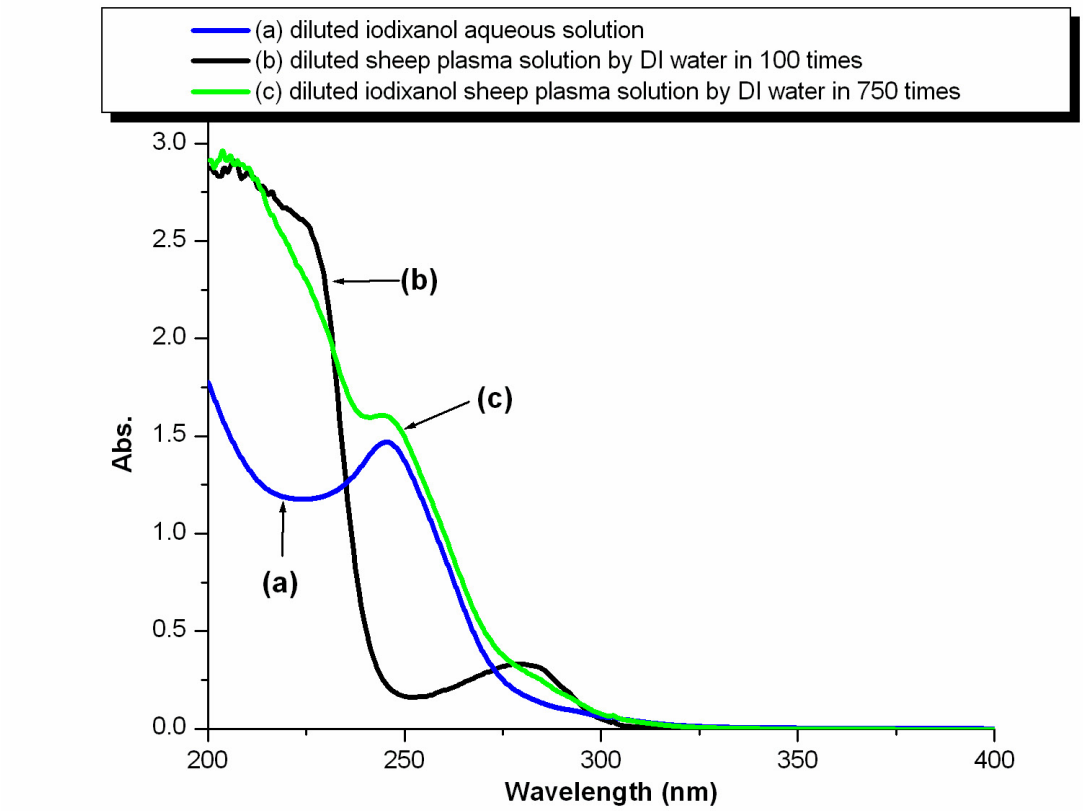

Figure 3.6: UV-Vis spectra of diluted iodixanol aqueous solution (a), diluted sheep plasma solution (b), and diluted iodixanol sheep plasma solution (c).

Moreover, in consideration of the actual circumstance for applying these imprinted polymers, few specific molecules are particularly found in plasma or blood as an ideal competitor to iodixanol molecule to evaluate the actual selectivity of synthetic MIPs. The desirable iodixanol competitors are defined to have similar sizes, shapes and chemical functionalities to iodixanol. Instead, various components in plasma or blood with a total number far larger than iodixanols would spontaneously become strong competitors. Thereby in this work plasma components including dissolved proteins, amino acid residues, glucose and mineral ions are native competitors in the binding tests. The difference of resulting BCs and IEs obtained respectively from aqueous as well as plasma solutions would indicate MIPs selectivity and binding capability of iodixanol targets.

In addition, an equilibrium binding experiment is performed to determine the binding equilibrium time in plasma. For the entire 40 hours aliquots of the stirred sheep plasma are taken periodically and analyzed using UV-Vis spectrometry. The binding capacities as a function of time are plotted to determine the equilibrium time. The total volume of the aliquots removed are less than 5% of the total test volume (10 ml), thereby minimizing the errors introduced in the test due to aliquot volume loss.

3.3 Experimental Results and Discussion

3.3.1 Structural Characteristics and Chemical Composition of Synthetic MIPs

Figure 3.7(a) shows a series of FT-IR spectra for MIPs samples of M4, M41-M45 with various feed ratios of EGDMA and 4-VP in polymerization, R_s, as listed in Table 3.1. The absorption bands observed at 1727 cm^{-1} and 1160 cm^{-1} are associated with the C=O and -C-O-C- groups in EGDMA [74], and the bands at 1675 cm^{-1}, 1600 cm^{-1}, 1560 cm^{-1}, and 1415 cm^{-1} are attributed to the pyridine rings [66]. The integrated peak area ratios of the two characteristic peaks at 1727 cm^{-1} and 1600 cm^{-1} are

utilized to quantitatively evaluate the actual ratios (R_a) of [EGDMA]:[4-VP] in the MIPs products. Further the value of R_a in the copolymer is plotted as a function of R_s as shown in Figure 3.7(b). This plot clearly shows that there is a linear relation between Ra and R_s indicating the consistency of experimental results (R_a) with the feed values (R_s). In the following sections, the feed ratios will be mainly used for discussions, where x represents the ratio of [template]:[monomer], and y stands for the ratio of [crosslinker]:[monomer].

3.3.2 Binding Capacities and Imprint Effects of MIPs

Binding capacities (BCs) and imprint effects (IEs) of the polymers in aqueous and sheep plasma solutions for an initial iodixanol concentration of 15 mg/ml are listed in Table 3.2. Results show that all of the MIPs that are synthesized by using 4-vinylpyridine (4-VP) as the functional monomer and ethylene glycol dimethacrylate (EGDMA) as the cross-linker can bind iodixanol in larger amounts than the analogous NIP control polymers, giving IE values exceeding unity. It indicates that basic 4-vinylpiridine (4-VP) is a proper functional monomer to imprint iodixanol, which is attributed to a combination of various associations in the entire imprinting system, such as the interactions between basic pyridines and acidic hydroxyl groups, $\pi - \pi$ stacking between pyridine and benzene rings as well as hydrophobic effects. Therefore the feasibility of non-covalent imprinting of iodixanol in aqueous solution is demonstrated by using 4-VP as the functional monomer.

As a comparison, methacrylic acid (MA) is also separately studied as the functional monomer to imprint iodixanol templates. Similar polymerization conditions are investigated. However, none of the poly(MA-*co*-EGDMA) products shows suitable binding capacity and imprint effect. It indicates that methacrylic acid (MA) is not a desirable functional monomer to imprint iodixanol. Although the functional MA monomers are, in theory, able to form certain non-covalent affinities with iodixanol

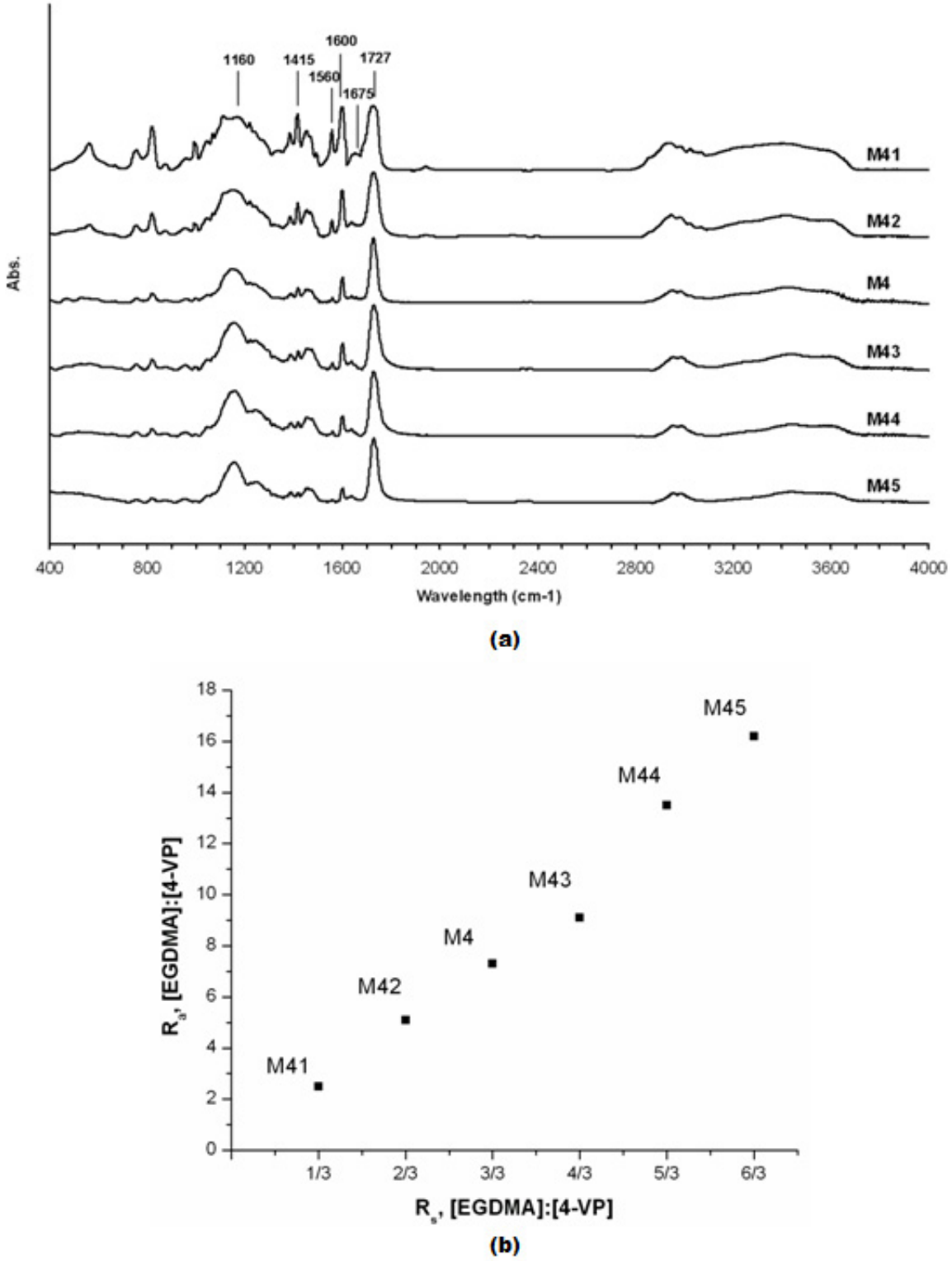

Figure 3.7: (a) FTIR spectra of MIPs (M4, M41-M45) with different feed ratios of [EGDMA]:[4-VP]; (b) the plot of the actual ratios (R_a) of [EGDMA]:[4-VP] in polymer products versus the feed ratios (R_s) of [EGDMA]:[4-VP] in polymerization.

Table 3.2: Binding capacities of MIPs and NIPs in aqueous and plasma solutions (at C_i = 15 mg/ml) and their imprint effects correspondingly.

Polymer Code Number	Aqueous Solution		Sheep Plasma	
	BC (mg /g)	IE	BC (mg /g)	IE
M1	128 ± 22.4	4.0	90 ± 13.5	1.7
M2	152 ± 26.6	4.7	96 ± 14.4	1.8
M3	190 ± 33.25	5.9	178 ± 26.7	3.3
M4	284 ± 49.7	8.8	232 ± 34.8	4.3
M5	186 ± 32.55	5.8	154 ± 23.1	2.8
M6	198 ± 25.2	6.1	178 ± 31.15	3.6
N1	32 ± 1.6	-	54 ± 2.8	-
M41	26 ± 4.55	2.2	10 ± 1.5	5
N2	12 ± 0.35	-	2 ± 0.2	-
M42	212 ± 37.1	3.9	16 ± 2.4	4
N3	54 ± 9.45	-	4 ± 0.3	-
M4	284 ± 49.7	8.8	232 ± 34.8	4.3
N1	32 ± 5.6	-	54 ± 81	-
M43	198 ± 34.65	7.1	84 ± 12.6	2.2
N4	28 ± 1.4	-	38 ± 5.7	-
M44	190 ± 33.25	6.8	14 ± 2.1	4.7
N5	28 ± 4.9	-	3 ± 0.2	-

templates, the results obviously indicate that the resulting non-covalent affinities in the MA-imprinting-iodixanol system are not as strong as those in 4-VP-imprinting-iodixanol system. Computational simulation and theoretical study can be taken in the future to understand the imprinting mechanism in detail.

Furthermore, by careful comparison of BCs and IEs achieved in aqueous solutions listed in the second column of Table 3.2, it is found that the highest BC obtained is 284 mg/g from M4 with an IE of 8.8. Although some other MIPs, such as M43 (BC = 198 mg/g and IE = 7.1) and M44 (BC = 190 mg/g, IE = 6.8), display good IEs (>5), their BCs are much lower than M4, thus they have poorer binding capabilities than M4. Meanwhile, similar observation and trend is also noticed from the results obtained in sheep plasma media listed in the third column of Table 3.2. The highest BC obtained of 232 mg/g is still from M4 with an IE of 4.3. Although M45 has the highest IE (4.7) in plasma, its low value of BC (14 mg/g) is too small to be of practical use. Thus these binding results indicate that M4 is the most desirable MIPs obtained in this work, with the potential engagement for biomedical applications as mentioned in section 4.1. Details about the material preparation optimization and structure-property relationship will be discussed the following sections 3.3.2.1∼3.3.2.4.

In addition, it is also noticed that all MIPs show higher binding capacities (BCs) and imprint effects (IEs) in aqueous than plasma solutions by a comparison of values summarized in Table 3.2. Among them, M4 is taken as an example for the following discussion. Figure 3.8 shows the column plot of BCs of M4 and its control polymer N1 obtained in aqueous and plasma solutions. It apparently shows that when M4 is tested in plasma mixture, its BC and IE are approximately reduced by 20% and 50% respectively from those values obtained in aqueous solution. This is primarily due to the complex nature of the plasma mixture, which consists of a large number of components that could compete with iodixanol targets to occupy a certain percentage of the imprinted binding sites. In addition, it is also possible that plasma

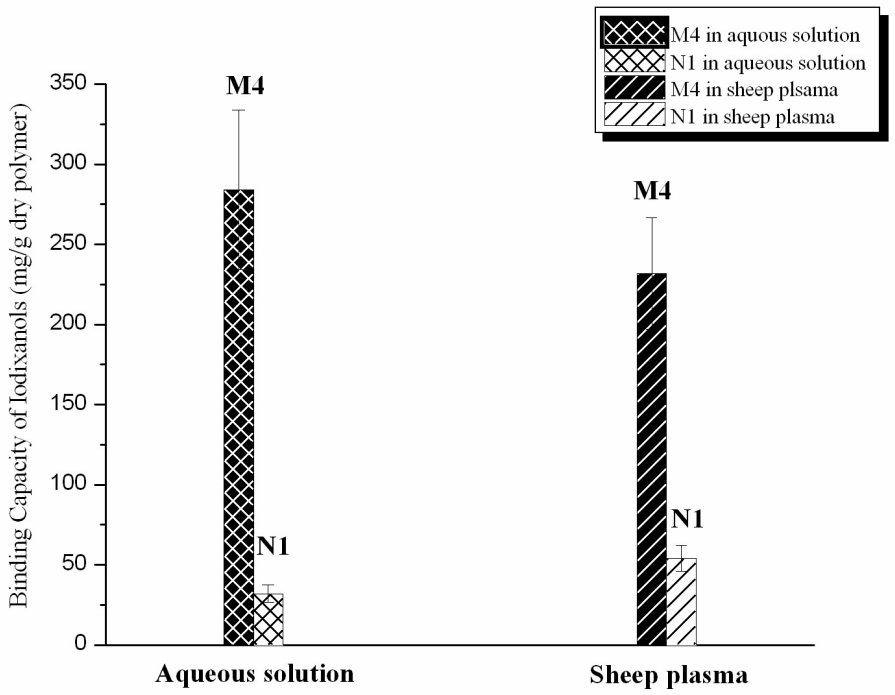

Figure 3.8: Binding capacities (BCs) of MIPs and NIPs in aqueous and sheep plasma.

components might potentially form complexes with iodixanol, thereby affecting the conformation and chemical functionality of iodixanol and resulting in a reduction of MIPs' BC and IE. From the current data it is not possible to distinguish which of these mechanisms, or possibly another one, cause the observed effects, and this would form part of the future research on MIPs. On the other hand, even if the achieved binding capability of iodixanol target is somewhat affected by the plasma components, M4 still shows high binding capacity (232 mg/g) and imprint effect (4.3) satisfying the application requirements, which indicates that M4 possesses a proper binding selectivity in plasma media, and it can function well to iodixanol targets in the presence of multiple competitors.

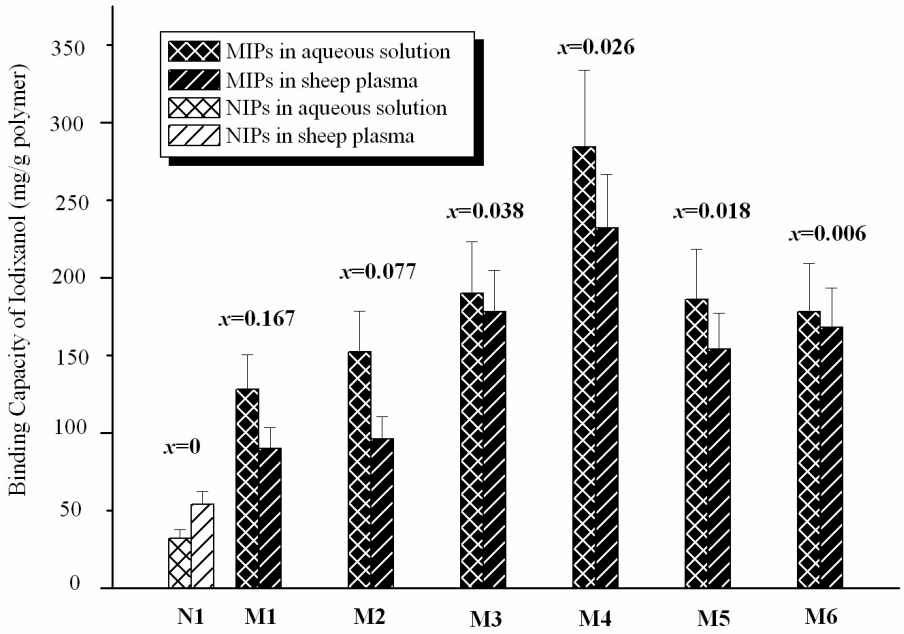

Figure 3.9: Binding capacities (BCs) of polymers with a preparation molar ratio of x:1:1, examined in aqueous solutions and sheep plasma.

3.3.2.1 Effect of the Molar Ratios

The efficiency of the studied MIP system is affected by several factors in polymerization, including the [template]:[monomer] (x) and the [crosslinker]:[monomer] (y) ratios as well as the solvent used. Of these parameters, the molar ratios of components are found to be the most important in determining the BC and IE of MIPs by analyzing the results of Table 3.2 in a graphical fashion shown in Figures 3.9 and 3.10. Figure 3.9 presents the variation of BCs for the various MIPs and NIPs as a function of x, at a constant y equal to 1. Figure 3.10 similarly presents the variation of BC as a function of y, at constant x (= 0.026). It apparently indicates the optimal [template]:[monomer]: [crosslinker] ratio (i.e. x:1:y) is 0.026:1:1 which can produce a maximum in the binding capacity (BC) in addition to a good imprint effect (IE).

In terms of the [template]:[monomer] ratio, functional monomers are usually used in an excess of moles compared to the template [16] (x <1). In general, there is an optimized [template]:[monomer] ratio, x_o, for a specific imprinting system. When $x < x_o$ the binding capacity (BC) of MIPs would be expected to increase with increasing x till x_o because of the increase of imprinting sites in the MIPs. However, when x exceeds x_o the binding capacity (BC) of MIPs decreases again since there is no sufficient amount of functional monomers used to imprint the template molecules. This leads to improper molecular imprinting and consequently the resulting MIPs do not have desirable binding capacity and imprint effect. It is also possible that the excess templates aggregate and form clusters, the resulting imprinted sites are shaped and functionalized regards to the clusters rather than isolated templates leading to poor recognition and binding capacity to template molecules [19, 80]. Experimental results (see Figure 3.9) show the maximal binding capacity appears when the ratio of [template]:[monomer] is 0.026, thus 0.026 is believed to be the optimized ratio, x_o, for this specific imprinting system.

The [crosslinker]:[monomer] ratio, y, plays another important role that affects the crosslink density and consequently the binding capacity of the polymers. Molecularly imprinted polymers are polymeric networks with an effective distance between crosslinks. If the crosslink density is too low, then the network is too flexible and dynamic and consequently the shape or size of the imprinted sites that the templates induced may not be retained. However, if the crosslink density is too high, then template molecular diffusion within the network may be reduced [16], which would have the effect of preventing not only template extraction but also iodixanol targets movement into the binding sites. In addition, in this work it is found that an excess of crosslinkers significantly affects the solubility of iodixanol in the reactant monomer/crosslinker solution, which can change the equilibration of non-covalent associations between monomers and templates. Figure 3.10 clearly shows

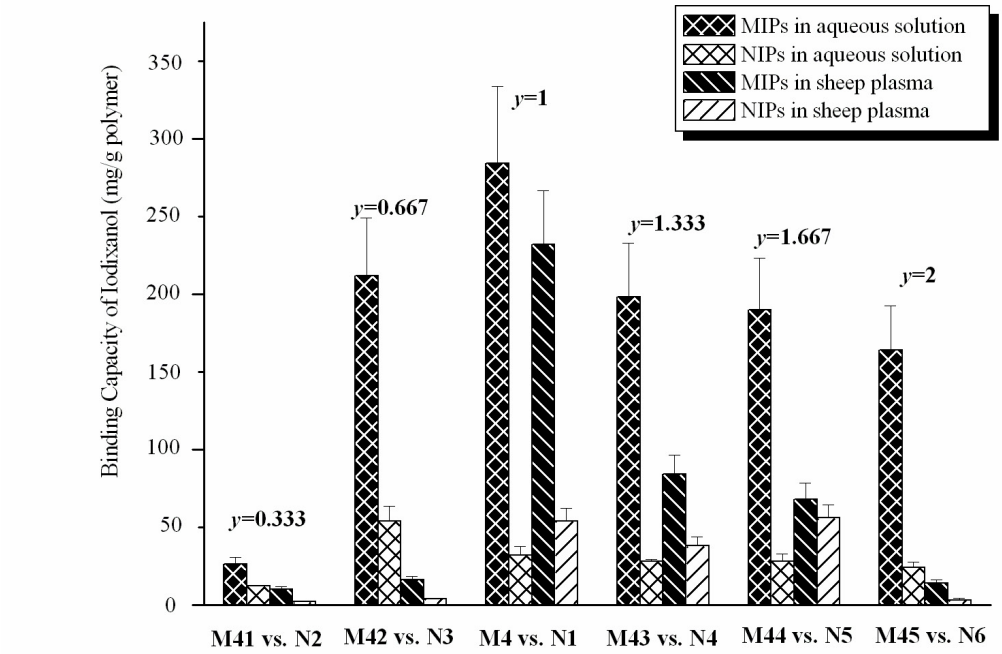

Figure 3.10: Binding capacities (BCs) of polymers with a preparation molar ratio of 0.026:1:y examined in aqueous solutions and sheep plasma.

the resulting behavior of MIPs to iodixanol targets in aqueous solutions and blood plasma, indicating the effects that these possible factors have on BCs, and the proper [crosslinker]:[monomer] ratio is 1:1.

3.3.2.2 Effect of the Initial Solution Concentration

In medical application, the actual injection amount of iodixanol for radiologic examination is dependent on patient body conditions and their actual tolerances, therefore patients might have different initial iodixanol concentration, C_i, in their blood. It is necessary to study the absorption profile of MIPs in solutions with different initial concentrations. Figure 3.11 shows absorption profiles for M4 and its control polymer N1 as a function of initial solution concentrations, C_i. The BC of MIPs is always a few times higher than that of NIPs, and both BCs increase with the rise of C_i. The theoretical BC (BC_t) of M4 is 132 mg/g and that of N1 is 0 mg/g based on the [template]:[monomer]:[crosslinker] ratio used in polymerization. It assumes all imprinted sites in the MIPs behave like antibodies to the iodixanol antigens where each binding site can properly absorb only one iodixanol target. The measured actual BC (BC_a) of MIPs is higher than its BC_t when C_i is larger than 5 mg/ml, while the BC_a of NIPs is never equal to zero. This is mainly attributed to the non-specific binding from "background" pores (non-template-induced sites present in the polymer matrix), which can be created by inherent local density fluctuations in the bulky polymer as well as porogenic solvents [136]. These "background" sites serve as binding sites to capture target molecules by non-specific, physical adsorption leading to a higher value of BC_a than the predicted BC_t [84]. Thus it is believed that the non-specific adsorption is the dominant effect on BC_a of NIPs. This effect increases when the number of available iodixanol molecules increase. In MIPs the BC_a results from a combination of specific (molecular recognition) absorption and non-specific adsorption, and the specific absorption is the dominant effect. Thus the BC_a of MIPs is always a few times

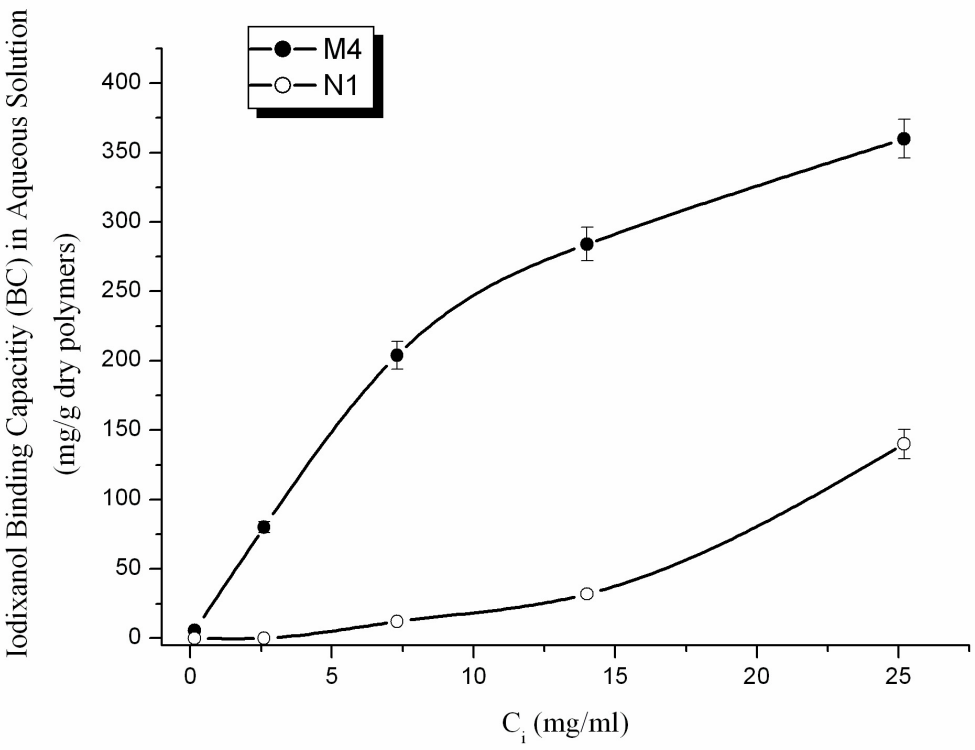

Figure 3.11: Binding capacities (BCs) of polymers versus the initial iodixanol concentration in aqueous solutions (C_i).

higher than NIPs' in varied solution concentrations. Additionally it is also possible that when the number of available target molecules exceeds the number of accessible template-induced binding sites, the bound target molecules might serve as nucleation centers for adjacent extra targets to deposit increasing the BCs of target molecules in MIPs compared to NIPs [68].

3.3.2.3 Binding Equilibrium in Sheep Plasma Solution

It is noticed earlier that the BC values of MIPs examined in aqueous solutions are slightly different from those in plasma because of the complex nature of the plasma media, which implies that the variation of media might impact the binding performance of MIPs as well as the binding equilibrium, for example requiring longer time

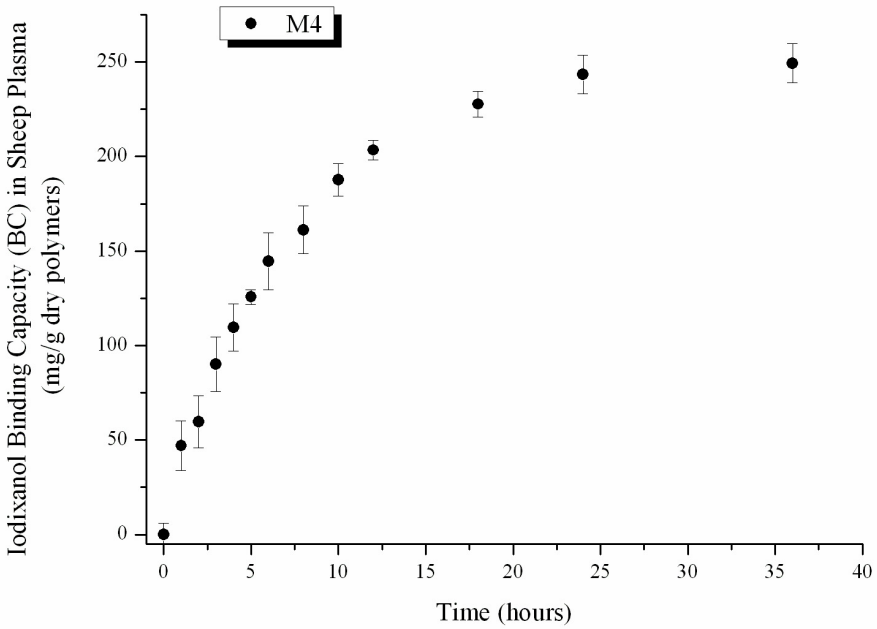

Figure 3.12: Absorption profile of M4 as a function of binding time in sheep plasma (C_i = 15 mg/ml).

to reach the equilibrium. Therefore the binding equilibrium profile of MIPs in plasma media is also studied, and M4 is tested as a representative of those synthetic MIPs. Figure 3.12 shows the time dependent absorption profile of M4 performed in sheep plasma within 40 hours (C_i = 15 mg/ml). It is observed that the initial binding rate of MIPs is the highest, ∼30 mg/g hour, and then gradually decreases along with the increased time. When the time scale is ∼24 hours the rate is reduced to zero indicating the entire system reaches equilibrium. Therefore the binding equilibrium time of MIPs in plasma is evaluated as 24 hours although a small amount of iodixanols might be still absorbed afterwards which is attributed to the non-specific binding or physical adsorption. Based on this characterization, all subsequent binding tests and BC measurements in plasma are determined within 24 hours.

3.3.2.4 Effect of the Solvent/Porogen

Selection of solvents is challenging, especially for water-soluble, medium or large size templates. It has been proposed that the presence of very polar solvents, e.g. DI water, could interfere with the monomer-template associations and thus polar solvents are generally not suitable for non-covalent molecular imprinting [16, 98]. However, in this work the extremely low solubility of iodixanol in apolar or weak polar solvents requires the use of polar solvents, such as ethanol:DI water (5:1) and DMSO. In practice, DMSO is a good solvent for all components in the imprinting system, including iodixanol, monomers, and crosslinkers, which eases the preparation of a homogeneous solution prior to polymerization. However, the high polarity of DMSO may interfere with monomer-template associations much more than aqueous ethanol. Comparison in the effects of the solvent is carried in samples M4 and M46 together with the control samples N1 and N7.

SEM images in Figure 3.13 show the surface morphologies of samples prepared in aqueous ethanol (M4 and N1) as well as those prepared in DMSO (M46 and N7). It is found that imprinted polymers are always slightly more porous than their non-imprinted control polymers, M4 vs. N1 and M46 vs. N7, which is attributed to the usage of templates in preparing imprinted polymers leading more pores formed in MIPs than NIPs after template extraction. Moreover, it is noticeable that MIPs prepared from aqueous ethanol, M4 in Figure 3.13(a), is less porous than that prepared in DMSO, M46 in Figure 3.13(c). BET surface analysis is used to quantitatively check and measure the surface areas (S) and pore volumes (V_p) of M4, M46 and their control polymers N1, N7. The BET results are summarized in Table 3.3. It is shown that samples from aqueous ethanol solvent system (M4 and N1) have lower surface area and pore volume than samples from DMSO solvent system (M46 and N7). Therefore BET results indicate that DMSO is a better porogenic solvent than aqueous ethanol leading to higher values of S and Vp, which is mainly understood by

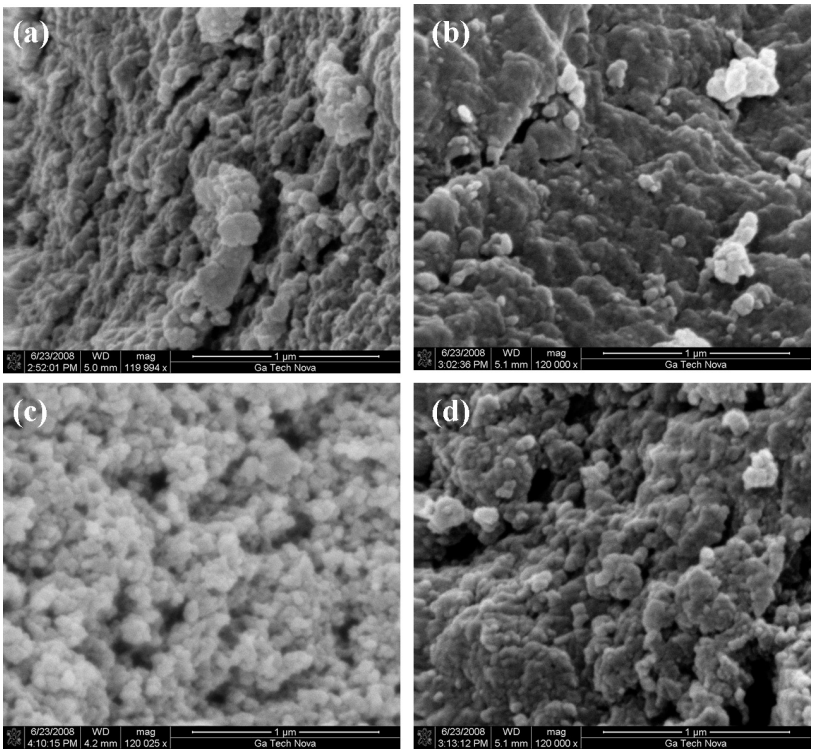

Figure 3.13: SEM images of polymers (a) M4, (b) N1, (c) M46 and (d) N7 with a scale bar of 1 μm.

the solvent nature. With a high value of S and V_p the equilibrium time for absorption in plasma might be reduced from 24 hours as obtained in Figure 3.12.

However, the resulting BC values for more porous M46 are much lower than those of M4 over the entire concentration range (from 0.15 mg/ml to 14 mg/ml) (Figure 3.14). Considering the results at C_i = 14 mg/ml, the BC for M4 is 275 mg/g, which is 8.8 times higher than its control polymer N1 (IE = 8.8). For M46 the BC is

Table 3.3: BET surface analysis of polymers prepared in different solvents.

Sample Code Number	Surface Area, S (m^2/g)	Total Pore Volume, V_p (cm^3/g)	Solvent
M4	6.83	0.019	Aqueous ethanol
N1	3.59	0.012	
M46	53.86	0.221	DMSO
N7	17.64	0.071	

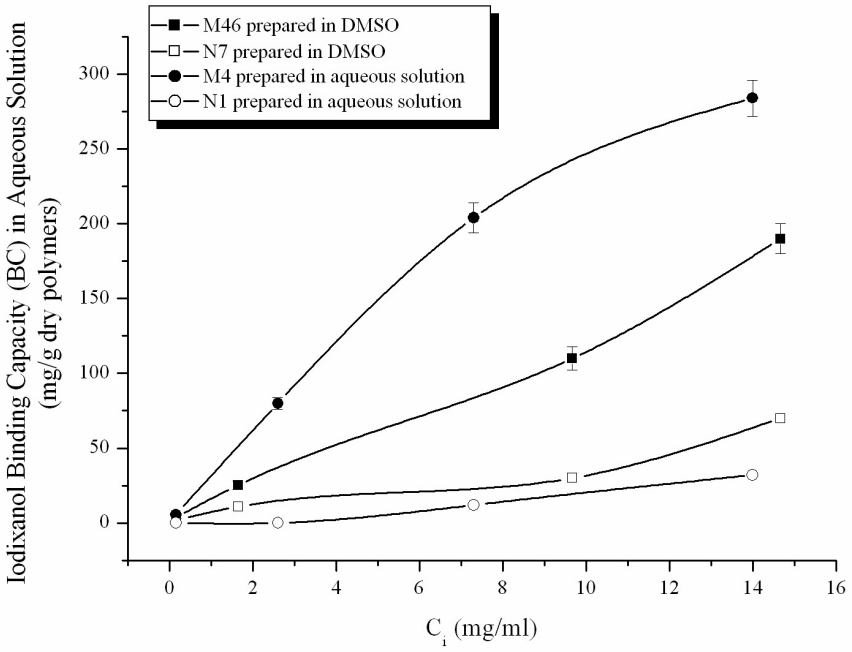

Figure 3.14: Plots of the BCs of polymers versus the initial iodixanol concentration (C_i).

190 mg/ml and only 2.7 times higher than that of its control polymers N7 (IE = 2.7). Clearly, although DMSO might be a better porogen increasing the porosity of produced polymers as mentioned before, aqueous ethanol is a better solvent than DMSO for imprinting iodixanol, which is mainly attributed to the effect of solvent polarity. In literature it is reported that some biomacromolecules dissolved in polar organic solvents, i.e. DMSO, would exhibit distinctly different activity compared to that in aqueous media [21]. Thereby it is possible that the configuration of iodixanols in DMSO is changed from that in aqueous solution which induces inferior imprinting.

3.4 Chapter Summary

As a summary of this chapter, molecularly non-covalent imprinting of the water-soluble X-ray contrast medium iodixanol is demonstrated in aqueous-based solvent using 4-vinylpyridine as the functional monomer and ethylene glycol dimethacrylate

as the crosslinker. Recognition and binding of iodixanol target molecules by imprinted polymers were investigated both in aqueous solution and sheep plasma *in vitro*. The binding equilibrium measured for both media can be reached within 24 hours. The best binding capacity achieved from the optimized imprinted polymers in this study is 284 mg/g in aqueous solution (C_i = 15 mg/ml), 8.8 times higher than that of the control polymers, and 232 mg/g in sheep plasma (C_i = 15 mg/ml), 4.3 times higher than the control polymers, respectively. The slight reduction on binding capability of MIPs examined in plasma media is attributed to the effects of the plasma components. However MIPs could still function well in plasma with satisfactory binding capability for biomedical applications. This work successfully demonstrates that non-covalent imprinting can be a desirable strategy to imprint water-soluble biomedical macromolecules, X-ray contrast agent for instance. In addition it serves as a pioneer directly leading non-covalent imprinting technology and formulated imprinted polymers to practical healthcare applications.

CHAPTER IV

NANOLITHOGRAPHY-BASED MOLECULAR MANIPULATION (NMM)

4.1 Introduction

Fabrication and investigation of nanometer-sized structures, devices and complex systems is an area of increasing technical and commercial importance with applications in areas such as microelectronics, functional biomimetics, chemistry and nanoelectromechanical systems (NEMS), where the scale confers particular functionality [33, 61].

Traditional "top-down" and "bottom-up" nanofabrication approaches have their limits. State-of-the-art nanolithography has demonstrated sub-100 nm patterns, such as EBL and X-ray lithography. However, it is still challenging for mass production. More importantly it is very hard to approach molecular-scale resolution. In contrast, the "bottom-up" chemical growth method can assemble molecules creating functional nanostructures. But thus far its ability to properly position the functional structures at specific locations for effectively fabricating useful devices has proven elusive, due to the necessity of relying on what is available from non-designed, spontaneous processes.

A recently emerging approach is to properly combine "bottom-up" with "top-down" means. This approach shows promise in the development of advanced nanotechnology, following the trend anticipated in Figure 1.1. This hybrid strategy allows the design and synthesis of various nanofabrication processes in a designated way. Some associated studies have been initiated, although they are still in their infancy. Examples include the integration of self-assembled block copolymers into conventional lithography for sub-10 nm patterning [38, 95, 96, 113], scanning probe lithography (SPL) based molecular manipulation [35, 40, 119], assembling of nanomaterials and

nanoparticles within lithographically fabricated templates [51, 81, 82, 90] as well as nanotube and nanowire integrated electrical/mechanical devices [48, 70, 123, 124, 129]. The concept of molecular assemblers was proposed several years ago as also indicated in Figure 1.1 [103]. However, based on our best knowledge to date it has not yet been demonstrated, and little has been reported on the development of hybrid approaches for fabricating artificial molecular assemblers or molecular manipulation templates.

We recently proposed a concept of nanolithography-based molecular manipulation (NMM). NMM basically defines a type of strategic hybrid nanofabrication process derived from nanolithography, but not solely relying on it. The essential objective is to combine "top-down" precise design with "bottom-up" molecular scale resolution to create a user-designated "smart" surface and volume that can interact with molecules in a designated way. In this work, we designed and demonstrated a NMM process which combines the "bottom-up" surface initiated polymerization (SIP) process [37] with the "top-down" nanolithography process of EBL. Further we demonstrated the prototype so-called "molecular manipulation templates" by the developed NMM process. Such templates have sub-10 nm feature size and surface tunable functionalities mimicking biocatalyst enzymes. Their capability of recognition and assembling of target molecules for synthesis of 3D morphological features of nanoparticles is also demonstrated.

Advantages of the proposed hybrid NMM process include: (1) it removes the challenge for the "top-down" EBL to directly produce molecular scale feature sizes (sub-10 nm); (2) it utilizes "bottom-up" SIP to reduce the scale gap to the desired one (e.g. sub-10 nm) by controlling the polymer layer thickness that are grown on the specific location. Meanwhile, anisotropic surface functionality is simultaneously accomplished by means of the grafted polymers. The chemical property of the deposited polymer layer can be tailored by appropriate selection of the polymer precursors or

functional monomer(s) according to the application requirements; (3) one important role of "top-down" EBL in NMM process is to appropriately define the locations of functional structures across the entire chip in order to properly design and fabricate useful devices and systems; (4) since the grafted organic layer can be easily removed by O_2 plasma, the chip is reusable for another SIP process without the need of repeating the EBL procedure; (5) it reduces the process cost and complexity.

In this work, three tasks are performed to demonstrate the NMM concept and the prototype molecular manipulation. They include (1) development and characterization of NMM process for fabricating nanopatterns with tunable surface chemical functionality, (2) implementation of NMM process to fabricate artificial molecular manipulation templates with 3D surface functionalized nanostructures, and (3) mechanosynthesis of 3D nanostructures with sub-10 nm feature size utilizing the fabricated molecular manipulation templates. Fabrication and characterization details will be given in the following sections accordingly.

4.2 Fabrication of Nanopatterns with Tunable Functionalities

4.2.1 Background and Motivation

Molecular nanotechnology is emerging as a key technical enabler of enormous applications in microelectronics, functional biomimetics and NEMS. In particular, to mimic biological mechanisms it is important to realize functionalized mechanical structures at the molecular scale, e.g. artificial molecular assemblers for guiding position-controlled mechano-chemistry. Many examples of steric-based functional enhancement exist in the chemical and biochemical worlds including multiple classes of enzymes and catalysts. Fabrication of chemomechanical structures at the molecular scale opens the door for the directed design of artificial enzymes and catalysts, efficient molecular assemblers, and validation of high-performance-computing-based

models of molecular interaction [60]. Some potential applications of the molecular-scale functionalized mechanical structures are conceptually illustrated in Figure 4.1. They may selectively recognize molecules and catalyze chemical reactions, such as addition reaction (Figure 4.1(I)) and bond cleavage (Figure 4.1(II)). They may recognize and positionally assemble molecules of interest resulting in CNT nanodevices (Figure 4.1(III)). They may allow the design of 3D functional nanostructures (Figure 4.1(IV)) and desirable polymer chain configurations (Figure 4.1(V)). The scenario shown in Figure 4.1(IV) is the research objective of this chapter.

Neither "top-down" nanolithography nor "bottom-up" chemical synthesis can be used alone to successfully fabricate nanostructures with as-designed physical dimensions at the molecular scale as well as desired surface functionality with minimal fabrication cost. In this section, we proposed and investigated the hybrid NMM strategy which combines the advantages of both "top-down" EBL and "bottom-up" free-radical SIP, and compensates for their individual disadvantages. The process begins with "top-down" patterning of the substrates by EBL at length scales far larger than the typical molecular sizes of sub-10 nm. SIP is then used for "bottom-up" growth of functional robust polymer brushes onto the EBL patterned surface. The consequent feature size can be reduced to a molecular scale, and the pattern functionality is varied by the covalently grafted polymers. The polymer studied in this work is the polyelectrolyte poly(4-vinyl pyridine) (PVP), which can present positive charge in aqueous solution and has biochemical compatibility and antimicrobial properties.

4.2.2 Materials

All chemicals were purchased in A.C.S. grade from Sigma-Aldrich chemical company, USA. Monomer 4-vinyl pyridine (4-VP) was washed with 10% aqueous solution of sodium hydroxide followed by vacuum distillation twice to remove the inhibitors and

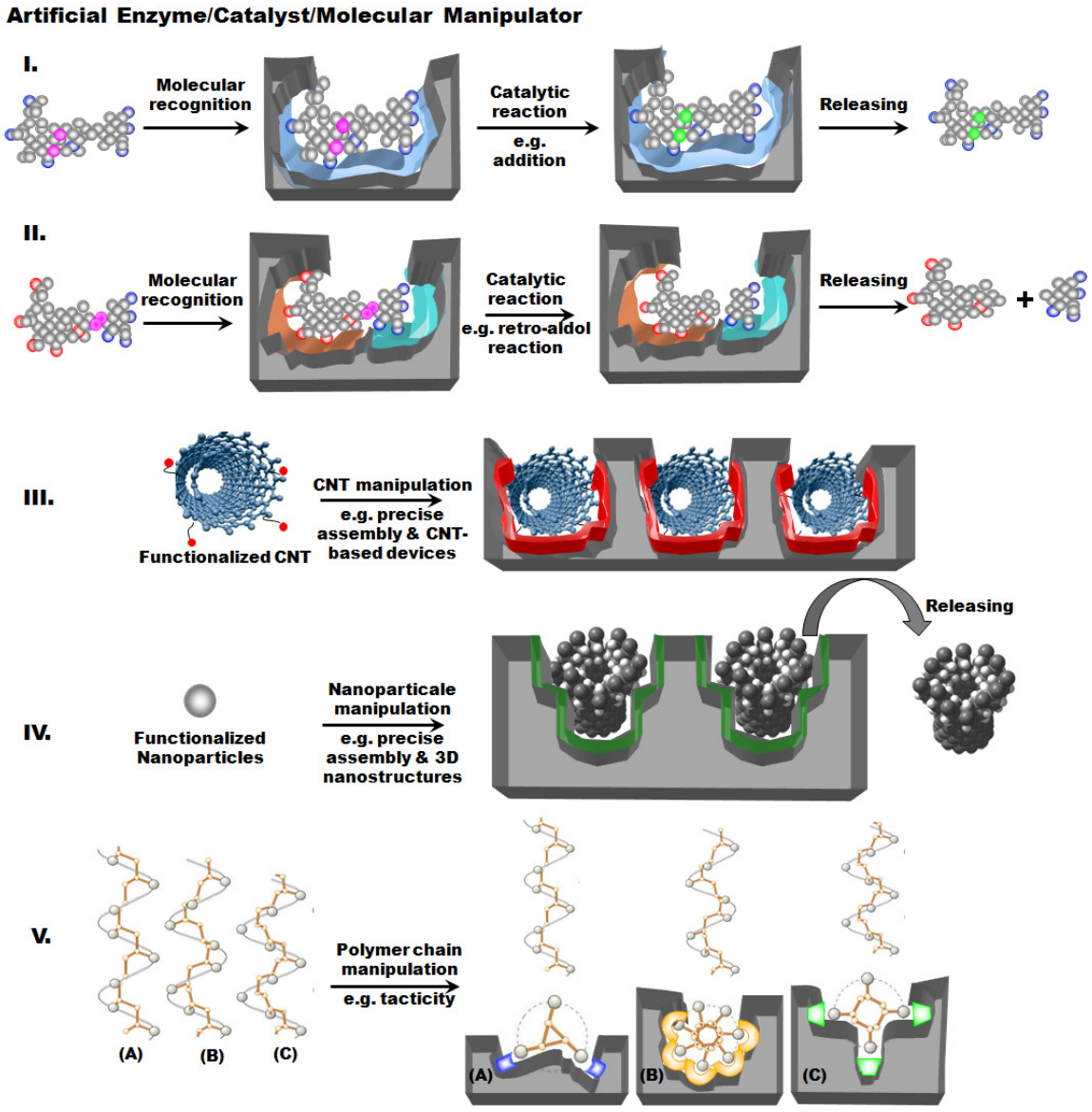

Figure 4.1: Conceptual schemes of applications of molecular scale chemo-mechanical structures in chemistry. They may selectively recognize molecules and catalyze the chemical reactions including addition reaction (I) and bond cleavage (II) producing new molecular products. They may recognize and positional assemble molecules of interest resulting CNT nanodevices (III), 3D functional nanostructures (IV), and desirable polymer chain configurations as designed (V).

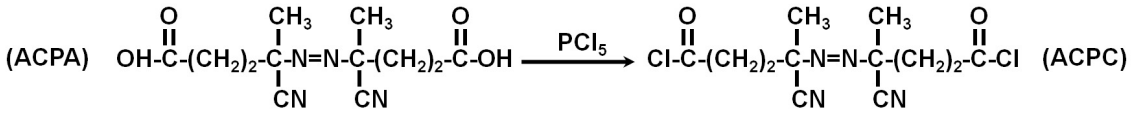

Figure 4.2: Schematic illustration of the chemical reaction to modify ACPA end groups.

impurities. γ-Aminopropyltriethoxy-silane (γ-APS) was used without further purification.

In this work modification of commercialized azo-based initiator 4,4'-azobis(4-cyanopentanoic acid) (ACPA) was performed to change the carboxylic acid end groups (-COOH) to acid chloride end groups [117] by using the chemical reaction as shown in Figure 4.2. The product 4,4'-azobis-(4-cyanopentaoic chloride) (ACPC) was further re-crystallized twice from n-hexane and characterized by ^{1}H-NMR. The produced ACPC initiator will be immobilized on the substrate surface to initiate SIP.

4.2.3 Fabrication

The NMM fabrication process is outlined in Figure 4.3. It begins with a "top-down" process (Figure 4.3(a)). A thermally oxidized Si substrate bearing ~100 nm SiO_2 is patterned by EBL (JEOL JBX-9300FS EBL system, 100 kV) followed by reactive ion etching (RIE) to create a series of nano-trenches in the SiO_2 layer. Trench widths of 85 nm and 65 nm are produced with depths of ~70 nm. The sample is then treated by piranha solution (98% H_2SO_4 and 30% H_2O_2 in volume ratio of 2:1 at 100 °C for 1 hour) resulting in a silanol surface. In subsequent processes (Figure 4.3(b)-(d)), all of the chemical reactions are performed in a closed dry-N_2 system using the setup shown in Figure 4.4. Figure 4.5 schematically illustrates each chemical reaction carried out. Typically, an oil pump is applied first to remove air followed by a N_2 purge flow to maintain the entire system in a dry-N_2 atmosphere. This procedure is repeated three times to ensure complete removal of O_2. All chemicals are injected separately under

N_2 flow, and an oil or ice bath is used to control the reaction temperature. Samples are stacked separately on a quartz frame, and the entire assembly is kept inside a beaker with a magnetic stirrer. Before the initiation of each chemical reaction, a degassing treatment is applied to the entire system (ultrasonication for approximately 2 hours) to remove air trapped inside the nano-patterns. The silanol groups react with γ-APS in ethanol solution, and thus the sample surface is modified with reactive amino groups (SiO_2-NH_2) as illustrated in Figure 4.3(b) and Figure 4.5(a). The reaction is kept at 130 °C for 6 hours with a $V_{\gamma-APS}$:$V_{ethanol}$ ratio of 3:20. The resulting sample (SiO_2-NH_2) is repeatedly washed by ethanol and deionized (DI) water and then dried in N_2. Then the amine-terminated SiO_2 sample (SiO_2-NH_2) is immersed in THF solution with an ACPC initiator concentration of 4 mg/ml. An excess amount of pyridine (0.4 ml) is added dropwise to the solution and the reaction is allowed to proceed for 24 hours (Figure 4.3(c) and Figure 4.5(b)). The resulting sample (SiO_2-azo) is washed a few times with THF and DI water followed by drying in N_2. Free-radical SIP of 4-vinyl pyridine onto the SiO_2-azo surface is performed at 60 °C for 4 hours in ethanol solution (Figure 4.3(d) and Figure 4.5(c)). The resulting surface is covalently coated by functional PVP brushes (SiO_2-PVP). The resulting sample is repeatedly cleaned by ethanol and DI water followed by drying in a vacuum oven at 60 °C for 24 hours. The grafted PVP thickness can be varied between 5 nm and 30 nm by tuning the initial monomer concentration.

4.2.4 Experimental Results and Discussion

4.2.4.1 Materials

Figure 4.6 shows a representative ^{1}H-NMR result of ACPC (solvent: $CDCl_3$). The signal at low chemical shift, 1-3 ppm, is attributed to the primary (-CH_3), secondary (-CH_2-) hydrogen bonded to aliphatic carbon. ∼7 ppm is attributed to the some percent of $CHCl_3$ impurity in $CDCl_3$ solvent. There is no noticeable peak at high ppm region of ∼12 ppm which indicates that the -COOH end groups on ACPA are

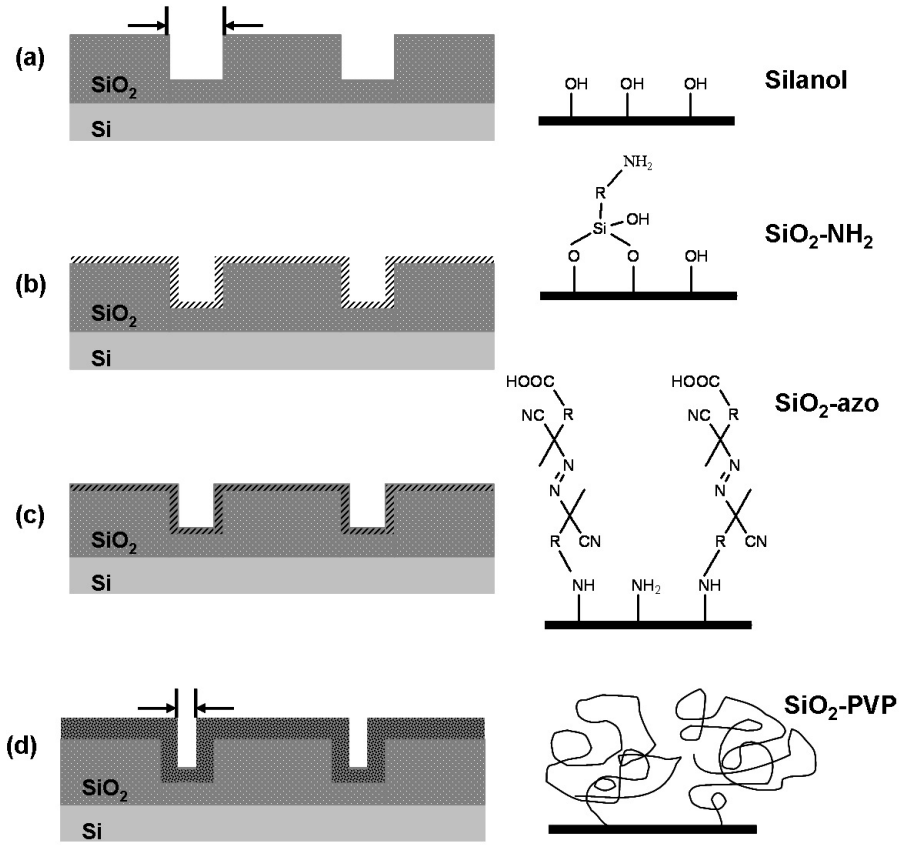

Figure 4.3: Schematic illustration of NMM process. (a) EBL followed by RIE, (b) surface functionalization of SiO_2 nano-patterns with amino groups, (c) surface modification of SiO_2 nano-patterns with azo-based initiators, (d) free radical surface initiated polymerization (SIP) to covalently grow functional polymer PVP brushes, SiO_2-PVP.

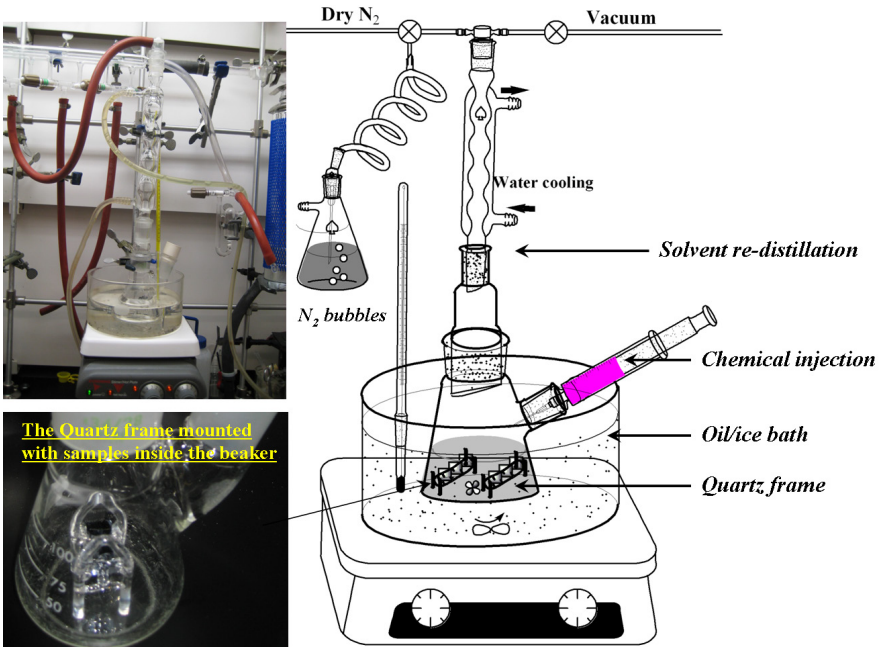

Figure 4.4: Reaction apparatus: a closed dry-N_2 enviroment for SIP process.

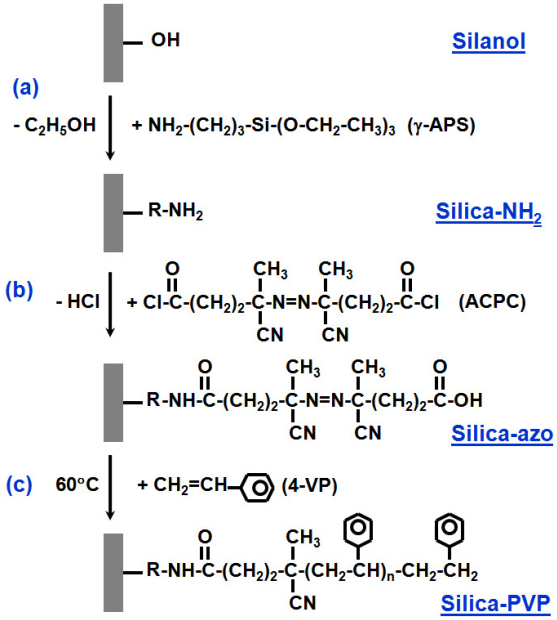

Figure 4.5: Schematic illustration of surface initiated polymerization on SiO_2 chip surface. (a) Surface modification by amine-terminated silane agent γ-APS to introduce amino groups onto substrate surface, (b) Immobilization of azo-initiator (ACPC) onto substrate surface by condensation reaction between surface amino groups and ACPC chloride groups, (b) Free radical surface polymerization initiated by the immobilized ACPC azo-initiator at 60 °C producing PVP polymer layer.

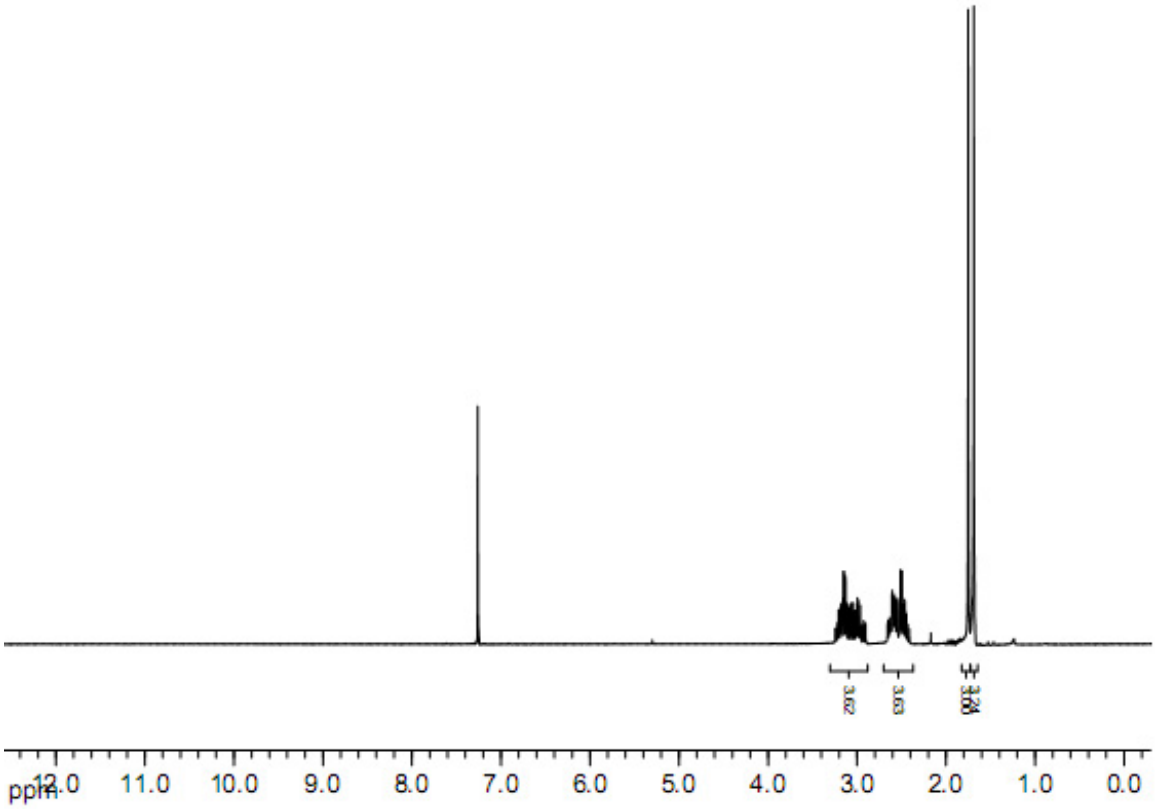

Figure 4.6: ^{1}H-NMR spectroscopy of 4,4'-azobis-(4-cyanopentaoic chloride) (ACPC).

successfully modified to acid chloride -COCl end groups.

4.2.4.2 NMM Process

Figure 4.7 shows SEM (Zeiss SEM Ultra60) images of a series of SiO_2 nano-trenches before and after SIP. As observed, the feature size is significantly reduced from the original 85 nm produced by "top-down" EBL/RIE (Figure 4.7(a)) to 35-45 nm after SIP (Figures 4.7(b)-(d)), resulting in a 50 nm size reduction in trench width. Additionally, the surface composition and functionality are chemically modified from the original hydrophilic SiO_2 to organic polyelectrolyte PVP with tailored biochemical compatibility. The grafted PVP molecules appear as particles in varied sizes of 5-30 nm (Figure 4.7(b)). In general, the size (the radius of gyration) of specific polymer molecules is affected by the average molecular weight (M_w), its polydispersity-PDI

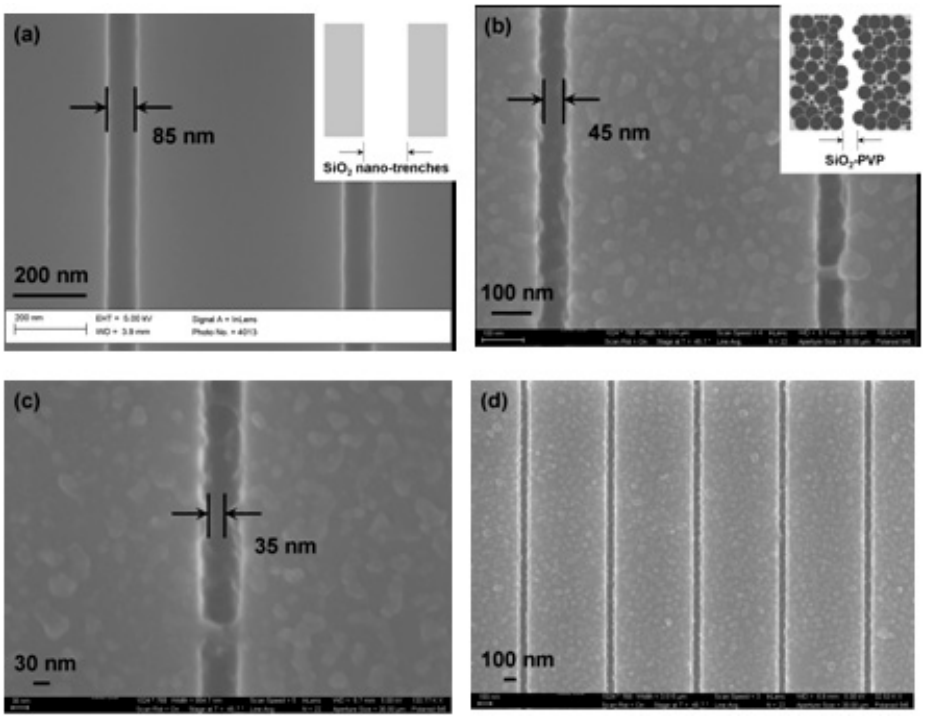

Figure 4.7: SEM images of SiO_2 nano-trenches (top view) (a) with 85 nm in width before SIP, (b) and (c) with the reduced width of 45 nm and 35 nm after SIP, respectively, and (d) in a lower magnification after SIP. The insets are cartoon illustrations before and after SIP.

(M_w/M_n), and its external environment [104]. The observed variation in size of the obtained PVP molecules can be explained by two factors: (1) the compact self/inter-entanglement of polymer chains since the sample surface is completely dried; and (2) a high molecular weight polydispersity (PDI) resulting from the free radical polymerization mechanism. The variation in size of grafted PVP molecules results in zigzag profiles of nanotrenches which are curved on the grafted polymer's molecular scale as illustrated in the insets of Figures 4.7(a) and (b).

Sub-10 nm trench patterns with functionalized surfaces are also obtained as shown in Figure 4.8. Both top and lateral views of the nanotrenches are compared. The observed feature size is apparently reduced from the original 65 nm (Figure 4.8(a)) to a molecular scale of sub-10 nm, e.g. 4 nm (Figure 4.8(b)) with a scalar reduction of approximately 55 nm. There is a noticeable size variation of approximately

15 nm between the minimum and maximum widths of the nanotrenches (i.e. 4 nm and 20 nm, see Figure 4.8(b)) which is of the same dimensions as the grafted PVP molecules. This implies that the resolution of this hybrid approach is affected by the size of the entangled polymer chains. When the patterned feature size and the grafted polymer molecules are on the same scale, the feature size variation in the nanopattern becomes apparent. Furthermore, Figure 4.8(d) shows a 20 nm thick continuous polymer layer which conformally coats the sub-70 nm nanotrenches, demonstrating the ability of SIP in conformally depositing ultrathin PVP polymer layer onto the entire patterned region. Compared to the SIP chemical deposition method, physical deposition or physisorption, including spin-casting and spray coating, can in principle also produce an ultrathin polymeric layer (a few nanometers) on nanopatterned substrate surfaces. However, the non-covalent adsorption may result in instability of the deposited ultrathin layer.

The sample surface elemental composition is characterized by X-ray photoelectron spectroscopy (XPS) (SSX-100, Al K-α radiation, 1486.6 eV). Figure 4.9 shows a series of XPS wide-energy scans on the sample after nanolithography (EBL and RIE) (Figure 4.9(a)), after surface modification with amino groups (SiO_2-NH_2) (Figure 4.9(b)), and after SIP (SiO_2-PVP) (Figure 4.9(c)), respectively. It is observed that the peak counts of C1s and N1s increase while O1s counts decrease for the samples SiO_2 (Figure 4.9(a)), SiO_2-NH_2 (Figure 4.9(b)) and SiO_2-PVP (Figure 4.9(c)), indicating successful introduction of amino groups and PVP brushes during fabrication as illustrated in Figures 4.3(b) and 4.3(d) respectively. C, N and O atomic weight ratios for each sample calculated from XPS results are listed in Table 4.1. The calculated ratio of C to N in the SiO_2-PVP sample obtained after SIP, 6.8, is very close to the theoretical value of 7 for PVP, indicating that PVP brushes are properly grafted onto nanopatterns at the molecular scale.

In general, it is technically more difficult to achieve a proper SIP on a recessed

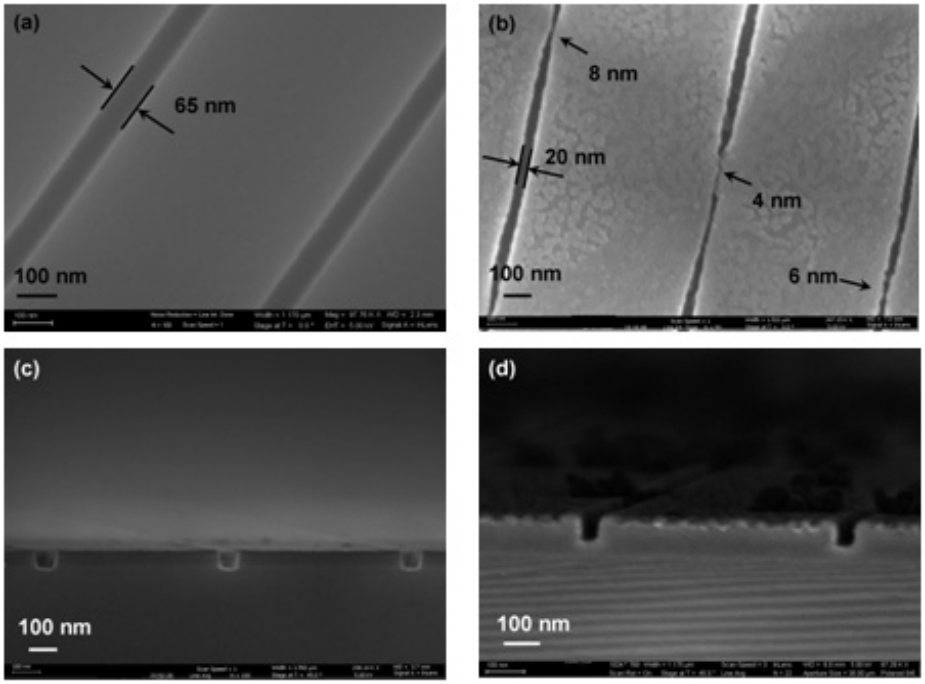

Figure 4.8: SEM images of SiO_2 nanotrenches (a) with 65 nm in width before SIP (top view), (b) with reduced size down to 4 nm after SIP (top view), (c) lateral view of nano-trenches with 65 nm sized opening before SIP, (d) lateral view of nano-trenches with reduced opening size after SIP.

Table 4.1: Elemental Compositions of SiO_2 nano-pattern surface in SIP.

Sample No.	Atom Weight %		
	C1s	***N1s***	***O1s***
a	15.42	0	84.58
b	40.21	5.08	54.71
c	64.38	9.40	26.22

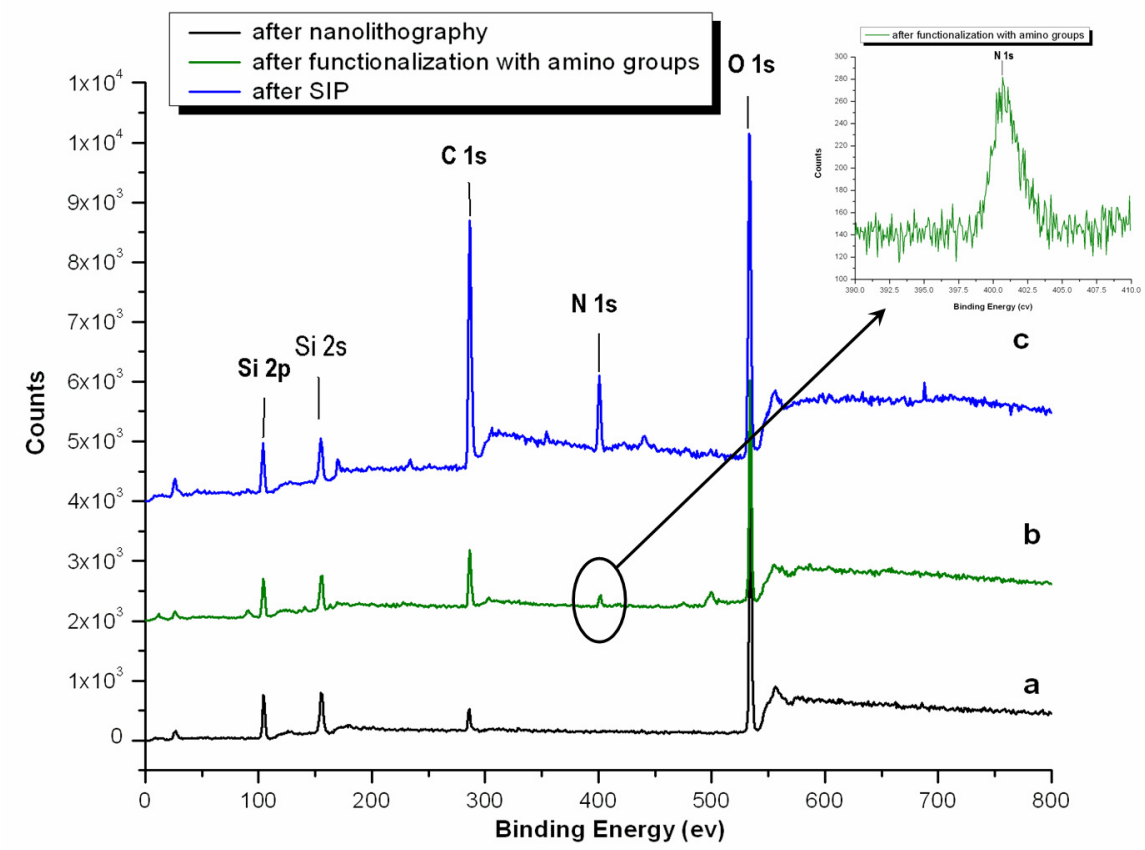

Figure 4.9: Wide-scan XPS spectra of SiO_2 nano-pattern surface (a) after "top-down" nanolithography, (b) after surface modification with amino groups (SiO_2-NH_2) and (c) after SIP (SiO_2-PVP). The insert is N1s XPS spectra of sample b.

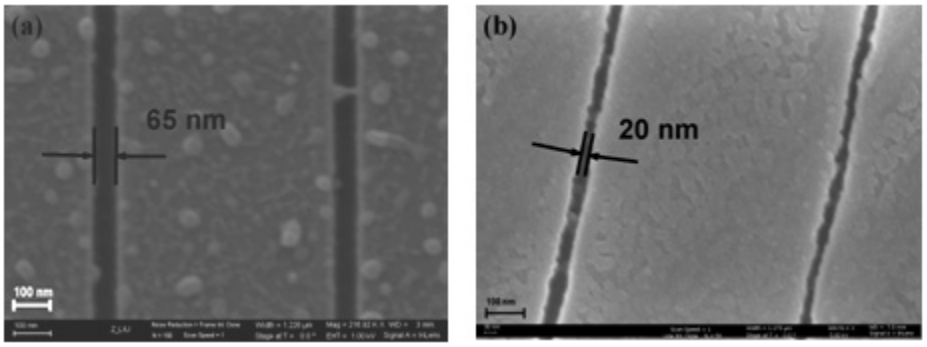

Figure 4.10: SEM images of SiO_2 nanotrenches after SIP (a) without and (b) with degassing.

nanopattern than on a protruding structure. In addition, patterning nano-sized recessed features becomes even more challenging when the feature size becomes smaller than 100 nm. A few studies have reported the successful grafting of polymers on protruding nanopatterns to amplify the pattern profile [65, 121], but very few on recessed nanopatterns at the sub-100 nm scale. In our study, one of the key factors that determine the success of grafting polymer brushes on the side walls of nano-trenches is the effective removal of the air trapped inside the nanotrenches prior to any chemical reaction. This problem is addressed by degassing the device under ultrasonication. As shown in Figure 4.10, only after degassing can the reactive chemicals enter into the nanotrenches for the following modifications to occur.

The utilization of free-radical SIP in this hybrid NMM is more convenient compared to using atom transfer radical polymerization (ATRP) [107] or living free-radical polymerization [121] for surface grafting, since it requires less stringent experimental conditions and reaction steps. In addition, this work does not require an additional process of nanometer-scale "lift-off" to pattern gold for anchoring thiol-based initiators [65, 107].

In summary, we have demonstrated a hybrid nanofabrication approach NMM by integrating "bottom-up" SIP into "top-down" EBL. The proposed method enables the capability of precisely producing molecular-scale structures down to 4 nm. Also,

it allows the potential of chemically tuning the pattern with proper bio/chemical functionalities to interact with the molecules of interest simply by choosing specific polymers. Further, this approach could be useful to fabricate extensive functional nanomachines including artificial heterogeneous enzymes/catalysts/molecular manipulation templates for activating favorable reactions as well as templates for assembling molecules, controlling molecules' conformations, and hierarchic integration, as are predicted and conceptually shown in Figure 4.1. The following section 4.3 takes the first steps in this direction, fabricating molecular manipulation templates by exploiting the developed NMM method for mechanochemical synthesis of 3D nanostructures (section 4.4). The templates are analogous to biocatalysts enzymes.

4.3 NMM Fabrication of Molecular Manipulation Templates

4.3.1 Background and Motivation

The NMM strategy that we demonstrated in section 4.2 enables "top-down" precise design and fabrication of artificial molecular assembler or molecular manipulation templates for synthesis of 3D nanostructures. Although traditional "bottom-up" strategies seem a natural approach for the fabrication of nanoparticles, since our knowledge of specific manipulation of "bottom-up" processes is limited, it is challenging to ideally control the fabrication process, and produce desirable nanostructures. In this section, we design and demonstrate a series of prototype molecular manipulation templates with both chemical and physical anisotropies by exploiting the NMM process for the proposed molecular assembly and synthesis of 3D nanostructures. Such programmed 3D nanoparticles can be used as enhanced therapeutic agents [36, 87, 114], as well as to mimic hierarchical assemblies and multiple classes of enzymes widely existent in the biochemical world [138].

4.3.2 Fabrication

The fabrication process of the molecular manipulation template is outlined in Figure 4.11. It begins with "top-down" e-beam lithography (EBL). A silicon substrate bearing a thin Si_3N_4 film (60 nm, deposited by low-pressure chemical vapor deposition) is patterned by EBL (JEOL JBX-9300FS EBL system, 100 kV) followed by two-step reactive ion etching (RIE) to create a series of nanoholes (100 nm and 200 nm in diameter respectively), as well as nanotrenches (100 nm in width) with an aspect ratio of approximately 1:1 (Figure 4.11(b)). A thermal oxidation (1100 °C) is carried out to reduce the pattern feature size, simultaneously creating 3D SiO_2/Si_3N_4 nanostructures (Figure 4.11(c)). "Bottom-up" surface initiated polymerization (SIP) is then used to functionalize 3D nanostructures, selectively grafting a basic polyelectrolyte layer (poly(vinyl pyridine), PVP) onto the SiO_2 surface in order to further reduce the feature size (Figure 4.11(d)). The resultant nanostructures are used as "binding sites" for molecular assembly and mechanochemical synthesis (Figure 4.14), which will be discussed in section 4.4.

4.3.3 Experimental Results and Discussion

Figure 4.12 shows SEM (Zeiss SEM Ultra60) images of a series of resulting nanostructures in Si-based templates before (Figure 4.12(b)) and after thermal oxidation (Figure 4.12(c)). It is apparently observed (Figure 4.12(a)-(b)) that the feature size of nanostructures patterned by EBL/RIE is reduced from 200 nm to 80 nm (inserts in Figure 4.12(a)-(b)), and the structure also simultaneously develops a 3D "nanomushroom" morphology. The morphology evolution is due to the anisotropic thermal oxidation in crystal Si and the usage of a Si_3N_4 layer (60 nm) as a thermal oxidation mask layer. Similarly, the feature sizes of 100 nm nanoholes and 100 nm nanotrenches are miniaturized to sub-10 nm (inserts of Figure 4.12(d)), and their profiles are developed to 3D recessed "nanospikes" and "nanofibers" respectively (Figure

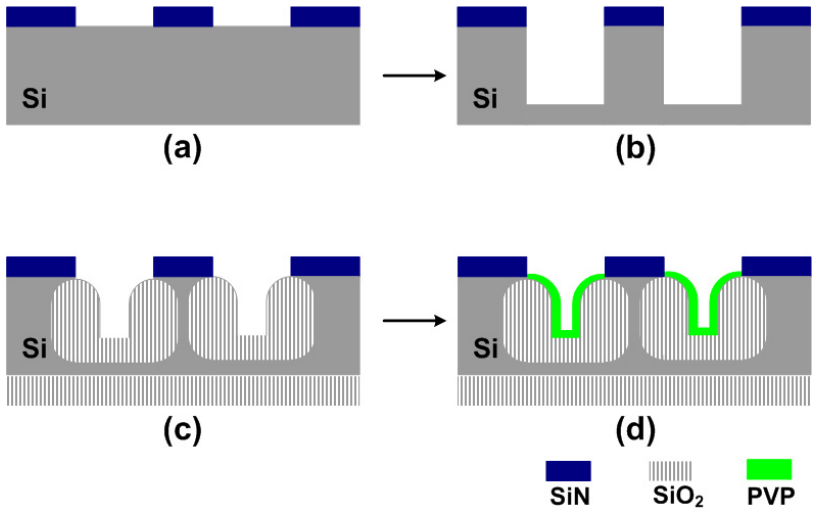

Figure 4.11: Schematic illustration of NMM fabrication of molecular manipulation templates. (a) EBL followed by RIE to pattern Si_3N_4 layer, (b) RIE to transfer the nanopattern into Si substrate, (c) thermal oxidation to reduce the feature size creating 3D SiO_2/Si_3N_4 nanostructures, (d) SIP to selectively functionalize the SiO_2 surface.

4.12(c)-(d)).

The resulting Si-based manipulation templates possess not only 3D physical nanostructures but also anisotropic surface functionalities through the grafted PVP polymers by SIP (Figure 4.11(d)). X-ray photoelectron spectroscopy (SSX-100, Al K-α radiation, 1486.6 eV) is used to characterize and compare the surface elemental composition of SiO_2 and Si_3N_4 control samples after SIP. The analysis result (Figure 4.13) reveals that the nitrogen peak (N1s, 400 eV) from the SiO_2 control sample after SIP corresponds to organic nitrogen from the grafted PVP polymer layer, and the nitrogen peak (N1s, 395 eV) from the Si_3N_4 sample correlates to the inorganic nitride, [92] which indicates that SiO_2 sample surface is successfully grafted by a PVP layer, while the Si_3N_4 sample surface remains the same. Composition analysis (Table 4.2) indicates that the molar ratio of C to N from SiO_2 sample surface is 6.9 which is very close to the stoichiometric ratio of C to N in pure PVP (7), while the ratio of Si to N from Si_3N_4 is 7.4 which is almost equal to the stoichiometric ratio of Si to N in Si_3N_4

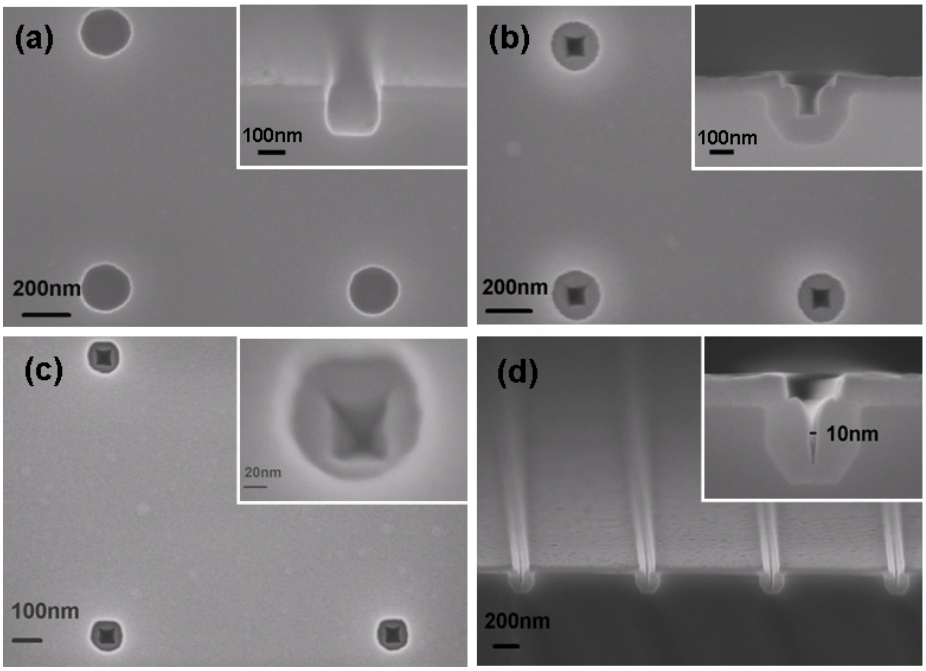

Figure 4.12: SEM images of 200 nm nanoholes (a) before and (b) after thermal oxidation, (c) 100 nm nanoholes after thermal oxidation, and (d) 100 nm nanotrenches after thermal oxidation. Inserts are corresponding lateral views in a higher magnification.

Table 4.2: Elemental Compositions of the SiO_2 and Si_3N_4 control samples after SIP.

Sample	Atomic Weight %			
	C	*N*	*O*	*Si*
Si_3N_4	41.01	9.87	34.47	14.65
SiO_2	45.70	7.73	32.96	13.61

(7.5). Therefore the chemical selectivity of SIP to SiO_2 rather than Si_3N_4 surface is demonstrated (Figure 4.11(d)).

4.4 Mechanochemical Synthesis of 3D Nanostructures

4.4.1 Background and Motivation

Nanoparticles hold significant promise as therapeutic agents in biomedical applications. However, there are a series of biological barriers in the body preventing them from efficiently localizing at their targets in sufficient amounts. For example, haemodynamic forces are effective barriers for injected nanoparticles to marginate and adhere onto vascular endothelia. Moreover, it is difficult to simultaneously attain preferential localization and avoid sequential biological barriers [114]. However, these issues can potentially be appropriately addressed by utilizing intrinsic 3D nanoparticles/nanostructures instead of simple constructs, e.g. 0D spherical or 1D tubular nanosubstances. Compared to 0D and 1D nanostructures, the forces acting on 3D nanoparticles are dependent on their orientation, surface property and surrounding environment. This would result in an enhanced performance of 3D nanostructures, e.g. *in situ* hierarchical assemblies with adaptable scales, chemically/physically tunable properties according to *in vivo* hydrodynamic and biological environments as well as improved margination and adhesive strength to the targets with a desirable therapeutic and imaging efficacy [87]. Oblate particles are demonstrated to adhere more effectively to the biological substrate than 0D spherical particles showing improved medical efficiency [36]. Therefore, 3D nanoparticles have been proposed as

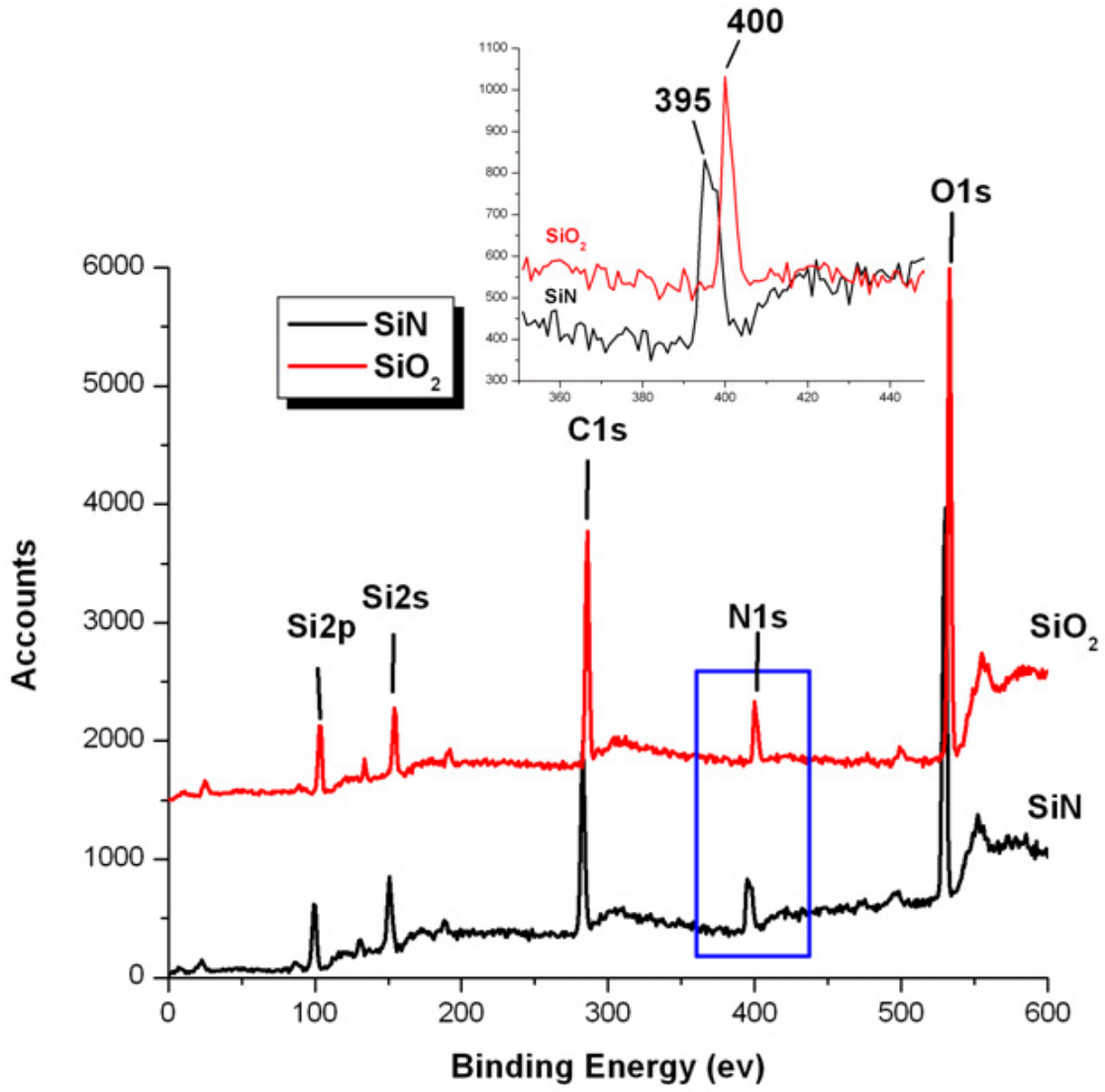

Figure 4.13: Wide-scan XPS spectra of SiO_2 and Si_3N_4 control samples after SIP. (black) Si_3N_4 sample after surface initiated polymerization. (red) SiO_2 sample after surface initiated polymerization.

improved therapeutic agents in biomedical applications, although advanced synthesis techniques remain largely unexplored in this area.

In this section we utilize the previously fabricated 3D manipulation templates to demonstrate the prototype NMM-driven "top-down" design and "bottom-up" synthesis of 3D polystyrene (PS) and polystyrene-iron oxide (PS-Fe_3O_4) composite nanostructures. Different types of 3D shapes with sub-10nm feature size have been successfully achieved including PS "nanomushrooms", PS "nanospikes", PS "nanofibers" and PS-Fe_3O_4 "nanoflowers". The specific motivations of study and synthesis of PS-Fe_3O_4 composite nanostructures are (1) to explore the fabrication feasibility of producing organic-inorganic hybrid nanostructures and (2) to investigate the corresponding performance of these magnetic 3D nanostructures by manipulating external magnetic field. Although surface fabrication techniques produce lower quantities of material compared to volumetric nanosphere synthesis, increased potency and specificity may compensate in many applications.

4.4.2 Materials

Water-soluble paramagnetic Fe_3O_4 nanocrystals (5 ± 2 nm in diameter) are prepared by a hydrolysis approach [42]. Typically, a sodium hydroxide (NaOH)/diethylene glycol (DEG) stock solution is prepared in advance by dissolving NaOH (50 mmol) in DEG (20 ml) at 120 °C for 1 hour under N_2 followed by cooling it down and keeping it at 70 °C. A mixture of poly(acrylic acid) (PAA, 288 mg), iron (III) chloride ($FeCl_3$, 3.55 g) and DEG (15 ml) are heated to 220 °C in N_2 atmosphere for 30 min under vigorous stirring forming a transparent light-yellow solution. A NaOH/DEG stock solution (4 ml) is injected rapidly into the above hot mixture. The reaction solution then turns black immediately. The resulting mixture is further heated for 10 min to yield magnetite nanocrystals with an average diameter of 5 ± 2 nm. Then the mixture is centrifuged. The product Fe_3O_4 is purified by three repeating cycles of re-dispersing

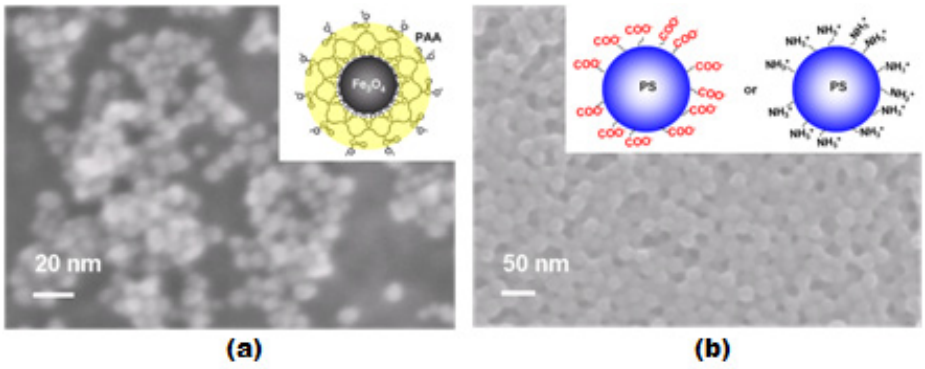

Figure 4.14: SEM images of (a) Fe_3O_4 nanoparticles (5 ± 2 nm in diameter, surface functionalized by PAA) and (b) PS nanoparticles (20 ± 5 nm in diameter, surface functionalized by carboxylic acid or amine groups). Inserts are schematic illustrations of the nanoparticle structures respectively.

in aqueous ethanol solution (ethanol:DI water = 1:1) and centrifugation. The purified Fe_3O_4 nanopaticles are characterized by SEM as shown in Figure 4.14(a). They would present negative charge in aqueous solution due to the surface functionalized PAA (see insert in Figure 4.14(a)).

The surface functionalized polystyrene spherical particles (20 ± 5 nm in diameter) were purchased from Molecular Probes Inc., USA, and characterized by SEM as shown in Figure 4.14(b). They present negative (surface carboxylic acid groups) or positive (surface amine groups) charge in aqueous solution respectively due to their respective surface functionalities (see insert in Figure 4.14(b)). All other chemicals were purchased in A.C.S. grade from Sigma-Aldrich chemical company, USA.

4.4.3 Synthesis

Figure 4.15 schematically illustrates the nanoscopic mechanosynthesis of 3D PS nanostructures utilizing the fabricated manipulation templates. The target molecules are 0D spherical PS nanoparticles (averagely 20 ± 5 nm in diameter) which are surface functionalized by carboxylic acid groups (-COOH) and suspended in aqueous solution in a concentration of 5×10^{11} to 5×10^{14} ml^{-1}. The template is first immersed in the

nanoparticle suspension, and ultrasonication is performed (30 min) for degassing of the entire system. A dip-coating technique is then used to uniformly introduce arrayed nanoparticles onto the template surface in a large area [63] (Figure 4.15(b)) using the setup shown in Figure 4.16. The substrate (approximately 10mm×15mm) is first vertically immersed into the nanoparticle suspension, and then pulled upward at a constant rate of 50 μm/min. The template is subsequently immersed into an alkaline bath (pH = 13-14), e.g. ammonium hydroxide ($NH_3 \cdot H_2O$) followed by ultrasonication (10∼15 min). This treatment causes the physisorbed nanoparticles to partition to the alkaline solution. Meanwhile, the remaining nanoparticles that are trapped in the artificial 3D nanostructure sites mechanically rub against each other and locally heated by the generated friction. The frictional heat allows the nanoparticles to melt and replicate the template's 3D sites. Additional annealing step is applied (100 °C, 1 hour) to facilitate the accomplishment of conformal replication (Figure 4.15(c)). Finally, the resulting 3D nanoreplicas are solution extracted from the sites by aqueous alkaline solution ($NH_3 \cdot H_2O$, pH=13∼14, 8∼10 hours) accompanied by an additional ultrasonication of 5 min. The 3D sites are thus ready for the next mechanochemical synthesis, mimicking a chemical or bio-catalyst (Figure 5.15(d)).

Similarly, 3D polystyrene-iron oxide composite nanostructures are synthesized using similar manipulation templates. Figure 4.17 schematically illustrates the nanofabrication process for 3D PS-Fe_3O_4 composite nanostructures adopted from the developed process illustrated in Figure 4.15. In particular, the lab-made water-soluble paramagnetic Fe_3O_4 nanoparticles (5 ± 2 nm in diameter) present negative charges in aqueous solution, while the PS nanoparticles (20 ± 5 nm in diameter) present positive charges (see insert in Figure 4.17). Both of them are suspended in DI water in a number ratio of Fe_3O_4 to PS approximately equal to 10:1. There is a probability of these mixed nanoparticles forming a composite structure due to the ionic associations (see insert in Figure 4.17). The process begins with a degassing step by

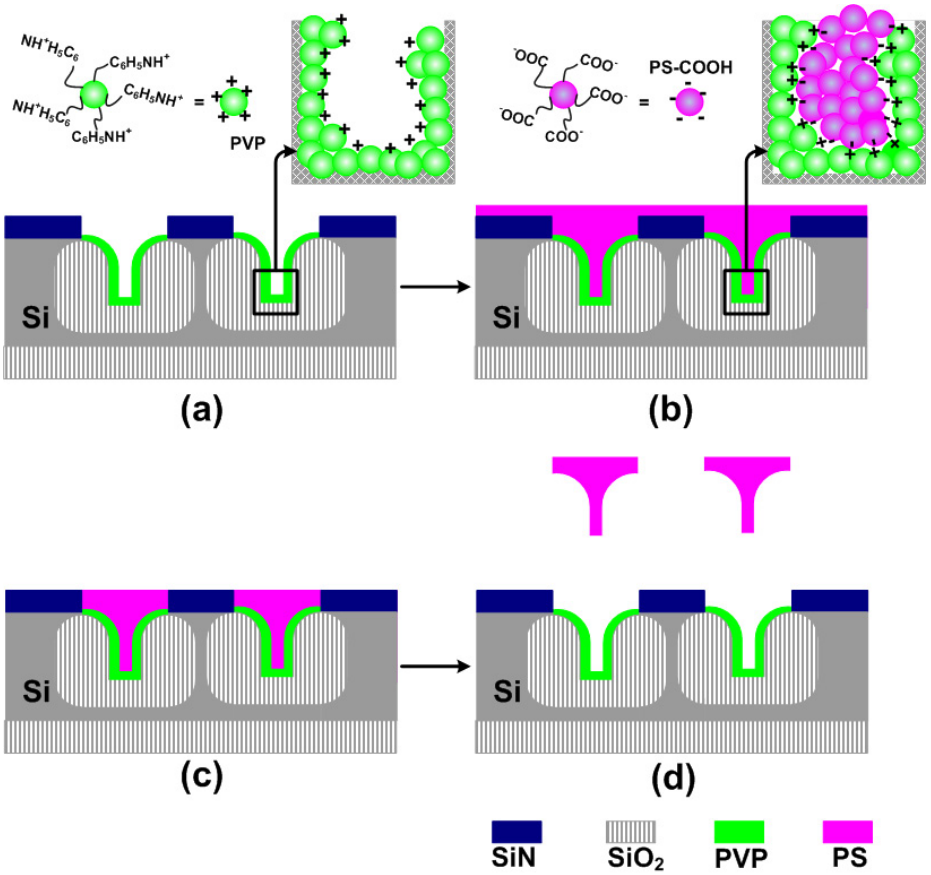

Figure 4.15: Schematic illustration of mechanosynthesis of 3D nanoparticles utilizing molecular manipulation templates. (a) immersion of the template in the nanoparticle suspension followed by degassing (5 min), (b) the dip-coating process at a constant rate of 50 μm/min, (c) removal of physically deposited nanoparticle residues by ultrasonicating the template in an alkaline bath (pH = 13-14) for 10-15 min followed by annealing the template at 100 °C for 1 hour, (d) releasing 3D replicated nanostructures by solution extraction (NaOH or $NH_3 \cdot H_2O$, pH = 13-14, 8∼10 hours) with an additional ultrasonication of 5 min.

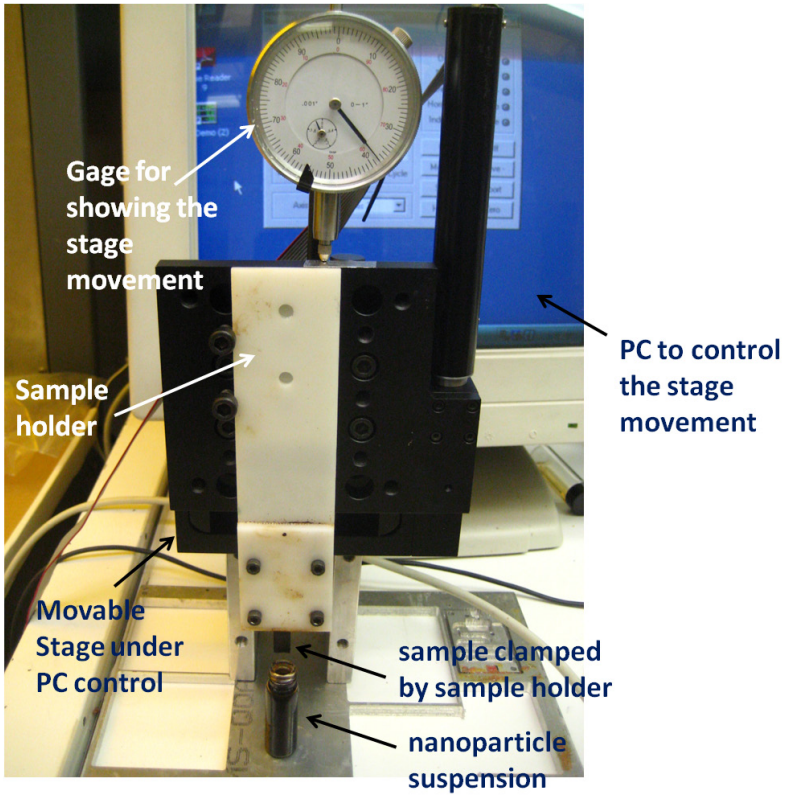

Figure 4.16: the apparatus for solution dip-coating process to uniformly introduce arrayed nanoparticles onto the template surface. The chip is clamped and held by the sample holder above the suspension solution. The sample holder is fixed on the movable stage which is programmed and controlled by the computer. There is a gage showing the movement of the stage either upward or downward.

immersing the templates in nanoparticle suspension under ultrasonication (30 min). A dip-coating process (50 μm/min) uniformly introduces the nanoparticle composite onto the template surface followed by annealing (120 °C, 2 hours) (Figure 4.17(b)). A cleaning procedure is carried out (Figure 4.17(c)) to release the physically adsorbed PS-Fe_3O_4 composite to aqueous solution by immersing the template in an alkaline bath ($NH_3{\cdot}H_2O$, pH = 13$\sim$14) under ultrasonication (5 min). The resulting replicated PS-Fe_3O_4 3D nanostructures are eventually extracted by the same alkaline solution (24 hours) accompanied by an ultrasonication (5 min) (Figure 4.17(d)). Then the template is ready for next cycle of synthesis analog to the chemical reaction catalyst.

4.4.4 Experimental Results and Discussion

4.4.4.1 3D PS Nanostructures

SEM images in Figure 4.18 show the mechanosynthesis procedure utilizing the prepared manipulation template with a 3D "nanomushroom" design. Figure 4.18(a) shows the resulting template surface morphology after the dip-coating process in the PS nanoparticle suspension as indicated in Figure 4.16(b), and Figure 4.18(b) presents the result after surface cleaning by alkaline solution as illustrated in Figure 4.16(c). The released 3D PS "nanomushroom" particles and their self-assemblies are shown in Figures 4.18(c) and (d) respectively. The inserts in Figure 4.18 are magnified SEM images of individual 3D nanostructures. The obtained cap diameter of the "mushroom" is 200 nm, and the width of the square stalk is 80 nm, indicating a conformal replication of the 3D sites in the templates. Therefore the feasibility of "top-down" design and fabrication of 3D PS nanostructuers is successfully demonstrated, which proves the concept of nanolithography-based molecular manipulation (NMM).

During mechanosynthesis, the surface functionality of the manipulation template plays an important role for molecular registration and assembling. It is observed that molecular targets deposited on bare Si_3N_4 surface can be efficiently removed by the alkaline solution under ultrasonication (5 min) (Figure 4.16(c)) which is understood

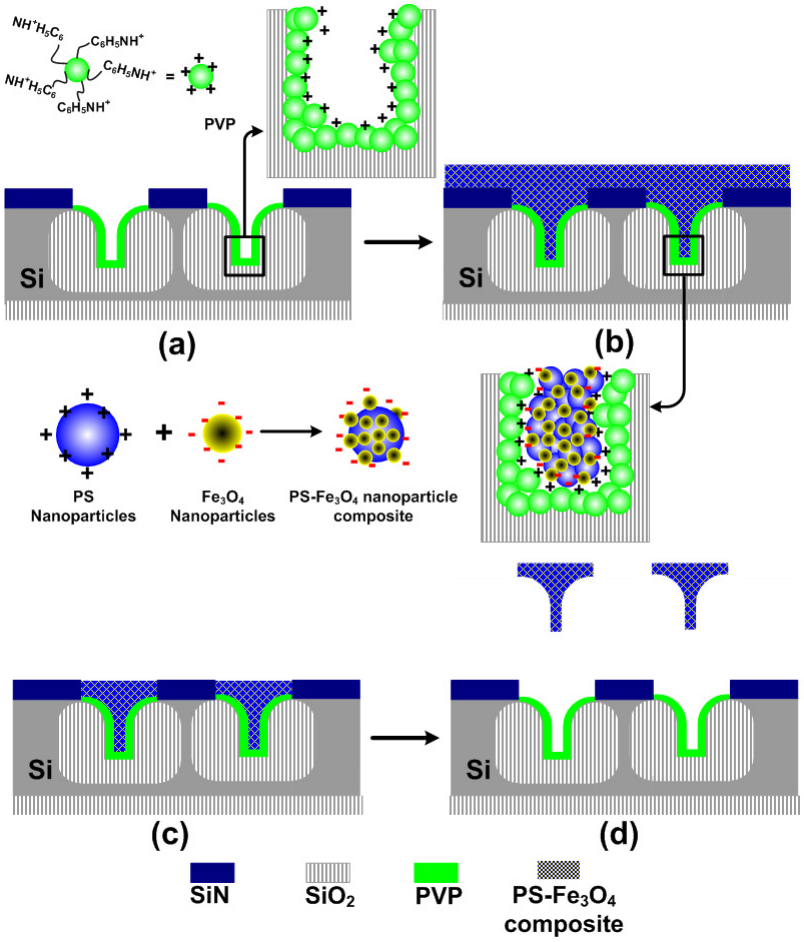

Figure 4.17: Schematic illustration of nanoscopic synthesis of 3D polymer-magnetite composite nanostructures. (a) immersion of the template in aqueous PS-Fe_3O_4 nanoparticle suspension followed by degassing (5 min), (b) the dip-coating at a constant rate of 50 μm/min followed by annealing at 120 °C for 2 hours, (c) removal of physically adsorbed PS-Fe_3O_4 nanoparticles by soaking the template in an alkaline bath (pH = 13∼14, 5 min) accompanied with ultrasonicating, (d) solution extraction to release the resulting 3D PS-Fe_3O_4 composite nanostructures ($NH_3{\cdot}H_2O$, pH = 13∼14, 24 hours) followed by an ultrasonication (5 min).

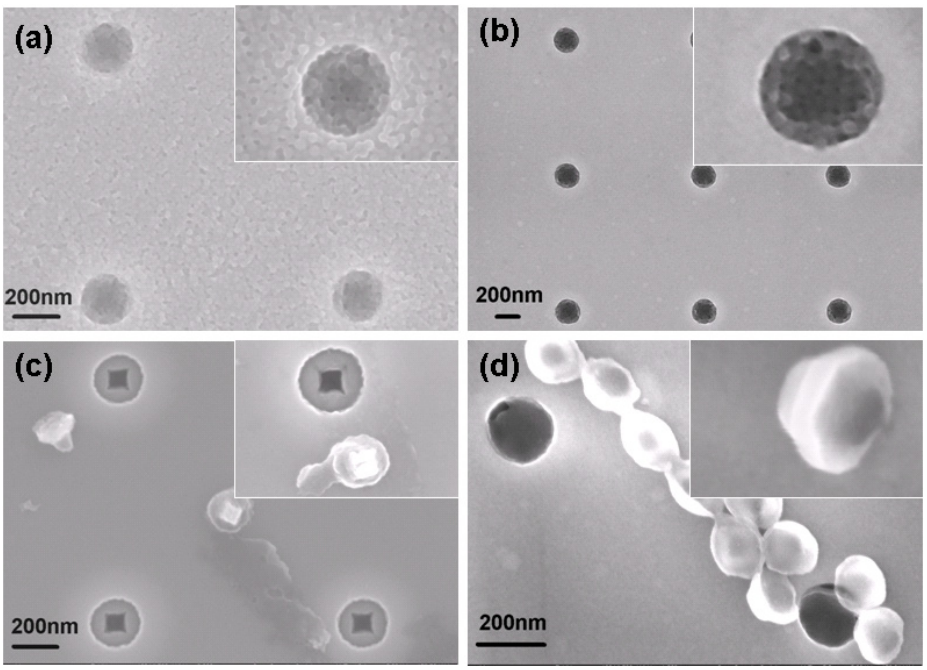

Figure 4.18: SEM images of nanomanipulation templates with 200 nm hole design (a) after dip-coating in PS nanoparticles suspension, (b) after cleaning by alkaline solution, (c) the released 3D PS "nanomushroom" and their self-assemblies. Inserts are magnified SEM images of individual structures.

due to the weak physical/static interactions between PS nanoparticles and Si_3N_4 surface. In contrast, nanoparticles that are assembled to the 3D polymer grafted SiO_2 sites have higher resistance to the attack of the alkaline solution. It is primarily due to a combination of physical and chemical protections from 3D nanosites (insert in Figure 4.15(b)). The yield based on this fabrication process is approximately 50%∼70%.

Similarly, "nanospikes" and "nanofibers" are also successfully synthesized as shown in Figure 4.19. The obtained "spike" cap is 100 nm in diameter, and the "spike" tip is sub-10 nm (Figures 4.19(a) and (b)). The achieved "nanofibers" have a feature size of sub-10 nm (Figures 4.19(c) and (d)). A very careful comparison between the resulting polymer nanostructures and the manipulation template indicates that the products

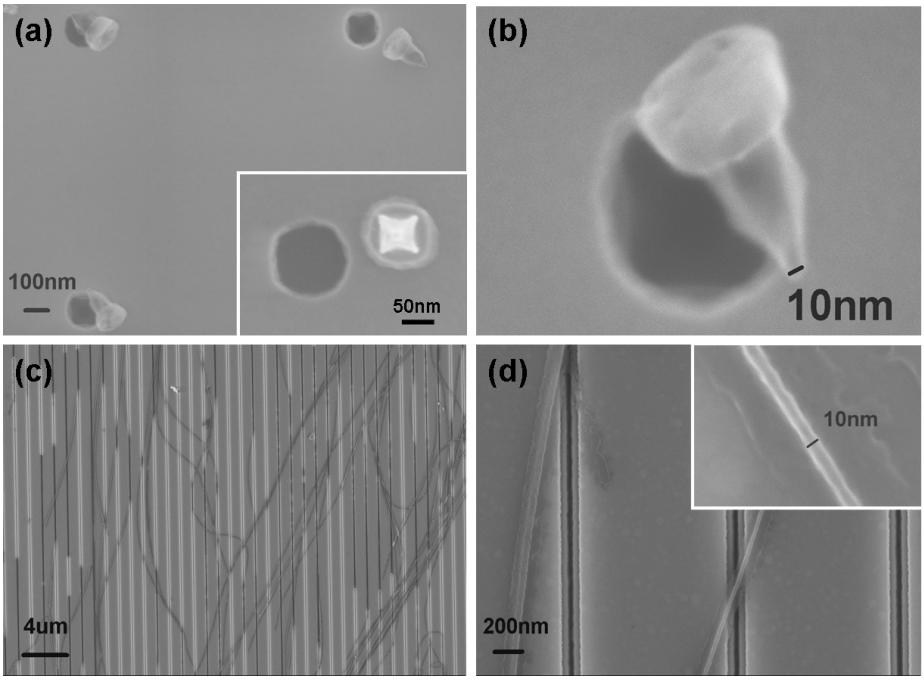

Figure 4.19: SEM images of resulting 3D replicated nanostructures. (a)-(b) "nanospikes", (c)-(d) "nanofibers". Inserts are amplified images.

have properly replicated the shape and dimension of 3D sites on the templates, although the tips of the "nanospikes" and the critical dimensions of the "nanofibers" achieved are still slightly "fatter" than their counterparts in the templates (approximately $1 \sim 2$ nm) (Figure 4.12(d)). It is attributed to the low surface tension and the limited wetting capability of amorphous hydrophobic polystyrene molecules on the SiO_2 surface. This issue could be potentially addressed by decreasing the molecular weight [76], reducing molecular size, or replacing PS by some other less hydrophobic molecule.

4.4.4.2 3D PS-Fe_3O_4 Composite Nanostructures

In addition to the 3D PS nanostructures, 3D polystyrene-iron oxide composite nanostructures, named as PS-Fe_3O_4 "nanoflowers", have also been successfully demonstrated using 3D nanohole templates. The essential motivations of conducting this

piece of work are (1) to study the fabrication feasibility of 3D organic-inorganic hybrid nanostructures using the demonstrated NMM strategy and (2) to investigate and understand the performance of these 3D magnetic nanostructures in an external controlled magnetic field with an attempt to properly manipulate them for applications. The template has a feature size of 50 nm (Figure 4.20(a)) which is properly preserved in the resulting composite "nanoflowers" (Figures 4.20(c)-(d)). It is also noticed that the resulting composite nanostructures have missed some structural details as the template sites have, such as the total height and precise square shape of the center feature. It is attributed to the implementation of Fe_3O_4 component to PS polymer for 3D nanostructure synthesis. The Fe_3O_4 nanoparticle is a metallic oxide unlike the PS component. During annealing (120 °C) Fe_3O_4 cannot melt, flow and wet the SiO_2 surface leading to difficulties of replicating the 3D nanosites. Therefore the resulting 3D nanostructures possess a similar shape and feature size as held by the 3D template sites however with more replication defects.

In fact, the issue associated with Fe_3O_4 component becomes severe when using the template with sub-20 nm feature size for synthesis. Figure 4.21 represents the typical nanohole template with sub-20 nm feature size as well as the resulting 3D replicated "nanoflowers". It can be apparently observed that the produced 3D "nanoflowers" have some similarities with the template 3D sites, but without too many feature details. This technical issue might be solved by careful selection and modification of the material component. It would form a part of future study.

The synthetic PS-Fe_3O_4 nanostructures and their aggregations show ferromagnetic properties in a gradient magnetic field as shown in Figure 4.22. Future study will be the characterization of the synthetic 3D nanostructures in a given external field to exploit the interrelationship between 3D nanostructure morphology and their performance for nanomedicines applications as conceptually illustrated in Figure 4.23.

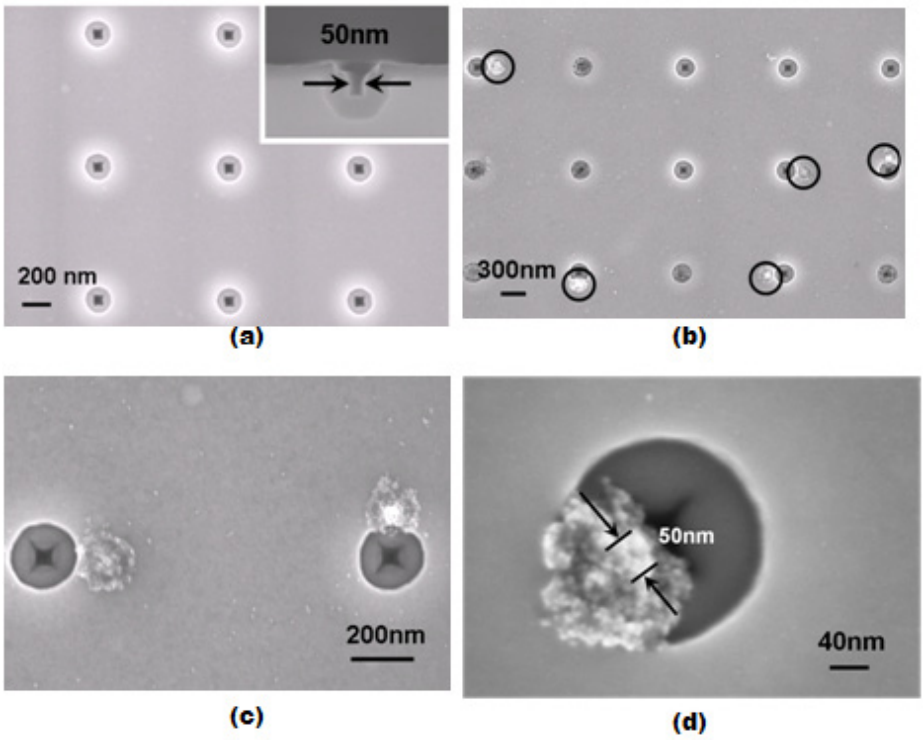

Figure 4.20: SEM images of prepared molecular manipulation template (a) and PS-Fe_3O_4 "nanoflowers" (b-d) with "petals" and "stamens" of 200 nm and 50 nm in diameter. The insert is the amplified lateral view of the template.

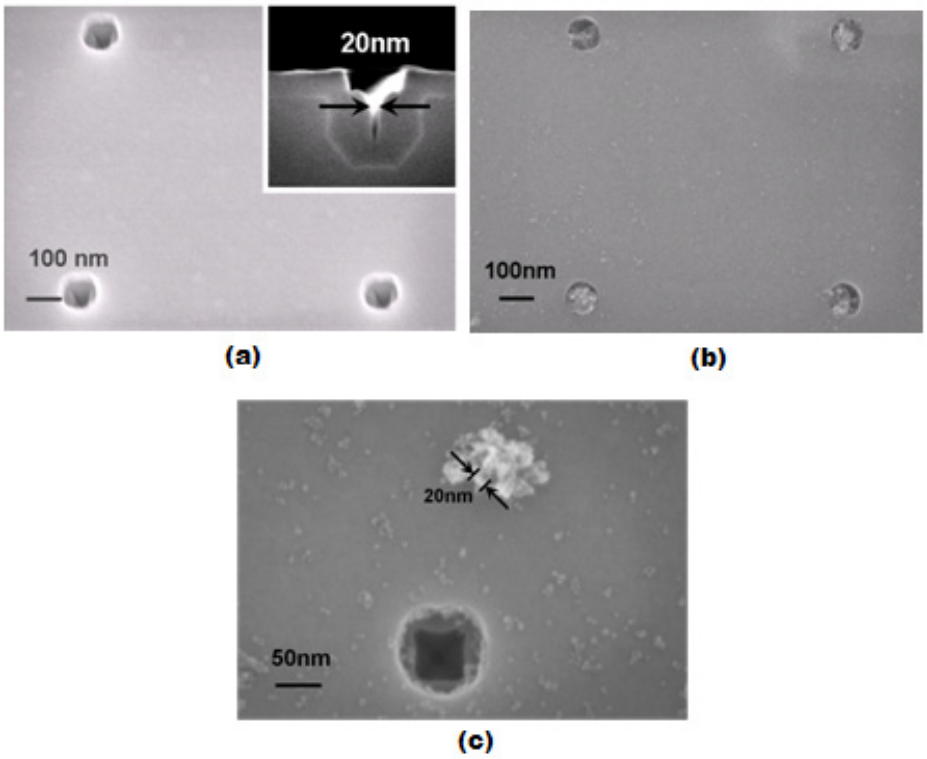

Figure 4.21: SEM images of 3D nanohole manipulation template (a) and 3D PS-Fe_3O_4 "nanoflowers" (b-c) with "petals" (100nm in diameter) and "stamens" (20 nm in diameter) respectively.

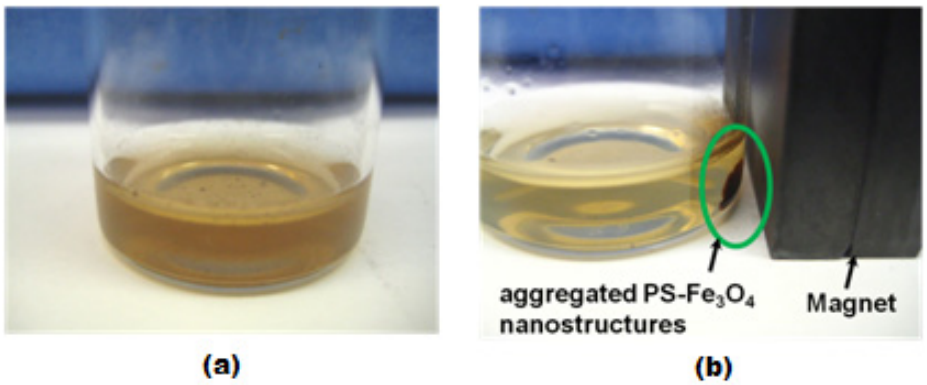

Figure 4.22: Photos of the response of released PS-Fe_3O_4 composite particles in aqueous solution without (a) and with (b) gradient magnetic field.

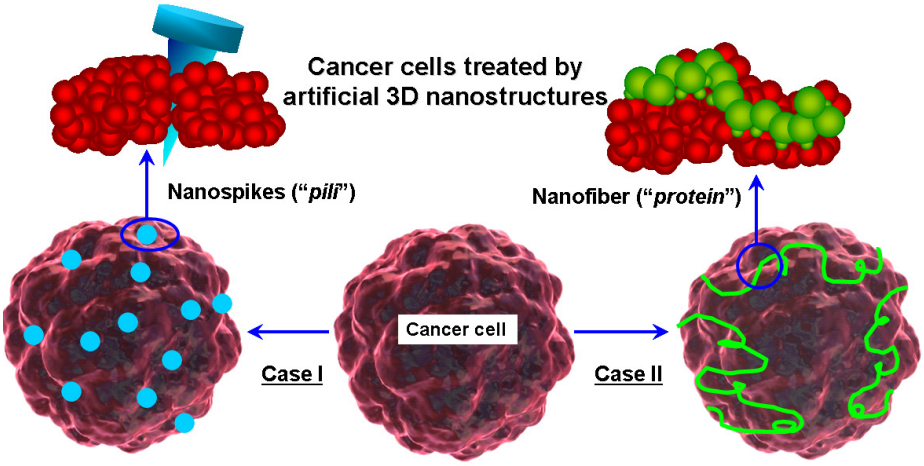

Figure 4.23: Schematic illustration of the potential medical applications of 3D nanostructures.

4.5 Chapter Summary

In a summary of this chapter, we successfully demonstrated the hybrid strategy of nanolithography-based molecular manipulation (NMM) by integrating "top-down" electron beam lithography with "bottom-up" surface initiated polymerization. It allows us to combine "top-down" precise design with "bottom-up" molecular size scale to create designated surfaces and volumes that can properly interact with molecules in a designated way. Experimentally a series of prototype molecular manipulation templates with 3D sub-10 nm sites and anisotropic surface functionalities are successfully fabricated by this approach. Such templates can properly "bottom-up" assemble polymer nanoparticles and mechano-chemically synthesize various polymeric 3D nanostructures. Different types of 3D nanostructures with sub-10 nm feature size are demonstrated in this work including PS "nanomushrooms", PS "nanospikes", PS "nanofibers" and PS-Fe_3O_4 "nanoflowers". The proposed NMM approach allows us the capability of "top-down" design and precise fabrication of various morphological features of nanostructures. Although this surface fabrication technique produces

relatively low quantitities of 3D nanostructures compared to the "bottom-up" volumetric classical chemical synthesis, increased potency and specificity may compensate in many applications. A number of potential applications can be envisaged by the demonstrated 3D nanostructures, such as improved medical agents. Most importantly, this strategic method enables us to manipulate molecules and fabrication procedures in a designated way with a great precise control. Although it is still in the early stage, it shows great promise and potential to advance molecular nanotechnology for various potential applications.

CHAPTER V

CONCLUSION

5.1 Thesis Summary

The motivation of this research was to explore advanced micro/nano patterning techniques for molecular manipulation by developing "top-down", "bottom-up" and hybrid approaches. The objectives were (1) to minimize the feature size bridging microns to nanometers and therefore the macromolecular scale to the molecular scale; and (2) to combine "top-down" precise design with "bottom-up" molecular processes to create designed surfaces and volumes to interact with molecules in a designated way.

The first study of "top-down" Inclined Nanoimprinting Lithography (INIL) allows the production of 3D nanopatterns of varying heights in a single step by manipulating anisotropic dewetting of polymers. The degree of asymmetry can be controlled by adjusting the magnitude of the inclination angle. It also allows feature size reduction from micrometers to nanometers. The underlying INIL mechanism was investigated and determined to be due to the inclination-dependent shear force on the polymer, leading to anisotropic polymer dewetting and consequent 3D nanopatterns with multiple heights. INIL is an inexpensive and convenient 3D nanofabrication approach. It is also compatible with other techniques allowing conformal pattern transfer from the polymer ink layer to other materials including silicon, PDMS silicone rubber, and metallic gold. Various nano-scale functional devices can be envisaged by the developed INIL technique including angle-resolved plasmonic/photonic crystals, solar cells and 3D chiral nanostructures/systems.

The second study has demonstrated that "bottom-up" non-covalent molecular imprinting is a viable strategy to produce tailor-made imprinted polymers (MIPs) with molecular scale feature size and functionality. In particular, MIPs capable of binding and sequestering the X-ray contrast agent iodixanol for biomedical applications was investigated. The produced synthetic imprinted polymers (MIPs) can properly recognize and efficiently bind iodixanol molecules in a desirable amount both in aqueous and sheep plasma solutions. The binding capacity and imprinting effect of MIPs can be optimized by tuning the functional monomer(s), the molar ratios between templates, functional monomers and crosslinkers as well as the solvent(s). The binding capacity and imprint effect of MIPs can be affected by the initial assay concentration and the binding time. The demonstrated MIPs are very encouraging for renal protection. MEMS-based sensor and nanomedicine applications are also envisaged by combining MIPs with "top-down" fabricated physical devices.

The third study of nanolithography-based molecular manipulation (NMM) realizes the combination of a "top-down" precise design with "bottom-up" size scale to create designed surfaces and volumes that can properly interact with target molecules in a designated way. It can conveniently and properly reduce the feature size from nanometers to sub-10nm. Various prototype molecular manipulation templates with different surface 3D nanostructures (sub-10 nm) and anisotropic surface functionalities can be fabricated by combining "top-down" electron-beam lithography (EBL) with "bottom-up" surface initiated polymerization (SIP). Such templates are able to recognize and assemble target molecules into designed 3D nanostructures mimicking the functionality of biocatalyst enzymes. Potential applications of the produced 3D nanostructures can be improved therapeutic agents for sensing and imaging due to the improved adhesion to the target. Although this demonstrated technique produces a relatively low quantity of 3D nanostructures compared to the classical "bottom-up" volumetric chemical synthesis, increased potency and specificity may compensate this

drawback in many applications.

5.2 Summary of Thesis Contribution

There are several contributions to both the academic and industry communities as a result of this work, not only by advancing the state-of-the-art nanotechnology but also by understanding associated fundamentals and underlying mechanisms. In particular both "top-down" and "bottom-up" nanofabrication approaches are studied, moreover, the prototype to the Nanolithography-based Molecular Manipulation (NMM) strategy has been demonstrated and studied as a pioneering effort. The most substantial contributions are summarized as follows:

5.2.1 Inclined Nanoimprinting Lithography (INIL)

To our knowledge, INIL (Inclined Nanoimprinting Lithography) is the first "top-down" approach demonstrated to produce 3D nanopatterns of varying heights in a single imprinting step. Significant advantages include (1) reduced process complexity, (2) high throughput with potential low cost, (3) process compatibility with other IC and MEMS techniques for conformally transferring such 3D nanopatterns into other materials. Furthermore, the process fundamentals are extensively studied, and the mechanism of shear force induced 3D asymmetric nanostructures is demonstrated. The thorough understanding of INIL theory, the associated factors and their relationship apparently allows us to design and adjust INIL in a precise manner. It is believed that the developed INIL technique combined with the numeric simulation optimized pattern design can enable various nano-scale functional devices including angle-resolved plasmonic/photonic crystals, solar cells and biomimic anisotropic self-cleaning surface.

5.2.2 Molecularly Imprinted Polymers (MIPs) for X-ray Contrast Agent

This work would be one of the few successful examples that properly demonstrate non-covalent imprinting of water-soluble macromolecules with promising binding results. Further the demonstrated imprinted polymers would be one of the very first examples that experimentally prove non-covalent molecular imprinting of suitable polymers can enhance their absorption capacity and imprinting effect, e.g. for X-ray contrast agent of iodixanol, to the point where clinical useful quantities can be bound. Manufacturing and eventually integrating such MIPs into dialysis columns or MEMS-based sensor devices would directly pave the path for clinical usage. In addition, the results of this research will also aid scientists and engineers to further understand the imprinting mechanism and improve application of MIT.

5.2.3 Nanolithography-based Molecular Manipulation (NMM)

The NMM concept represents a significant hybrid strategy for fabricating nanosystems and molecular systems, e.g. by fusing "top-down" nanolithography (e.g. EBL) with "bottom-up" molecular manipulation (e.g. SIP) approaches, as demonstrated in this work. Advantages of this integration include removing the challenge and difficulty for "top-down" EBL to directly produce molecular scale feature sizes. Instead, it utilizes "bottom-up" SIP to minimize the scale gap to the desired one (e.g. sub-10 nm) by molecularly controlling the polymer layer thickness. In addition, pattern surface functionalization is simultaneously accomplished through the grafted polymer material. "Top-down" EBL can appropriately define the locations of functional structures across the entire chip for properly fabricating useful devices as well as system integration. The demonstrated mechanosynthesis of 3D nanostructures in sub-10 nm feature sizes by using the prototype molecular manipulation templates is the first example that proves the NMM strategy and allows us to manipulate molecules and molecular-scale fabrication in a designated way. Although it is at an early stage, it

shows potential and a bright future toward molecular nanotechnology. In addition, the produced novel 3D polymeric nanostructures are of significant specificity and thus enable applications that require chemical and physical anisotropies, such as improved therapeutic agents and near molecular self-assemblies.

5.3 Suggestions for Future Work

Based on the results presented in this dissertation, some issues associated with these three investigations have been encountered and need to be addressed in the future. Moreover, according to the current research progress, each investigation has some aspects that are of great interest to further explore and study.

In the INIL study, we have successfully demonstrated the technique and its mechanism, and have the capability to manipulate polymer material properties and process conditions to properly produce designed 3D nanopatterns of varying heights. One meaningful research extension of this project is to apply the demonstrated technique for device fabrication in the fields of nanophotonics and plasmonics. It would consist of careful device design and simulation, as well as process optimization and characterization. Moreover, 3D chiral nanostructures assembled from the demonstrated nanopattern component of varying height would be of great interest to explore. On the other hand, further studies on process mechanism, including numerical simulation and thermodynamics analysis, will be important and helpful for us to completely understand and manipulate INIL.

In the MIPs investigation, we have demonstrated the non-covalent imprinting of iodixanol in aqueous ethanol using 4-vinylpyridine as the functional monomer and ethylene glycol dimethacrylate as the crosslinker. The optimized MIPs show proper binding capacity and imprint effect both in aqueous and sheep plasma solutions. Three aspects of this work are of particular interest for future study. First, one missing yet important part of the MIPs project is the *in vitro* binding performance

characterization of MIPs in blood. Its fulfillment will lead MIPs to actual clinical applications. Collaboration with hospitals or some licensed labs will be needed to perform this study. It is also very interesting and meaningful to study the effect of MIPs particle size and porosity on MIPs binding performance and the diffusion of target molecules into MIPs. Secondly, the integration of demonstrated MIPs with MEMS devices for sensor applications would be an interesting yet challenging research topic. Such combination would enable a number of significant applications and serve as a good example of integrating "top-down" MEMS techniques with "bottom-up" molecular assembly strategies. The third potential study would be associated with the fundamental understanding of the imprinting mechanism and the molecular associations by using high-performance computing and molecular-level simulation methods.

In the NMM work, we proposed the NMM concept and have demonstrated a hybrid NMM process by integrating "top-down" EBL with "bottom-up" SIP for fabricating a series of molecular manipulation templates with 3D sub-10 nm nanostructures and tailor-made surface functionalities. The templates are utilized to mechanosynthesize various 3D novel polymeric nanostructures with sub-10 nm feature size. Future work under this topic would include (1) characterization of the synthetic 3D nanostructures in a given external field to exploit the interrelationship between 3D nanostructure morphology and their performance for nanomedicine applications; (2) template pattern redesign and process optimization to increase the yield; (3) selection and extensive study of other kinds of molecules and functional materials to meet the potential application needs, e.g. targeted drug delivery. With regard to the first issue, precise tools that only require a small amount of sample would be utilized to perform this characterization, such as Transmission Electron Microscopy (TEM), Atomic Force Microscopy (AFM) and Nuclear Magnetic Resonance (NMR). Careful experimental design and setup would be needed to properly translate and transfer the existent molecular-level information and their associations. This will pave the

away for the ultimate vision of top-down-designed molecular catalysts and enzymes inherent in this investigation.

REFERENCES

[1] http://www.molecular-imprinting.org/story/MIT.htm Nov 1, 2010.

[2] http://www.nanolithography.gatech.edu/EBL_current_research.pdf Nov 1, 2010.

[3] Ahn, S., Cha, J., Myung, H., Kim, S., and Kang, S., "Continuous ultraviolet roll nanoimprinting process for replicating large-scale nano-and micropatterns," *Applied Physics Letters*, vol. 89, p. 213101, 2006.

[4] Aldaye, F., Palmer, A., and Sleiman, H., "Assembling materials with DNA as the guide," *Science*, vol. 321, no. 5897, p. 1795, 2008.

[5] Alexander, C., Andersson, H., Andersson, L., Ansell, R., Kirsch, N., Nicholls, I., O'Mahony, J., and Whitcombe, M., "Molecular imprinting science and technology: a survey of the literature for the years up to and including 2003," *Journal of molecular recognition*, vol. 19, no. 2, pp. 106–180, 2006.

[6] Almen, T., "Visipaque–a step forward. A historical review.," *Acta radiologica. Supplementum*, vol. 399, p. 2, 1995.

[7] Aoki, Y. and Tanaka, T., "Viscoelastic Properties of Miscible Poly (methyl methacrylate)/Poly (styrene-co-acrylonitrile) Blends in the Molten State," *Macromolecules*, vol. 32, no. 25, pp. 8560–8565, 1999.

[8] Austin, M., Ge, H., Wu, W., Li, M., Yu, Z., Wasserman, D., Lyon, S., and Chou, S., "Fabrication of 5 nm linewidth and 14 nm pitch features by nanoimprint lithography," *Applied Physics Letters*, vol. 84, p. 5299, 2004.

[9] Austin, M., Zhang, W., Ge, H., Wasserman, D., Lyon, S., and Chou, S., "6 nm half-pitch lines and 0.04 Ám2 static random access memory patterns by nanoimprint lithography," *Nanotechnology*, vol. 16, p. 1058, 2005.

[10] Baca, A., Truong, T., Cambrea, L., Montgomery, J., Gray, S., Abdula, D., Banks, T., Yao, J., Nuzzo, R., and Rogers, J., "Molded plasmonic crystals for detecting and spatially imaging surface bound species by surface-enhanced Raman scattering," *Applied Physics Letters*, vol. 94, p. 243109, 2009.

[11] Bao, L., Cheng, X., Huang, X., Guo, L., Pang, S., and Yee, A., "Nanoimprinting over topography and multilayer three-dimensional printing," *Journal of Vacuum Science & Technology B: Microelectronics and Nanometer Structures*, vol. 20, p. 2881, 2002.

[12] Barbey, R., Lavanant, L., Paripovic, D., Schüuwer, N., Sugnaux, C., Tugulu, S., and Klok, H., "Polymer brushes via surface-initiated controlled radical polymerization: synthesis, characterization, properties, and applications," *Chem. Rev*, vol. 109, no. 11, pp. 5437–5527, 2009.

[13] Barth, J., "Molecular architectonic on metal surfaces," *Physical Chemistry*, vol. 58, no. 1, p. 375, 2007.

[14] Baumberg, J., Kelf, T., Sugawara, Y., Cintra, S., Abdelsalam, M., Bartlett, P., and Russell, A., "Angle-resolved surface-enhanced Raman scattering on metallic nanostructured plasmonic crystals," *Nano Lett*, vol. 5, no. 11, pp. 2262–2267, 2005.

[15] Berg, K., Rolfsen, B., and Stake, G., "Iodixanol is readily eliminated by hemodialysis," *Acta Radiologica*, vol. 39, no. 4, pp. 372–374, 1998.

[16] Bergmann, N. and Peppas, N., "Molecularly imprinted polymers with specific recognition for macromolecules and proteins," *Progress in Polymer Science*, vol. 33, no. 3, pp. 271–288, 2008.

[17] Bermel, P., Luo, C., Zeng, L., Kimerling, L., and Joannopoulos, J., "Improving thin-film crystalline silicon solar cell efficiencies with photonic crystals," *Appl. Phys. Lett*, vol. 43, pp. 579–581, 1983.

[18] Bolisay, L., Culver, J., and Kofinas, P., "Molecularly imprinted polymers for tobacco mosaic virus recognition," *Biomaterials*, vol. 27, no. 22, pp. 4165–4168, 2006.

[19] Bolisay, L., Culver, J., and Kofinas, P., "Optimization of virus imprinting methods to improve selectivity and reduce nonspecific binding," *Biomacromolecules*, vol. 8, no. 12, pp. 3893–3899, 2007.

[20] Bossi, A., Bonini, F., Turner, A., and Piletsky, S., "Molecularly imprinted polymers for the recognition of proteins: the state of the art," *Biosensors and Bioelectronics*, vol. 22, no. 6, pp. 1131–1137, 2007.

[21] Bromberg, L. and Klibanov, A., "Transport of proteins dissolved in organic solvents across biomimetic membranes," *Proceedings of the National Academy of Sciences of the United States of America*, vol. 92, no. 5, p. 1262, 1995.

[22] Brongersma, M. and Shalaev, V., "The Case for Plasmonics," *Science*, vol. 328, no. 5977, p. 440, 2010.

[23] Bruggemann, O., Haupt, K., Ye, L., Yilmaz, E., and Mosbach, K., "New configurations and applications of molecularly imprinted polymers," *Journal of Chromatography A*, vol. 889, no. 1-2, pp. 15–24, 2000.

[24] Bucknall, D., "Influence of interfaces on thin polymer film behaviour," *Progress in Materials Science*, vol. 49, no. 5, pp. 713–786, 2004.

[25] Cao, Y., Steigerwald, M., Nuckolls, C., and Guo, X., "Current Trends in Shrinking the Channel Length of Organic Transistors Down to the Nanoscale," *Advanced Materials*, vol. 22, no. 1, pp. 20–32, 2010.

[26] Casey, B. and Kofinas, P., "Selective binding of carcinoembryonic antigen using imprinted polymeric hydrogels," *Journal of Biomedical Materials Research Part A*, vol. 87, no. 2, pp. 359–363, 2008.

[27] Chen, Y. and Pépin, A., "Nanofabrication: Conventional and nonconventional methods," *Electrophoresis*, vol. 22, no. 2, pp. 187–207, 2001.

[28] Chou, S., "Nanoimprint lithography," June 30 1998. US Patent 5,772,905.

[29] Chou, S., Keimel, C., and Gu, J., "Ultrafast and direct imprint of nanostructures in silicon," *Nature*, vol. 417, no. 6891, pp. 835–837, 2002.

[30] Chou, S., Krauss, P., and Renstrom, P., "Imprint of sub-25 nm vias and trenches in polymers," *Applied physics letters*, vol. 67, p. 3114, 1995.

[31] Chou, S., Krauss, P., Zhang, W., Guo, L., and Zhuang, L., "Sub-10 nm imprint lithography and applications," *Journal of Vacuum Science and Technology-Section B-Microelectronics Nanometer Structur*, vol. 15, no. 6, pp. 2897–2904, 1997.

[32] Chutinan, A., Kherani, N., and Zukotynski, S., "High-efficiency photonic crystal solar cell architecture," *Optics Express*, vol. 17, no. 11, pp. 8871–8878, 2009.

[33] Craighead, H., "Nanoelectromechanical systems," *Science*, vol. 290, no. 5496, p. 1532, 2000.

[34] Cui, X., Tawa, K., Kintaka, K., and Nishii, J., "Enhanced Fluorescence Microscopic Imaging by Plasmonic Nanostructures: From a 1D Grating to a 2D Nanohole Array," *Advanced Functional Materials*, vol. 20, no. 6, pp. 945–950, 2010.

[35] Davis, J., Morgan, D., Wrathmell, C., Axford, D., Zhao, J., and Wang, N., "Molecular bioelectronics," *Journal of Materials Chemistry*, vol. 15, no. 22, pp. 2160–2174, 2005.

[36] Decuzzi, P. and Ferrari, M., "The adhesive strength of non-spherical particles mediated by specific interactions," *Biomaterials*, vol. 27, no. 30, pp. 5307–5314, 2006.

[37] Edmondson, S., Osborne, V., and Huck, W., "Polymer brushes via surface-initiated polymerizations," *Chemical society reviews*, vol. 33, no. 1, pp. 14–22, 2004.

[38] Edwards, E., Muller, M., Stoykovich, M., Solak, H., de Pablo, J., and Nealey, P., "Dimensions and shapes of block copolymer domains assembled on lithographically defined chemically patterned substrates," *Macromolecules*, vol. 40, no. 1, pp. 90–96, 2007.

[39] Fennimore, A., Yuzvinsky, T., Han, W., Fuhrer, M., Cumings, J., and Zettl, A., "Rotational actuators based on carbon nanotubes," *Nature*, vol. 424, no. 6947, pp. 408–410, 2003.

[40] Garcia, R., Martinez, R., and Martinez, J., "Nano-chemistry and scanning probe nanolithographies," *Chemical Society Reviews*, vol. 35, no. 1, pp. 29–38, 2006.

[41] Gates, B., Xu, Q., Love, J., Wolfe, D., and Whitesides, G., "Unconventional nanofabrication," *Materials Research*, vol. 34, no. 1, p. 339, 2004.

[42] Ge, J., Hu, Y., Biasini, M., Dong, C., Guo, J., Beyermann, W., and Yin, Y., "One-step synthesis of highly water-soluble magnetite colloidal nanocrystals," *Chemistry-A European Journal*, vol. 13, no. 25, pp. 7153–7161, 2007.

[43] Ge, Y. and Turner, A., "Too large to fit? Recent developments in macromolecular imprinting," *Trends in biotechnology*, vol. 26, no. 4, pp. 218–224, 2008.

[44] Glinsner, T., Lindner, P., Muhlberger, M., Bergmair, I., Schoftner, R., Hingerl, K., Schmid, H., and Kley, E., "Fabrication of 3D-photonic crystals via UV-nanoimprint lithography," *Journal of Vacuum Science & Technology B: Microelectronics and Nanometer Structures*, vol. 25, p. 2337, 2007.

[45] Guo, L., "Nanoimprint lithography: methods and material requirements," *Advanced materials*, vol. 19, no. 4, pp. 495–513, 2007.

[46] Haupt, K., Dzgoev, A., and Mosbach, K., "Assay system for the herbicide 2, 4-dichlorophenoxyacetic acid using a molecularly imprinted polymer as an artificial recognition element," *Anal. chem*, vol. 70, no. 3, pp. 628–631, 1998.

[47] Heo, C., Kim, S., Jang, S., Lee, S., and Yang, S., "Gold Nanograils with Tunable Dipolar Multiple Plasmon Resonances," *Advanced Materials*, vol. 21, no. 17, pp. 1726–1731, 2009.

[48] Hierold, C., Jungen, A., Stampfer, C., and Helbling, T., "Nano electromechanical sensors based on carbon nanotubes," *Sensors and Actuators A: Physical*, vol. 136, no. 1, pp. 51–61, 2007.

[49] Hishiya, T., Shibata, M., Kakazu, M., Asanuma, H., and Komiyama, M., "Molecularly Imprinted Cyclodextrins as Selective Receptors for Steroids1," *Macromolecules*, vol. 32, no. 7, pp. 2265–2269, 1999.

[50] Hua, F., Sun, Y., Gaur, A., Meitl, M., Bilhaut, L., Rotkina, L., Wang, J., Geil, P., Shim, M., Rogers, J., and others, "Polymer imprint lithography with molecular-scale resolution," *Nano Lett*, vol. 4, no. 12, pp. 2467–2471, 2004.

[51] Huang, Y., Duan, X., Wei, Q., and Lieber, C., "Directed assembly of one-dimensional nanostructures into functional networks," *Science*, vol. 291, no. 5504, p. 630, 2001.

[52] Itani, T., Wakamiya, W., Cashmore, J., and Gower, M., "157-nm lithography with high numerical aperture lens for sub-70 nm node," *Microelectronic Engineering*, vol. 67, pp. 39–46, 2003.

[53] Jacobsen, P., "On-line dialysis and quantitative high-performance liquid chromatography analysis of iodixanol in human, rat and monkey plasma," *Journal of Chromatography B: Biomedical Sciences and Applications*, vol. 749, no. 1, pp. 135–142, 2000.

[54] Jacobsen, P., Larsen, Å., Konarboland, R., and Skotland, T., "Biotransformation of nonionic X-ray contrast agents in vivo and in vitro," *Drug Metabolism and Disposition*, vol. 27, no. 10, p. 1205, 1999.

[55] Jalabert, L., Bottier, C., Kumemura, M., and Fujita, H., "Embedded vertical nanosheets of SiO in PDMS using an alternative nanopatterning process," *Journal of Vacuum Science & Technology B: Microelectronics and Nanometer Structures*, vol. 27, p. 3055, 2009.

[56] Janiak, D., Ayyub, O., and Kofinas, P., "Effects of Charge Density on the Recognition Properties of Molecularly Imprinted Polymeric Hydrogels," *Macromolecules*, vol. 42, no. 5, pp. 1703–1709, 2009.

[57] Jeon, N., Choi, I., Whitesides, G., Kim, N., Laibinis, P., Harada, Y., Finnie, K., Girolami, G., and Nuzzo, R., "Patterned polymer growth on silicon surfaces using microcontact printing and surface-initiated polymerization," *Applied Physics Letters*, vol. 75, p. 4201, 1999.

[58] Jeon, S., Menard, E., Park, J., Maria, J., Meitl, M., Zaumseil, J., and Rogers, J., "Three-dimensional nanofabrication with rubber stamps and conformable photomasks," *Advanced Materials*, vol. 16, no. 15, pp. 1369–1373, 2004.

[59] Jeon, S., Park, J., Cirelli, R., Yang, S., Heitzman, C., Braun, P., Kenis, P., and Rogers, J., "Fabricating complex three-dimensional nanostructures with high-resolution conformable phase masks," *Proceedings of the National Academy of Sciences of the United States of America*, vol. 101, no. 34, p. 12428, 2004.

[60] Jiang, L., Althoff, E., Clemente, F., Doyle, L., Rothlisberger, D., Zanghellini, A., Gallaher, J., Betker, J., Tanaka, F., Barbas III, C., and others, "De novo computational design of retro-aldol enzymes," *Science*, vol. 319, no. 5868, p. 1387, 2008.

[61] Joachim, C., Gimzewski, J., and Aviram, A., "Electronics using hybrid-molecular and mono-molecular devices," *Nature*, vol. 408, no. 6812, pp. 541–548, 2000.

[62] Jones, D. and Huck, W., "Controlled surface-initiated polymerizations in aqueous media," *Advanced Materials*, vol. 13, no. 16, pp. 1256–1259, 2001.

[63] Juillerat, F., Solak, H., Bowen, P., and Hofmann, H., "Fabrication of large-area ordered arrays of nanoparticles on patterned substrates," *Nanotechnology*, vol. 16, p. 1311, 2005.

[64] Juluri, B., Kumar, A., Liu, Y., Ye, T., Yang, Y., Flood, A., Fang, L., Stoddart, J., Weiss, P., and Huang, T., "A mechanical actuator driven electrochemically by artificial molecular muscles," *ACS nano*, vol. 3, no. 2, pp. 291–300, 2009.

[65] Kaholek, M., Lee, W., Ahn, S., Ma, H., Caster, K., LaMattina, B., and Zauscher, S., "Stimulus-responsive poly (N-isopropylacrylamide) brushes and nanopatterns prepared by surface-initiated polymerization," *Chem. Mater*, vol. 16, no. 19, pp. 3688–3696, 2004.

[66] Kantouch, A. and El-Sayed, A., "Polyvinyl pyridine metal complex as permanent antimicrobial finishing for viscose fabric," *International journal of biological macromolecules*, vol. 43, no. 5, pp. 451–455, 2008.

[67] Karnik, R., Fan, R., Yue, M., Li, D., Yang, P., and Majumdar, A., "Electrostatic control of ions and molecules in nanofluidic transistors," *Nano Lett*, vol. 5, no. 5, pp. 943–948, 2005.

[68] Katz, A. and Davis, M., "Investigations into the mechanisms of molecular recognition with imprinted polymers," *Macromolecules*, vol. 32, no. 12, pp. 4113–4121, 1999.

[69] Kim, D., Lin, Z., Kim, H., Jeong, U., and Russell, T., "On the replication of block copolymer templates by poly (dimethylsiloxane) elastomers," *Advanced Materials*, vol. 15, no. 10, pp. 811–814, 2003.

[70] Kim, P. and Lieber, C., "Nanotube nanotweezers," *Science*, vol. 286, no. 5447, p. 2148, 1999.

[71] Kinkhabwala, A., Yu, Z., Fan, S., Avlasevich, Y., Mullen, K., and Moerner, W., "Large single-molecule fluorescence enhancements produced by a bowtie nanoantenna," *Nature Photonics*, vol. 3, no. 11, pp. 654–657, 2009.

[72] Korczagin, I., Golze, S., Hempenius, M., and Vancso, G., "Surface micropatterning and lithography with poly (ferrocenylmethylphenylsilane)," *Chem. Mater*, vol. 15, no. 19, pp. 3663–3668, 2003.

[73] Kung, H., Hoyert, D., Xu, J., and Murphy, S., "Deaths: final data for 2005," *National vital statistics reports*, vol. 56, no. 10, pp. 1–120, 2008.

[74] Lee, J. and Bucknall, D., "Swelling behavior and network structure of hydrogels synthesized using controlled UV-initiated free radical polymerization," *Journal of Polymer Science Part B: Polymer Physics*, vol. 46, no. 14, pp. 1450–1462, 2008.

[75] Lee, K., Itharaju, R., and Puleo, D., "Protein-imprinted polysiloxane scaffolds," *Acta biomaterialia*, vol. 3, no. 4, pp. 515–522, 2007.

[76] LeGrand, D., Gaines, G., and others, "The molecular weight dependence of polymer surface tension," *Journal of Colloid and Interface Science*, vol. 31, no. 2, pp. 162–167, 1969.

[77] Leopoldes, J., Dupuis, A., Bucknall, D., and Yeomans, J., "Jetting micron-scale droplets onto chemically heterogeneous surfaces," *Langmuir*, vol. 19, no. 23, pp. 9818–9822, 2003.

[78] Li, M., Chen, L., and Chou, S., "Direct three-dimensional patterning using nanoimprint lithography," *Applied Physics Letters*, vol. 78, p. 3322, 2001.

[79] Li, M., Wang, J., Zhuang, L., and Chou, S., "Fabrication of circular optical structures with a 20 nm minimum feature size using nanoimprint lithography," *Applied Physics Letters*, vol. 76, p. 673, 2000.

[80] Lin, Y., Tang, S., Mao, X., and Bao, L., "Protein recognition via molecularly imprinted agarose gel membrane," *Journal of Biomedical Materials Research Part A*, vol. 85, no. 3, pp. 573–581, 2008.

[81] Ling, X., Phang, I., Reinhoudt, D., Vancso, G., and Huskens, J., "Free-standing porous supramolecular assemblies of nanoparticles made using a double-templating strategy," *Faraday Discussions*, vol. 143, pp. 117–127, 2009.

[82] Ling, X., Phang, I., Schonherr, H., Reinhoudt, D., Vancso, G., and Huskens, J., "Freestanding 3D Supramolecular Particle Bridges: Fabrication and Mechanical Behavior," *Small*, vol. 5, no. 12, pp. 1428–1435, 2009.

[83] Liss, P., Persson, P., Hansell, P., and Lagerqvist, B., "Renal failure in 57 925 patients undergoing coronary procedures using iso-osmolar or low-osmolar contrast media," *Kidney international*, vol. 70, no. 10, pp. 1811–1817, 2006.

[84] Liu, X., Ding, X., Guan, Y., Peng, Y., Long, X., Wang, X., Chang, K., and Zhang, Y., "Fabrication of temperature-sensitive imprinted polymer hydrogel," *Macromolecular bioscience*, vol. 4, no. 4, pp. 412–415, 2004.

[85] Loo, Y., Willett, R., Baldwin, K., and Rogers, J., "Additive, nanoscale patterning of metal films with a stamp and a surface chemistry mediated transfer process: Applications in plastic electronics," *Applied Physics Letters*, vol. 81, p. 562, 2002.

[86] MA, A., "Next Wave of Metamaterials Hopes to Fuel the Revolution," *Science*, vol. 327, no. 5962, p. 138, 2010.

[87] Matsuura, N. and Rowlands, J., "Towards new functional nanostructures for medical imaging," *Medical physics*, vol. 35, p. 4474, 2008.

[88] McAlpine, M., Friedman, R., Jin, S., Lin, K., Wang, W., and Lieber, C., "High-performance nanowire electronics and photonics on glass and plastic substrates," *Nano letters*, vol. 3, no. 11, pp. 1531–1535, 2003.

[89] Medeiros, D., Aviram, A., Guarnieri, C., Huang, W., Kwong, R., Magg, C., Mahorowala, A., Moreau, W., Petrillo, K., and Angelopoulos, M., "Recent progress in electron-beam resists for advanced mask-making," *IBM Journal of Research and Development*, vol. 45, no. 5, pp. 639–650, 2001.

[90] Messer, B., Song, J., and Yang, P., "Microchannel networks for nanowire patterning," *J. Am. Chem. Soc*, vol. 122, no. 41, pp. 10232–10233, 2000.

[91] Mosbach, K. and Ramstrom, O., "The emerging technique of molecular imprinting and its future impact on biotechnology," *Nature Biotechnology*, vol. 14, no. 2, pp. 163–170, 1996.

[92] Moulder, J. and Chastain, J., *Handbook of X-ray photoelectron spectroscopy*. Perkin-Elmer Eden Prairie, MN, 1992.

[93] Nagpal, P., Lindquist, N., Oh, S., and Norris, D., "Ultrasmooth patterned metals for plasmonics and metamaterials," *Science*, vol. 325, no. 5940, p. 594, 2009.

[94] Oral, E. and Peppas, N., "Hydrophilic molecularly imprinted poly (hydroxyethyl-methacrylate) polymers," *Journal of Biomedical Materials Research Part A*, vol. 78, no. 1, pp. 205–210, 2006.

[95] Park, J., Khandekar, A., Park, S., Mawst, L., Kuech, T., and Nealey, P., "Selective MOCVD growth of single-crystal dense GaAs quantum dot array using cylinder-forming diblock copolymers," *Journal of Crystal Growth*, vol. 297, no. 2, pp. 283–288, 2006.

[96] Park, S., Craig, G., La, Y., Solak, H., and Nealey, P., "Square arrays of vertical cylinders of PS-b-PMMA on chemically nanopatterned surfaces," *Macromolecules*, vol. 40, no. 14, pp. 5084–5094, 2007.

[97] Persson, P., "Contrast-induced nephropathy," *European Radiology Supplements*, vol. 15, pp. 65–69, 2005.

[98] Piletska, E., Guerreiro, A., Whitcombe, M., and Piletsky, S., "Influence of the Polymerization Conditions on the Performance of Molecularly Imprinted Polymers," *Macromolecules*, vol. 42, no. 14, pp. 4921–4928, 2009.

[99] Pisignano, D., Sariconi, E., Mazzeo, M., Gigli, G., and Cingolani, R., "High-temperature microfluidic lithography," *Advanced Materials*, vol. 14, no. 21, pp. 1565–1567, 2002.

[100] Prodan, E., Radloff, C., Halas, N., and Nordlander, P., "A hybridization model for the plasmon response of complex nanostructures," *Science*, vol. 302, no. 5644, p. 419, 2003.

[101] Qi, M., Lidorikis, E., Rakich, P., Johnson, S., Joannopoulos, J., Ippen, E., and Smith, H., "A three-dimensional optical photonic crystal with designed point defects," *Nature*, vol. 429, no. 6991, pp. 538–542, 2004.

[102] Reiter, G., "Unstable thin polymer films: rupture and dewetting processes," *Langmuir*, vol. 9, no. 5, pp. 1344–1351, 1993.

[103] Roco, M., "International perspective on government nanotechnology funding in 2005," *Journal of Nanoparticle Research*, vol. 7, no. 6, pp. 707–712, 2005.

[104] Roiter, Y. and Minko, S., "AFM Single Molecule Experiments at the Solid-Liquid Interface: In Situ Conformation of Adsorbed Flexible Polyelectrolyte Chains," *J. Am. Chem. Soc*, vol. 127, no. 45, pp. 15688–15689, 2005.

[105] Rudnick, M., Davidson, C., Laskey, W., Stafford, J., and Sherwin, P., "Nephrotoxicity of iodixanol versus ioversol in patients with chronic kidney disease: the Visipaque Angiography/Interventions with Laboratory Outcomes in Renal Insufficiency (VALOR) Trial," *American Heart Journal*, vol. 156, no. 4, pp. 776–782, 2008.

[106] Schillemans, J. and van Nostrum, C., "Molecularly imprinted polymer particles: synthetic receptors for future medicine," *Nanomedicine*, vol. 1, no. 4, pp. 437–447, 2006.

[107] Schilp, S., Ballav, N., and Zharnikov, M., "Fabrication of a Full-coverage Polymer Nanobrush on an Electron-beam-activated Template," *Angewandte Chemie International Edition*, vol. 47, no. 36, pp. 6786–6789, 2008.

[108] Schmelmer, U., Jordan, R., Geyer, W., Eck, W., Golzhauser, A., Grunze, M., and Ulman, A., "Surface-initiated polymerization on self-assembled monolayers: amplification of patterns on the micrometer and nanometer scale," *Angewandte Chemie International Edition*, vol. 42, no. 5, pp. 559–563, 2003.

[109] Shi, H., Tsai, W., Garrison, M., Ferrari, S., and Ratner, B., "Template-imprinted nanostructured surfaces for protein recognition," *Nature*, vol. 398, no. 6728, pp. 593–597, 1999.

[110] Singh, B. and Chauhan, N., "Preliminary evaluation of molecular imprinting of 5-fluorouracil within hydrogels for use as drug delivery systems," *Acta Biomaterialia*, vol. 4, no. 5, pp. 1244–1254, 2008.

[111] Stewart, M., Johnson, S., Sreenivasan, S., Resnick, D., and Willson, C., "Nanofabrication with step and flash imprint lithography," *Journal of Microlithography, Microfabrication, and Microsystems*, vol. 4, p. 011002, 2005.

[112] Stewart, M., Mack, N., Malyarchuk, V., Soares, J., Lee, T., Gray, S., Nuzzo, R., and Rogers, J., "Quantitative multispectral biosensing and 1D imaging using quasi-3D plasmonic crystals," *Proceedings of the National Academy of Sciences*, vol. 103, no. 46, p. 17143, 2006.

[113] Stoykovich, M. and Nealey, P., "Block copolymers and conventional lithography," *Materials Today*, vol. 9, no. 9, pp. 20–29, 2006.

[114] Tasciotti, E., Liu, X., Bhavane, R., Plant, K., Leonard, A., Price, B., Cheng, M., Decuzzi, P., Tour, J., Robertson, F., and others, "Mesoporous silicon particles as a multistage delivery system for imaging and therapeutic applications," *Nature nanotechnology*, vol. 3, no. 3, pp. 151–157, 2008.

[115] Tiron, R., Mollard, L., Louveau, O., and Lajoinie, E., "Ultrahigh-resolution pattern using electron-beam lithography hf wet etching," *Journal of Vacuum Science & Technology B: Microelectronics and Nanometer Structures*, vol. 25, no. 4, pp. 1147–1151, 2007.

[116] Truong, T., Maria, J., Yao, J., Stewart, M., Lee, T., Gray, S., Nuzzo, R., and Rogers, J., "Nanopost plasmonic crystals," *Nanotechnology*, vol. 20, p. 434011, 2009.

[117] Ueda, J., Sato, S., Tsunokawa, A., Yamauchi, T., and Tsubokawa, N., "Scale-up synthesis of vinyl polymer-grafted nano-sized silica by radical polymerization of vinyl monomers initiated by surface initiating groups in the solvent-free dry-system," *European Polymer Journal*, vol. 41, no. 2, pp. 193–200, 2005.

[118] Venkatesh, S., Sizemore, S., and Byrne, M., "Biomimetic hydrogels for enhanced loading and extended release of ocular therapeutics," *Biomaterials*, vol. 28, no. 4, pp. 717–724, 2007.

[119] Vettiger, P., Despont, M., Drechsler, U., Durig, U., Haberle, W., Lutwyche, M., Rothuizen, H., Stutz, R., Widmer, R., and Binnig, G., "The Millipede: more than one thousand tips for future AFM data storage," *IBM Journal of Research and Development*, vol. 44, no. 3, pp. 323–340, 2000.

[120] Vieu, C., Carcenac, F., Pepin, A., Chen, Y., Mejias, M., Lebib, A., Manin-Ferlazzo, L., Couraud, L., and Launois, H., "Electron beam lithography: resolution limits and applications," *Applied Surface Science*, vol. 164, no. 1-4, pp. 111–117, 2000.

[121] Von Werne, T., Germack, D., Hagberg, E., Sheares, V., Hawker, C., and Carter, K., "A versatile method for tuning the chemistry and size of nanoscopic features by living free radical polymerization," *J. Am. Chem. Soc*, vol. 125, no. 13, pp. 3831–3838, 2003.

[122] Weisbord, S., "Iodinated contrast media and the kidney.," *Reviews in cardiovascular medicine*, vol. 9, p. S14, 2008.

[123] Williams, P., Papadakis, S., Patel, A., Falvo, M., Washburn, S., and Superfine, R., "Fabrication of nanometer-scale mechanical devices incorporating individual multiwalled carbon nanotubes as torsional springs," *Applied Physics Letters*, vol. 82, p. 805, 2003.

[124] Wind, S., Appenzeller, J., and Avouris, P., "Lateral scaling in carbon-nanotube field-effect transistors," *Physical review letters*, vol. 91, no. 5, p. 58301, 2003.

[125] Wizeman, W. and Kofinas, P., "Molecularly imprinted polymer hydrogels displaying isomerically resolved glucose binding.," *Biomaterials*, vol. 22, no. 12, p. 1485, 2001.

[126] Wulff, G., "Molecular imprinting in cross-linked materials with the aid of molecular templates-a way towards artificial antibodies," *Angewandte Chemie International Edition in English*, vol. 34, no. 17, pp. 1812–1832, 1995.

[127] Xia, Y., "WHITESIDES. GM:Soft lithography," *Angew. Chem., Int. Ed. Engl*, vol. 37, pp. 550–575, 1998.

[128] Xu, Q., Mayers, B., Lahav, M., Vezenov, D., and Whitesides, G., "Approaching zero: using fractured crystals in metrology for replica molding," *J. Am. Chem. Soc*, vol. 127, no. 3, pp. 854–855, 2005.

[129] Xu, S., Qin, Y., Xu, C., Wei, Y., Yang, R., and Wang, Z., "Self-powered nanowire devices," *Nature Nanotechnology*, vol. 5, no. 5, pp. 366–373, 2010.

[130] Yamashita, T., "Unraveling photonic bands: characterization of self-collimation effects in two-dimensional photonic crystals," 2005.

[131] Yan, J., Du, Y., Liu, J., Cao, W., Sun, X., Zhou, W., Yang, X., and Wang, E., "Fabrication of integrated microelectrodes for electrochemical detection on electrophoresis microchip by electroless deposition and micromolding in capillary technique," *Anal. Chem*, vol. 75, no. 20, pp. 5406–5412, 2003.

[132] Yanik, A., Huang, M., Artar, A., Chang, T., and Altug, H., "Integrated nanoplasmonic-nanofluidic biosensors with targeted delivery of analytes," *Applied Physics Letters*, vol. 96, p. 021101, 2010.

[133] Yao, D., Zhang, W., and Zhou, J., "Controllable Growth of Gradient Porous Structures," *Biomacromolecules*, vol. 10, no. 5, pp. 1282–1286, 2009.

[134] Yao, J., Yan, X., Lu, G., Zhang, K., Chen, X., Jiang, L., and Yang, B., "Patterning colloidal crystals by lift-up soft lithography," *Advanced Materials*, vol. 16, no. 1, pp. 81–84, 2004.

[135] Ye, L. and Mosbach, K., "Molecular Imprinting: Synthetic Materials As Substitutes for Biological Antibodies and Receptors," *Chem. Mater*, vol. 20, no. 3, pp. 859–868, 2008.

[136] Yungerman, I. and Srebnik, S., "Factors contributing to binding-site imperfections in imprinted polymers," *Chem. Mater*, vol. 18, no. 3, pp. 657–663, 2006.

[137] Zaumseil, J., Meitl, M., Hsu, J., Acharya, B., Baldwin, K., Loo, Y., and Rogers, J., "Three-dimensional and multilayer nanostructures formed by nanotransfer printing," *Nano letters*, vol. 3, no. 9, pp. 1223–1227, 2003.

[138] Zhang, C., He, Y., Su, M., Ko, S., Ye, T., Leng, Y., Sun, X., Ribbe, A., Jiang, W., and Mao, C., "DNA self-assembly: from 2D to 3D," *Faraday Discussions*, vol. 143, pp. 221–233, 2009.

[139] Zhang, H., Bucknall, D., and Dupuis, A., "Uniform Nanoscopic Polystyrene Patterns Produced from a Microscopic Mold," *Nano Letters*, vol. 4, no. 8, pp. 1513–1519, 2004.

[140] Zhang, W. and Chou, S., "Fabrication of 60-nm transistors on 4-in. wafer using nanoimprint at all lithography levels," *Applied physics letters*, vol. 83, p. 1632, 2003.

[141] Zhao, B. and Brittain, W., "Polymer brushes: surface-immobilized macromolecules," *Progress in Polymer Science*, vol. 25, no. 5, pp. 677–710, 2000.

[142] Zhao, X., Xia, Y., and Whitesides, G., "Fabrication of three-dimensional micro-structures: Microtransfer molding," *Advanced Materials*, vol. 8, no. 10, pp. 837–840, 1996.

[143] Zimmerman, S., Wendland, M., Rakow, N., Zharov, I., and Suslick, K., "Synthetic hosts by monomolecular imprinting inside dendrimers," *Nature*, vol. 418, no. 6896, pp. 399–403, 2002.

VITA

Ms. Zhan Liu received B.S. in Chemistry and M.S. in material Science from Tsinghua University, Beijing, China, in 2002 and 2005 respectively. Zhan's bachelor thesis is titled "Synthesis and investigation of dodecylamine supported layered tin iodide as a semiconductor". Her B.S. thesis adviser is Prof. Gao-quan Shi. Zhan's master thesis is "synthesis and characterization of water-soluble comb-like grafted copolymers poly(acrylic acid)-*g*-poly(ethylene glycol) with crystallizable PEG side chains". Her M.S. thesis adviser is Prof. Xu-ming Xie.

Zhan came to Georgia Institute of Technology in fall 2005 pursuing her PhD degree in school of Polymer, Textile & Fiber Engineering. She joined Prof. Mark G. Allen's research group in fall 2005, and since then she has been conducting research projects towrad the Ph.D. degree. Her research interest is design and development of advanced micro/nanofabrication techniques for nano/molecular scale functional patterns/devices, functional and nanostructured polymer materials and systems including the synthesis, characterization and assembly, molecular manipulation and self-assembly.